THE UNIVERSITY OF QUEENSLAND

SCHOOL OF CIVIL ENGINEERING

REPORT CH74/09

AN EXPERIMENTAL STUDY OF TIDAL BORE PROPAGATION: THE IMPACT OF BRIDGE PIERS AND CHANNEL CONSTRICTION

AUTHOR: Hubert CHANSON

HYDRAULIC MODEL REPORTS

This report is published by the School of Civil Engineering at the University of Queensland. Lists of recently-published titles of this series and of other publications are provided at the end of this report. Requests for copies of any of these documents should be addressed to the Civil Engineering Secretary.

School of Civil Engineering
The University of Queensland
Brisbane QLD 4072
AUSTRALIA

Telephone: (61 7) 3365 3619
Fax: (61 7) 3365 4599

URL: http://www.eng.uq.edu.au/civil/

First published in 2009 by
School of Civil Engineering
The University of Queensland, Brisbane QLD 4072, Australia

ISBN No. 9781864999600

The University of Queensland, St Lucia QLD

AN EXPERIMENTAL STUDY OF TIDAL BORE PROPAGATION: THE IMPACT OF BRIDGE PIERS AND CHANNEL CONSTRICTION

by

Hubert CHANSON

Professor in Hydraulic Engineering, School of Engineering,

The University of Queensland, Brisbane QLD 4072, Australia

Ph.: (61 7) 3365 3619, Fax: (61 7) 3365 4599, Email: h.chanson@uq.edu.au

Url: http://www.uq.edu.au/~e2hchans/

REPORT No. CH74/09

ISBN 9781864999600

School of Civil Engineering, The University of Queensland

July 2009

Tidal bore (*mascaret*) of the Sélune River passing beneath the Pont Aubault (France) looking upstream

Abstract

A tidal bore is an unsteady flow motion generated by the rapid water level rise at the river mouth during the early flood tide when the tidal range exceeds 4 to 6 m, the estuary bathymetry amplifies the tidal wave and the freshwater level is low. The tidal bore is an abrupt rise in water depth associated with a discontinuity in water depth and velocity at the bore front. The present study examines the turbulence and turbulent mixing generated by the passage of an undular tidal bore in a short channel constriction such as a set of bridge piers. Some new experiments were conducted in a large rectangular prismatic channel. Then a short channel constriction that was a 1/20 scale model of the Pont Aubaud on the Sélune River in the Baie du Mont Saint Michel was installed. The free-surface properties of undular tidal bores were carefully documented for both configurations. The analysis of the parametric relationship between momentum function and specific energy showed that the undular flow properties were restricted to the subcritical branch of the M-E diagram, while the quantitative results indicated that the effects of streamline curvature could not be ignored. The free-surface undulation profiles exhibited a quasi-periodic shape, but both field measurements and laboratory observations demonstrated that neither the linear wave theory nor the Boussinesq equation theory captured the fine details of the free-surface profiles. An analysis of the potential energy of the undular tidal bore showed that the potential energy of the free-surface undulations represented up to 30% of the potential energy of the tidal bore. The presence of the channel constriction had a major impact on the free-surface properties. In the channel throat, the wave motion was three-dimensional, pseudo-chaotic and energetic and the undular bore lost nearly one third of its potential energy per surface area as it propagated through the channel constriction. The velocity data sets suggested the upstream advection of energetic turbulent events and vorticity behind the bore front. It is proposed that these energetic turbulent events were some macro-turbulence generated by secondary currents. With the channel constriction, some intense large-scale turbulence was further produced by the constriction. The proposed mechanism was consistent with some field observations in the Daly River tidal bore in 2003. Overall the presence of a channel constriction (e.g. bridge piers) does impact onto the bore propagation. It is associated with some energy loss and the development of large-scale coherent structures, and these processes might induce some river bed scour on the vicinity of the bridge piers.

The technical report is supported by a digital appendix (Appendix B) containing five movies available at the University of Queensland institutional open access repository UQeSpace {http://espace.library.uq.edu.au/}.

Keywords : Turbulence, Positive surges, Tidal bores, Bridge piers, Physical modelling, Energy dissipation, Wave transformation, Bore front, Turbulent mixing, Secondary current, Bridge structures.

TABLE OF CONTENTS

APPENDICES

List of symbols

The following symbols are used in this report:

a_w	wave amplitude (m);
B	channel width (m);
d	flow depth (m) measured normal to the invert;
d_c	critical flow depth (m);
d_{conj}	conjugate flow depth (m) measured immediately behind the bore front;
d_{max}	water depth (m) measured at the first wave crest;
d_o	initial flow depth (m) measured normal to the invert;
E	specific energy (m); for a horizontal channel with hydrostatic pressure distribution: $E = d + \frac{V^2}{2 \times g}$;
E_p	potential energy per surface area (J/m^2);
F	sampling frequency (Hz);
Fr	bore Froude number defined as: $Fr = (V_o + U) / \sqrt{g \times d_o}$;
Fr_o	Froude number of the initially steady flow defined as: $Fr_o = V_o / \sqrt{g \times d_o}$;
g	gravity constant (m/s^2): g = 9.80 m/s^2 in Brisbane, Australia;
h	tainter gate opening (m) after gate closure;
K.E.	kinetic energy (J);
L	length (m);
L_w	wave length (m) measured from crest to crest;
M	momentum function (m^2); for a horizontal channel with hydrostatic pressure distribution: $M = \frac{d^2}{2} + \frac{q^2}{g \times d}$;
P	pressure (Pa);
P.E.	potential energy (J);
Q	volume flow rate (m^3/s);
q	volume flow rate per unit width (m^2/s): q = Q/B;
S_o	bed slope : $S_o = \sin\theta$;
T	wave period (s); free-surface undulation period (s) for an observer standing on the bank
T.E.	total energy (J);
t	time (s);
t_o	reference time (s);
U	bore front celerity (m/s) for an observer standing on the bank, positive upstream;
V	(a) cross-sectional averaged flow velocity (m/s) positive downstream; (b) instantaneous velocity component (m/s);
V_o	initial flow velocity (m/s) positive downstream: $V_o = Q/(d_o \times B)$;
V_x	instantaneous longitudinal velocity (m/s) positive downstream;
V_y	instantaneous transverse velocity (m/s) positive towards the left sidewall;
V_z	instantaneous vertical velocity (m/s) positive upwards;

$\overline{V}$	depth-averaged velocity (m/s);
v'	root mean square of turbulent velocity component (m/s);
x	longitudinal distance (m) measured from the channel upstream end, positive downstream;
x_s	bore front location (m);
y	transverse distance (m) measured from the channel centreline, positive towards the left sidewall;
z	distance (m) normal to the bed; it is the vertical distance (m) for a horizontal channel;

Greek symbols

δ	boundary layer thickness (m) defined in terms of 99% of the free-stream velocity;
η	water elevation (m) above the mean water level;
π	π = 3.14159265358979323846264 3;
θ	bed slope angle with the horizontal, positive downwards;
ρ	water density (kg/m^3);
ψ	stream function (m^2/s);

Subscript

ADV	acoustic Doppler velocimeter;
conj	conjugate flow conditions: i.e., immediately behind the positive surge front;
x	longitudinal component positive downstream;
y	component transverse to the channel centreline;
z	component normal to the invert;
o	initial flow conditions : i.e., upstream of the positive surge front;

Abbreviations

ADV	acoustic Doppler velocimeter;
D/S	downstream;
U/S	upstream;

Notation

Ø	diameter;
$\frac{\partial}{\partial y}$	partial differentiation with respect to y.

1. Introduction

1.1 Presentation

A bore is an unsteady flow motion generated by the rapid water level rise at the river mouth during the early flood tide when the tidal range exceeds 4.5 to 6 m, the estuary bathymetry amplifies the tidal wave and the freshwater level is low. When the tidal level at the river mouth rises with time during the early flood tide, the leading edge of the tide, called the tidal wave, becomes steeper and steeper, until it forms an abrupt front that is the tidal bore (Fig. 1-1). The tidal bore is a positive surge associated with a discontinuity in water depth and velocity, and the bore front is a flow singularity. In Nature, however, a tidal bore may have a variety of different shapes, and the photographs illustrate in particular that the bore front is not a sharp, vertical discontinuity of the water surface because of the necessary curvature of the streamline and the associated pressure and velocity redistributions (Fig. 1-1).

A tidal bore may occur during the spring tide conditions when the funnel shape of the river mouth amplifies the tidal wave. The driving process is the large tidal amplitude (at least 4.5 to 6 m). The tides are forced oscillations generated by the attractions of the Moon and Sun, and have the same periods as the motion of the Sun and Moon relative to the Earth. The Sun exerts a somewhat smaller attraction force than the Moon, but it is especially important every fourteenth day at full moon or new moon when the attraction forces of the Sun and Moon reinforce one another. These conditions give the largest tidal ranges called spring tide conditions, and these may be locally amplified by a number of factors including when the natural resonance of the bay and estuary is close to the tidal period (CLANCY 1968, Open University 1999). The coincidence implies that the general sloshing of the waters around the inlet or bay becomes synchronised with the lunar tides and amplify their effect, like in the Bay of Fundy (Canada) and at Cook Inlet (Alaska).

The tidal bores were studied by hydraulic engineers and applied mathematicians for a couple of centuries. Major contributions on positive surges and bores included the works of BAZIN (1865), BARRÉ de SAINT VENANT (1871), BOUSSINESQ (1877), LEMOINE (1948), SERRE (1953), BENJAMIN and LIGHTHILL (1954), and PEREGRINE (1966). More recent studies encompass MADSEN et al. (2005), KOCH and CHANSON (2008,2009) and CHANSON (2008a).

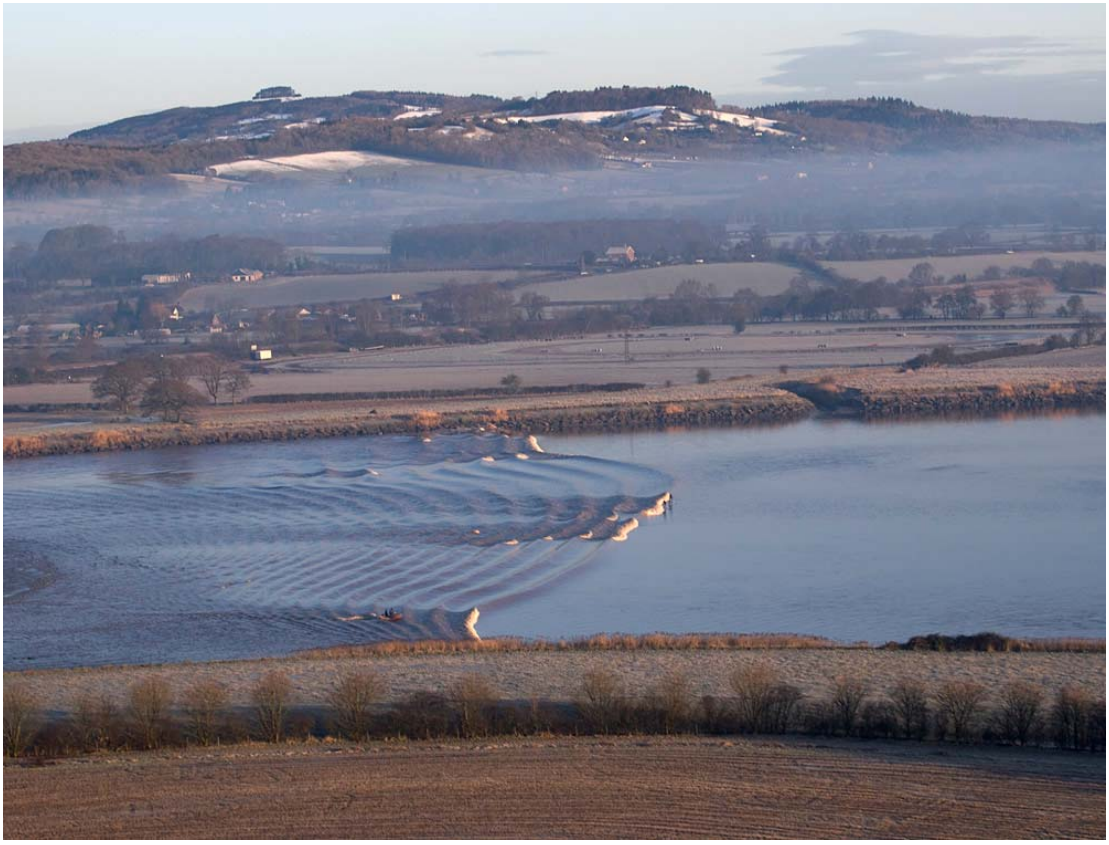

(A) Aerial photograph on 11 February 2099 at 09:15:45 (Courtesy of Mark HUMPAGE) - Note the various shape of the bore across the river: breaking near the banks and above sand banks, and undular in deeper waters

(B) Tidal bore in the Kent River estuary (UK) at Jenny Browns Point in Spring 2007 (Courtesy of Arnold

PRICE)

(C) Tidal bore of the Garonne River at Langoiran (France) on 1 October 2008 at sunset (18:48) - Shutter speed: 1/800 s

(D) Undular tidal bore the Dordogne River in front of Port de Saint Pardon (France) on 27 September 2008 at 15:50 - Bore front passing in front of the boat ramp - The two kayakers were riding the second wave and

Fabrice COLAS was surfing on the third wave - Shutter speed: 1/800 s

(E) Tidal bore in Turnagain Arm, Cook Inlet (Alaska) propagating from right to left (Courtesy of Walter TAPE)

Fig. 1-1 - Photographs of tidal bores

1.2 Discussion

The impact of tidal bores on hydraulic structures (e.g. bridges, gates) was rarely discussed but a few studies. ZHU and CHENG (2008) studied the impact of the Qiantang River tidal bore on the Caoe River Dam that is a series of sluices built on the right bank of the Qiantang River estuary, at the mouth of the Caoe River. Also in China, several physical and numerical studies were conducted on the Qiantang River bore impact on the Hangzhou Bay bridge opened in 2008. The bridge is a 35.6 km long, S-shaped cable-stayed structure with six traffic lanes in both directions, linking Cixi county in the South to Jiaxing in the North.

The most common type of tidal bore impact on man-made structures is the tidal bore passage beneath the bridge structures across tidal bore affected estuaries. For example, along the Garonne, Dordogne, Severn Rivers. One most illustrious bridge is the Pont Aubaud across the Sélune River at the town of Pontaubault in France. The Pont Aubaud is a 15th century stone bridge that was used by the troops of General Patton during the "breakthrough of Avranches" on 31 July 1944 nearly 65 years ago (Fig. 1-2). In 1944, the Pont Aubaud was the only available bridge across the Sélune river and 7 divisions of Patton's army crossed it in 72 hours! A commemorative engraving summarised the bridge historical heritage:

"*Pont Aubaud - Road to Freedom*

15th century: construction of the bridge

1793: Battle between the "Chouans" and the "Bleus" ([1])

31-7-1944: Battle between German and American soldiers

Crossing in 72 hours of 7 divisions of Patton's army for the liberation of France

'The issue of the war depended upon one bridge' (by P. CARELL)"

Fig. 1-3 illustrates the propagation of a small undular tidal bore beneath the Pont Aubaud on the Sélune River (France). Figure 1-3A shows the incoming tidal bore while Figure 1-3B highlights the chaotic wave motion between the piers shortly after the passage of the bore. Note the bridge piers shaped to cut the tidal bore flow (Fig. 1-2). The bridge structure has sustained the tidal bores for a number of centuries and it demonstrates the sound design.

Further photographs of tidal propagation beneath bridge structures are presented in Appendix E.

(A) Old postcard of the Pont Aubaud in the 1900s - View from the left bank

[1] During the French Revolution, battle between the partisans of the King ("Chouans") and the republican armies ("Bleus").

(B) At low tide on 31 Aug. 2008 evening, view from downstream - Note the siltation of the bridge piers on the right bank

Fig. 1-2 - Pont Aubault across the Sélune River at Pontaubault (France)

(A) Note the kayaker riding the first wave of the undular tidal bore just before the bridge

(B) Looking upstream at the turbulence between bridge piers 43 s late with the bore front in the background

Fig. 1-3 - Propagation of the Sélune River tidal bore beneath the Pont Aubault, Pontaubault (France) on 1 September 2008 at 09:04 - View from the left bank looking upstream

1.3 Structure of the report

The present study examines in details the turbulence and turbulent mixing generated by the passage of an undular tidal bore in a short channel constriction, such as a set of bridge piers, for a range of flow conditions. The experimental facility and instrumentation are described in section 2. The basic flow patterns are presented in section 3. The free-surface measurements are discussed in section 4. The turbulent velocity measurements are shown and developed in section 5.

The technical report is supported by a digital appendix (Appendix B) containing 5 movies available at the University of Queensland institutional open access repository UQeSpace {http://espace.library.uq.edu.au/}. Several appendices are further presented with relevant photographs, experimental data and technical details.

2. Experimental facility and methods

2.1 Experimental facilities

Some new experiments were performed in the large tilting flume at the University of Queensland previously used by KOCH and CHANSON (2005,2008,2009) and CHANSON (2008) (Table 2-1). The channel was 0.5 m wide 12 m long, and its slope was set horizontal for all experiments. The flume was made of smooth PVC bed and glass walls, and the waters were supplied by a constant head tank. A radial gate was located at the channel downstream end (x = 11.9 m) while a fast-closing tainter gate was located next to and just upstream of the radial gate at x = 11.15 m (Fig. 2-1). The radial gate was used to create a range of subcritical flow conditions in the initially steady flow; its position and opening were fixed (unchanged) during a whole experiment. The tainter gate was a fast-closing gate used to generate the tidal bore.

The water discharge was measured with two orifice meters that were designed based upon the British Standards (British Standard 1943). The percentage of error was expected to be less than 2%. In steady flows, the water depths were measured using rail mounted pointer gauges and acoustic displacement meters. The unsteady water depths were measured with a series of acoustic displacement meters. A Microsonic™ Mic+35/IU/TC unit was located at x = 10.8 m immediately upstream of the tainter gate and a further 6 acoustic displacement meters Microsonic™ Mic+25/IU/TC were spaced along the channel between x = 8 m and 3 m, where x is the longitudinal distance from the channel upstream end. Further informations on the sensor characteristics are reported in Table 2-2.

The turbulent velocity measurements were conducted with an acoustic Doppler velocimeter Nortek™ Vectrino+ (Serial No. VNO 0436) equipped with a three-dimensional side-looking head. For the experiments, the velocity range was 1.0 m/s or 0.3 m/s depending upon the initially-steady flow conditions. The sampling rate was 200 Hz and the data accuracy was 1%. The ADV was set up with a transmit length of 0.3 mm and a sampling volume of 6 mm diameter and 1.5 mm height. Both the acoustic displacement meters and acoustic Doppler velocimeter were synchronised within +/- 1 ms, and they were sampled simultaneously at 200 Hz using a high-speed data acquisition system NI DAQCard-6024E (maximum sampling rate: 200 kHz). For all experiments, the ADV unit was located between x = 4 m, 4.55 m and 5 m.

The translation of the ADV probe in the vertical direction was controlled by a fine adjustment travelling mechanism connected to a Mitutoyo™ digimatic scale unit. The error on the vertical position of the probe was $\Delta z < 0.025$ mm. The accuracy on the longitudinal position was estimated as $\Delta x < +/- 2$ mm. The accuracy on the transverse position of the probe was less than 1 mm, and all the measurements were taken on the channel centreline.

Some additional information was obtained with a digital camera Panasonic™ Lumix DMC-FZ20GN (shutter: 1/2,000 to 8 s). Several photographs of the experimental facility and of the experiments are presented in Appendix A. Some movies of the experiments are available in the form of a digital appendix (Appendix B).

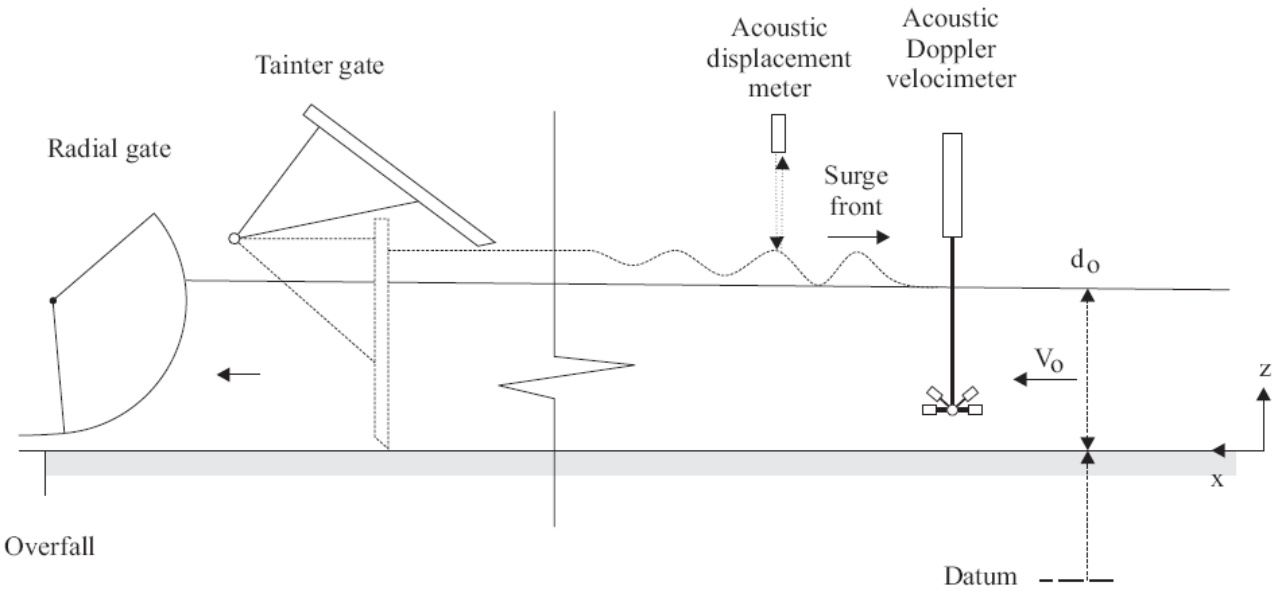

Fig. 2-1 - Sketch of the experimental facility

Table 2-1- Experimental flow conditions

Reference	S_o	Q	d_o	Gate opening h	Surge type at x = 5 m	U	Fr	Remarks
		m^3/s	m	m		m/s		
(1)	(2)	(3)	(4)	(5)	(6)	(7)	(8)	(9)
HORNUNG et al. (1995)	0	0	--	N/A	Undular to breaking (+)	--	1.5 to 6	Smooth bed. L = 24 m.
KOCH and CHANSON (2005)	0	0.040	0.079	0.010 to 0.092	Undular to breaking	0.14 to 0.68	1.31 to 1.93	Smooth PVC bed. L = 12 m, B = 0.5 m.
CHANSON (2008a)								
Series 1A	0	0.058	0.137	0.010 to 0.110	Undular to breaking	0.56 to 0.90	1.17 to 1.49	Smooth PVC bed. L = 12 m, B = 0.5 m.
Series 1B	0	0.058	0.142 (*)	0.010 to 0.105	Undular to breaking	0.50 to 0.89	1.13 to 1.47	Rough screens (k = 8 mm). L = 12 m, B = 0.5 m.
Series 2A	0.0145	0.058	0.070	0.091	Decelerating & breaking	0.03	2.02	Smooth PVC bed. L = 12 m, B = 0.5 m.
Series 2B	0.009 to 0.027	0.035 to 0.06	0.040 to 0.072	0.015 to 0.100	Decelerating: undular to breaking	0.002 to 0.22	1.71 to 2.83	Smooth PVC bed. L = 12 m, B = 0.5 m.
Present study								Smooth PVC bed. L = 12 m, B = 0.5 m.
Series 1	0	0.0089 to 0.0511	0.056 to 0.212	0 to 0.07	Undular to breaking	0.67 to 1.37	1.04 to 1.95	Free-surface measurements. Runs 090122_01 to 090423_803
Series 2a	0	0.0190	0.115	0	Undular	1.05	1.16	Turbulence measurements. Runs 090424_901-906
Series 2b	0	0.0190	0.165 to 0.170	0	Undular	1.20 to 1.21	1.10 to 1.13	Turbulence measurements. Runs 090427_911-927.
Series 2c	0	0.0188	0.199	0	Undular	1.32	1.08	Turbulence measurements. Runs 090429_930-939.

Notes: d_o: initial depth measured at x = 5 m in absence of constriction or x = 3.6 m with channel constriction;

Fr: surge Froude number ($Fr = (V_o + U)/\sqrt{g \times d_o}$); h: tainter gate opening after closure; Q: initial steady flow rate; U: surge front celerity measured at x = 5 m in absence of constriction or x = 3.6 m with channel constriction; (*) above rough screens.

Table 2-2 - Characteristics of the ultrasonic acoustic displacement meters (Ref. Microsonic™ {http://www.microsonic.de})

Characteristic (1)	Microsonic™ Mic+25/IU/TC (2)	Microsonic™ Mic+35/IU/TC (3)	Units (4)
Accuracy	0.18	0.18	mm
Response time	50	70	ms
Ultrasonic frequency	320	400	kHz
Wave length (at 20 C)	1.1	0.9	mm
Detection zone radius at operating range	22	37.5	mm
Blind zone	30	60	mm
Operating range	250	350	mm
Maximum range	350	600	mm

Channel constriction

For some experiments, two half-channel constrictions were introduced between x = 4.88 m and 4.21 m (Fig. 2-2). Both sides were identical, made of mortar and painted. The convergent and divergent shapes were sloped at 1:1 roughly. The channel constriction model was designed as a scale model (~ 1:20) of the Pont Aubault bridge piers across the Sélune River in the Baie du Mont Saint Michel (Fig. 1-2 & 1-3).

During the experiments, in steady flow conditions, the visual observations showed the presence of shock waves/cross-waves between the half-bridge piers when the upstream Froude number $Fr_o = V_o/\sqrt{g \times d_o}$ was larger than 0.2 (Fig. 2-2B). When the Froude number Fr_o of the initially steady flow was less than 0.2, only small ripples were seen in the channel constriction.

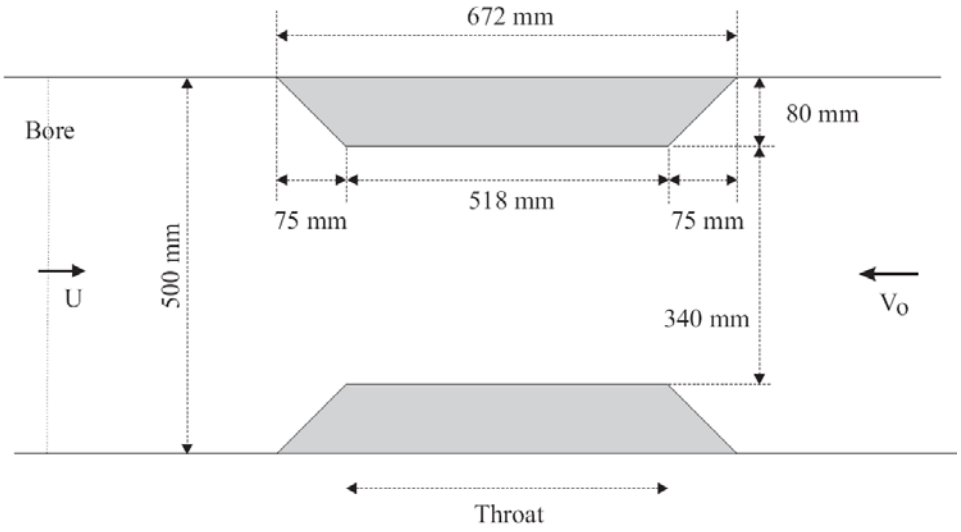

(A) Dimensioned sketch

(B) Shock waves between bridge pier model for Q = 0.0193 m^3/s, d_o = 0.117 m at x = 3.6 m, Fr_o = 0.31 - Steady flow from right to left

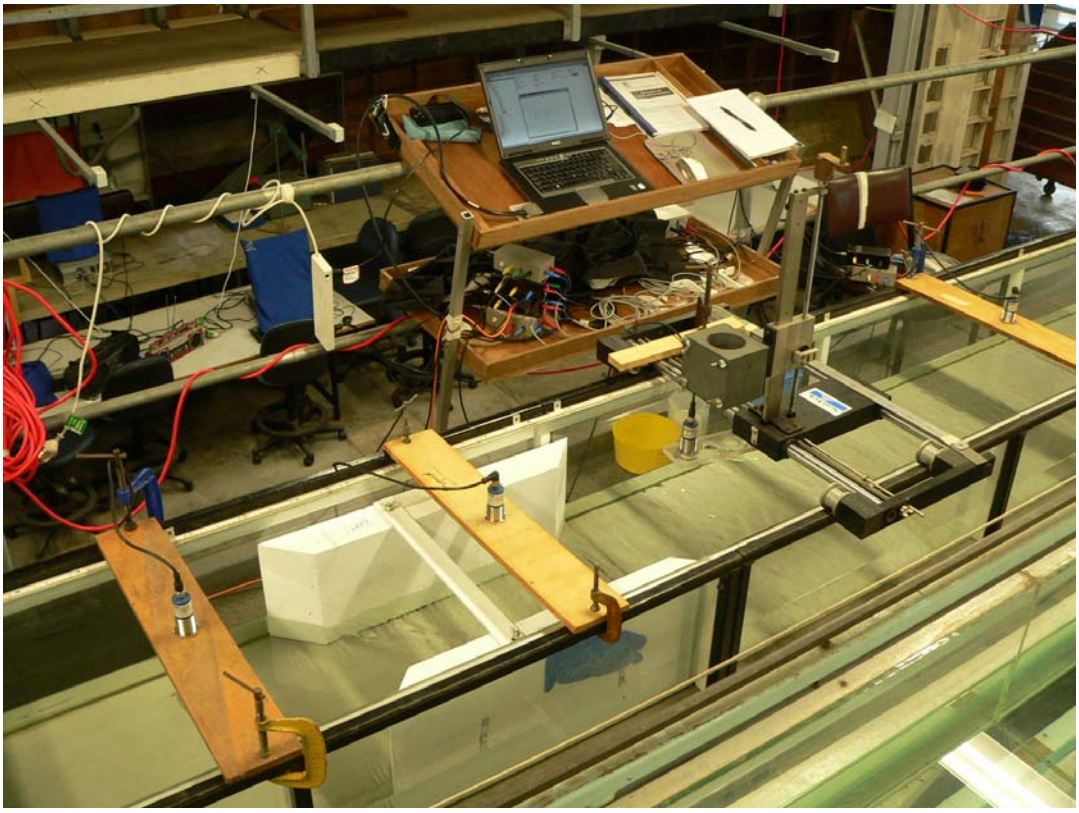

(C) General view of the experimental channel and constriction for Q = 0.00895 m^3/s, d_o = 0.0845 m at x = 3.6 m, Fr_o = 0.23 - Steady flow from left to right

Fig. 2-2 - Channel constriction installation in the rectangular channel

2.2 Inflow conditions

The initial flow conditions were partially developed at x = 4 to 5 m. This was tested at x = 5 m in absence of constriction and at x = 4 m in presence of the constriction. Figure 2-3 illustrates some vertical distributions of longitudinal velocity V_x and standard deviations of the longitudinal, vertical and transverse velocity components v_x', v_z' and v_y'. For the data set, the relative boundary layer thickness was about δ/d_o = 0.3 to 0.4. The results were consistent with the earlier studies of KOCH and CHANSON (2005,2008,2009) and CHANSON (2008a) in the same channel facility.

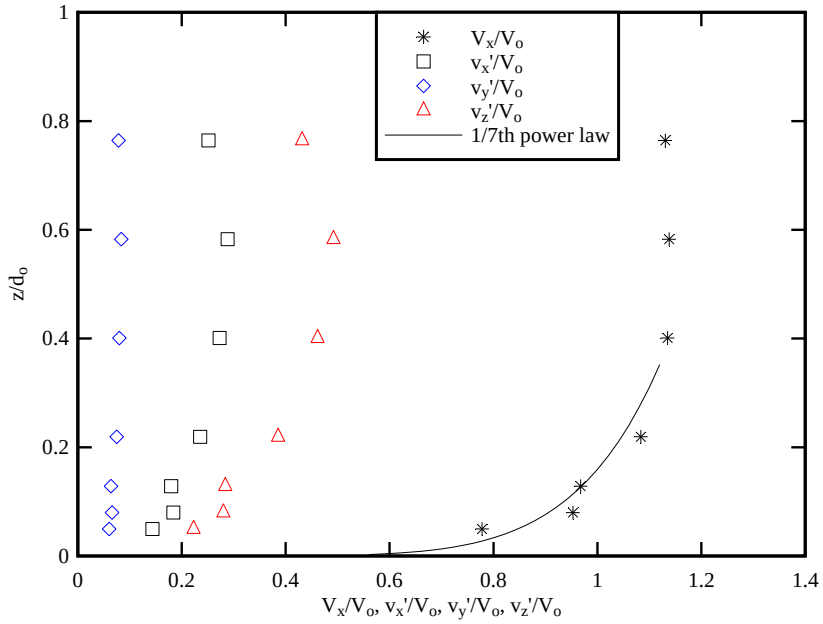

Fig. 2-3 - Dimensionless velocity profiles in the initially steady flow at x = 4.0 m - Run 090427_911a, Q = 0.0190 m^3/s, d_o = 0.1703 m at x=3.6 m, V_o = 0.223 m/s, Fr_o = 0.17

2.3 Tidal bore generation

The new experiments were conducted for a range of flow conditions summarised in Table 2-1. The experimental setup was selected to generate an initially steady, subcritical flow for a given initial flow rate Q. The opening of the downstream radial gate located at x = 11.9 m was set to control the initial steady flow depth (Fig. 2-4), and the opening was kept constant during each tidal bore experiment. The steady gradually-varied flow conditions were established for at least 15 minutes prior to the measurements and the data acquisition was started about 30 s minutes prior to the tainter gate closure.

The tidal bore was generated by the rapid (partial or complete) closure of the downstream tainter gate located at x = 11.15 m (Fig. 2-4). The gate was identical to that used by KOCH and CHANSON (2005,2008,2009) and CHANSON (2008a), and the gate closure time was less than 0.2 s. Some photographs of the bore formation immediately after the tainter gate closure are presented in Appendix A. After closure, the bore propagated upstream and each experiment was stopped when the bore front reached the intake structure to avoid any wave reflection interference.

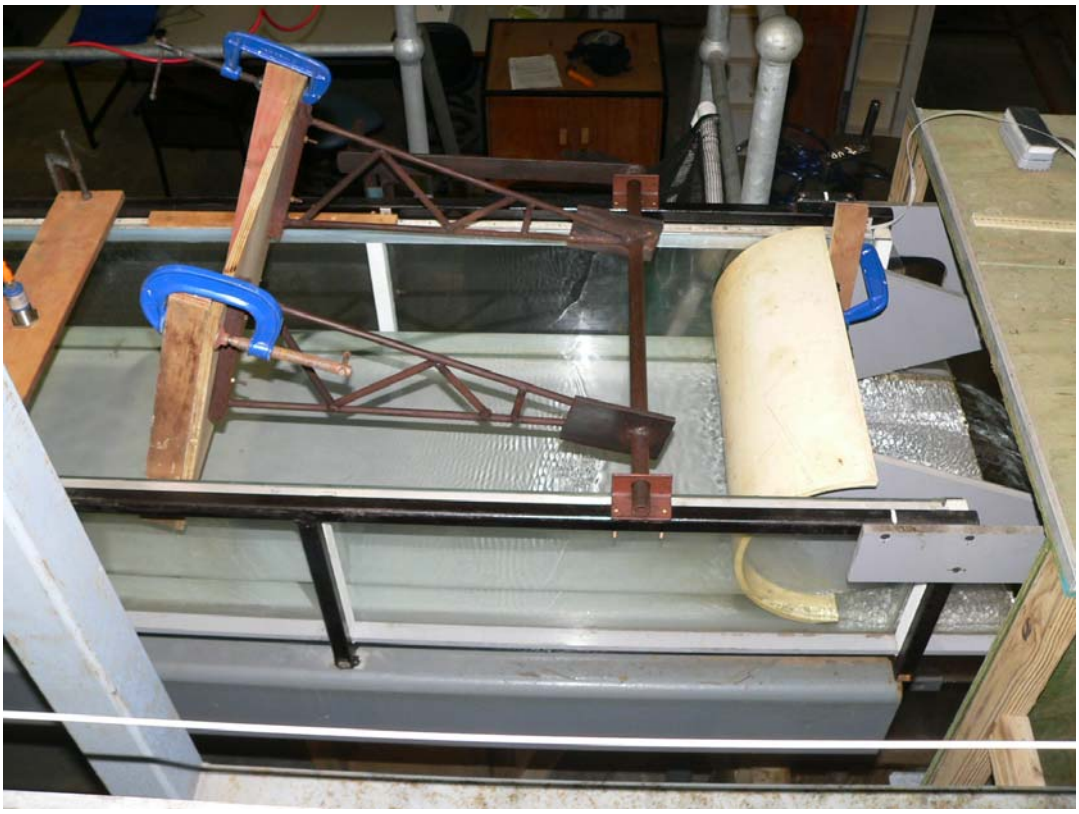

Fig. 2-4 - Photograph of tainter gate (fully-opened) and radial gate (right) - Initially steady flow (Q = 0.00895 m^3/s) from left to right

The acoustic displacement meters were located on the channel centreline at x = 10.8 m, 8.0 m, 6.0 m, 5.0 m, 4.55 m, 4.0 m, and 3.0 m. In addition, there was always a sensor sampling the free-surface elevation immediately above the ADV sampling volume when the ADV measurements were performed.

2.4 ADV signal processing and analysis

The acoustic Doppler velocimetry (ADV) measurements are performed by measuring the velocity of particles in a remote sampling volume based upon the Doppler shift effect (e.g. VOULGARIS and TROWBRIDGE 1998, McLELLAND and NICHOLAS 2000, CHANSON 2008b). An ADV system records simultaneously four values with each component of a sample: the velocity component, the signal strength value, the correlation value and the signal-to-noise ratio. Past and present experiences demonstrated many problems because the signal outputs combine the effects of velocity fluctuations, Doppler noise, signal aliasing, turbulent shear and other disturbances.

For all experiments, the present experience demonstrated some recurrent problems with the velocity data, including low correlations and low signal to noise ratios when the waters were not seeded. The situation improved drastically by a combination of measures, including the stirring of dirts in the intake chamber and the injection of kaolin powder in the intake chamber prior to each run.

In steady flows, the signal processing removed all the samples with communication errors, average correlation below 60% or signal-to-noise ratio (SNR) below 5 dB. Further the data were "despiked" using a

phase-space thresholding technique (GORING and NIKORA 2002, WAHL 2003, CHANSON et al. 2008) ([2]). The signal checks indicated that the streamwise and transverse velocity data were little affected by the presence of the channel bed, but the vertical velocity data were adversely affected by the presence of the PVC bed for $z < 0.030$ m (CHANSON 2008a,2008b).

While several ADV post-processing techniques were devised for steady flows, these post-processing techniques are not applicable to unsteady flows. In the present study, unsteady flow post-processing was limited to a removal of communication errors, and it is acknowledged that the V_z vertical velocity component data may be adversely affected.

[2] The signal processing was performed with WinADV 2.025.

3. Experimental observations

3.1 Basic flow patterns

The visual observations and free-surface measurements were conducted for a range of flow conditions with an initially-steady subcritical flow. A number of photographs of the experiments are presented in Appendix A. Some movies of the experiments are available in the form of a digital appendix (Appendix B). Some experimental data are presented in the Appendices E and F. Table 3-1 summarises the experimental flow conditions.

Several flow patterns were observed depending upon the tidal bore Froude number defined as:

$$Fr = \frac{V_o + U}{\sqrt{g \times d_o}} \quad (3\text{-}1)$$

where d_o is the initial flow depth, V_o is the initial flow velocity positive downstream, g is the gravity acceleration and U is the surge front celerity for an observer standing on the bank, positive upstream. The tidal bore was undular for a Froude number less than 1.5 to 1.6 and a breaking bore for larger bore Froude numbers. Table 3-2 summarises the findings.

For Fr < 1.5 to 1.6, the tidal bore propagated upstream relatively slowly and the front was followed a train of well-formed, quasi-periodic undulations: i.e., an undular tidal bore. The undular bore had a smooth, quasi-two-dimensional profile for Fr < 1.25 (Fig. 3-1). For 1.25 < Fr, some slight cross-waves (shock waves) were observed, starting next to the sidewalls upstream of the first wave crest and intersecting next to the first crest. A similar cross-wave pattern was observed in stationary undular hydraulic jumps and in undular tidal bores (CHANSON and MONTES 1995, MONTES and CHANSON 1998, BEN MEFTAH et al. 2007, CHANSON and KOCH 2008). For 1.3 < Fr < 1.5 to 1.6, some slight wave breaking was observed at the bore front (i.e. the first wave crest), and the ensuing free-surface undulations were flatter. The cross-waves were also observed. The findings are detailed in Table 3-2 where they are compared to a number of earlier studies. Table 3-2 shows a close agreement between all the studies.

At the largest bore Froude numbers (i.e. Fr > 1.5 to 1.6), a breaking bore was observed. The surge front propagated relatively rapidly, and the free-surface appeared to be quasi-two-dimensional with a marked roller. Some air entrainment and intense mixing was observed in the bore roller.

For the entire range of investigations, the basic flow patterns were consistent with the earlier findings of FAVRE (1935), BENET and CUNGE (1971), TRESKE (1994), KOCH and CHANSON (2008,2009) and CHANSON (2008a). Note that the flow patterns were basically independent of the initial steady flow Froude number $Fr_o = V_o / \sqrt{g \times d_o}$, while an earlier study showed that these were also independent of the bed roughness (CHANSON 2008a).

Fig. 3-1 - Gentle undular bore (Fr = 1.15, no cross-wave) propagating from left to right - Run 090305_22, Q = 0.019 m^3/s, d_o = 0.1015 mm (at x = 4.8 m), Fr = 1.15, U = 0.781 m/s, Shutter speed: 1/40 s

Table 3-1- Experimental observations of tidal bores in a horizontal, rectangular, prismatic channel

Reference	d_o m	Fr_o	Surge type at x = 5 m	Fr	Remarks
(1)	(3)	(3)	(4)	(6)	(7)
HORNUNG et al. (1995)	--	0	Undular to breaking ($^+$)	1.5 to 6	Smooth bed. L = 24 m.
KOCH and CHANSON (2008,2009)	0.079	1.15	Undular to breaking	1.31 to 1.93	Smooth PVC bed. L = 12 m, B = 0.5 m.
CHANSON (2008a)					
Series 1A	0.137	0.71 to 0.73	Undular to breaking	1.17 to 1.49	Smooth PVC bed. L = 12 m, B = 0.5 m.
Series 1B	0.142 (*)	0.70	Undular to breaking	1.13 to 1.47	Rough screens (k = 8 mm). L = 12 m, B = 0.5 m.
Present study					Smooth bed. L = 12 m, B = 0.5 m.
Series 1	0.056 to 0.212	0.12 to 1.05	Undular to breaking	1.04 to 1.95	Free-surface measurements
Section 2	0.115 to 0.199	0.14 to 0.31	Undular	1.08 to 1.16	Turbulence measurements.

Notes: d_o: initial depth measured at x = 5 m in absence of constriction or x = 3.6 m with channel constriction; Fr_o: initial flow Froude number ($Fr = V_o / \sqrt{g \times d_o}$); Fr: surge Froude number ($Fr = (V_o + U) / \sqrt{g \times d_o}$); (*): measured above rough screens.

Table 3-2- Tidal bore flow patterns in a horizontal, rectangular channel: experimental observations

Reference	Q m^3/s	d_o m	Undular bore			Breaking bore	Remarks
			Two-dimensional	With cross-waves	With breaking & cross-waves		
(1)	(2)	(3)	(4)	(5)	(6)	(7)	(8)
HORNUNG et al. (1995)	0	--	Fr < 1.6	--	1.6 < Fr < 1.9	1.9 < Fr	Smooth bed
KOCH and CHANSON (2005)	0.040	0.079	--	Fr < 1.4 to 1.5	1.5 < Fr < 1.7	1.7 < Fr	Smooth PVC bed. B = 0.5 m.
CHANSON (2008a)							
Series 1A	0.058	0.137	Fr < 1.2	1.2 < Fr < 1.3	1.3 < Fr < 1.45	1.45 < Fr	Smooth PVC bed. B = 0.5 m.
Series 1B	0.058	0.142	Fr < 1.2	1.2 < Fr < 1.3	1.3 < Fr < 1.5	1.5 < Fr	Rough screens. B = 0.5 m.
Present study Series 1 & 2	0.0089 to 0.0511	0.056 to 0.212	Fr < 1.25	1.25 < Fr < 1.3	1.3 < Fr < 1.5 to 1.6	1.5 to 1.6 < Fr	Smooth PVC bed. B = 0.5 m.

Notes: d_o: initial depth measured at x = 5 m; Fr: surge Froude number; (--): data not available.

3.2 Effects of channel constriction

The effects of the channel constriction were documented for a range of flow conditions. These corresponded to an initially steady subcritical flow ($0.12 \leq Fr_o \leq 0.31$) with a focus on the upstream propagation of undular tidal bores travelling against the flow ($1.04 \leq Fr \leq 1.31$). A number of photographic illustrations are reported in Appendix A.

The visual observations showed that the entrance of the bore into the constriction convergent was associated with some reflection propagating back towards the channel downstream end, together with the development of a turbulent free-surface motion in the throat. As the tidal bore progressed into the constriction throat, the free-surface exhibited some strongly three-dimensional pattern. When the bore exited the constriction, it tended to regain its quasi-two-dimensional appearance about 0.75 to 1.5 m after the constriction divergent. Figure 3-2 illustrates the propagation of an undular bore (Fr = 1.23) in the channel constriction, looking upstream. Each photograph was taken 0.5 s apart. It is presently unknown why the undular bore regained so rapidly its two-dimensional profile. This might be linked with the properties of positive surges and tidal bores to absorb any random disturbances that may exist at the free-surface in front of and behind the bore front (HENDERSON 1966, CHANSON 2004). It is also a well-known observation in the field.

The shock reflection on the constriction convergent was associated with the development of surface scars that illustrated the existence of some large turbulent structures. Figure 3-3 shows some surface scar development as the bore front advanced in the throat. The bore propagation through the constriction was further linked with some free-surface turbulence and pseudo-chaotic surface motion in the throat. These were possibly best observed using the light glare and reflection at the free-surface. Some surface turbulence was

observed also next to the exit/divergent ([3]) in the wake of the sidewall expansions (Fig. 3-4). Figure 3-4 illustrates the turbulent vortices delimited by the surface scars as the undular bore front (first wave crest) exited the constriction.

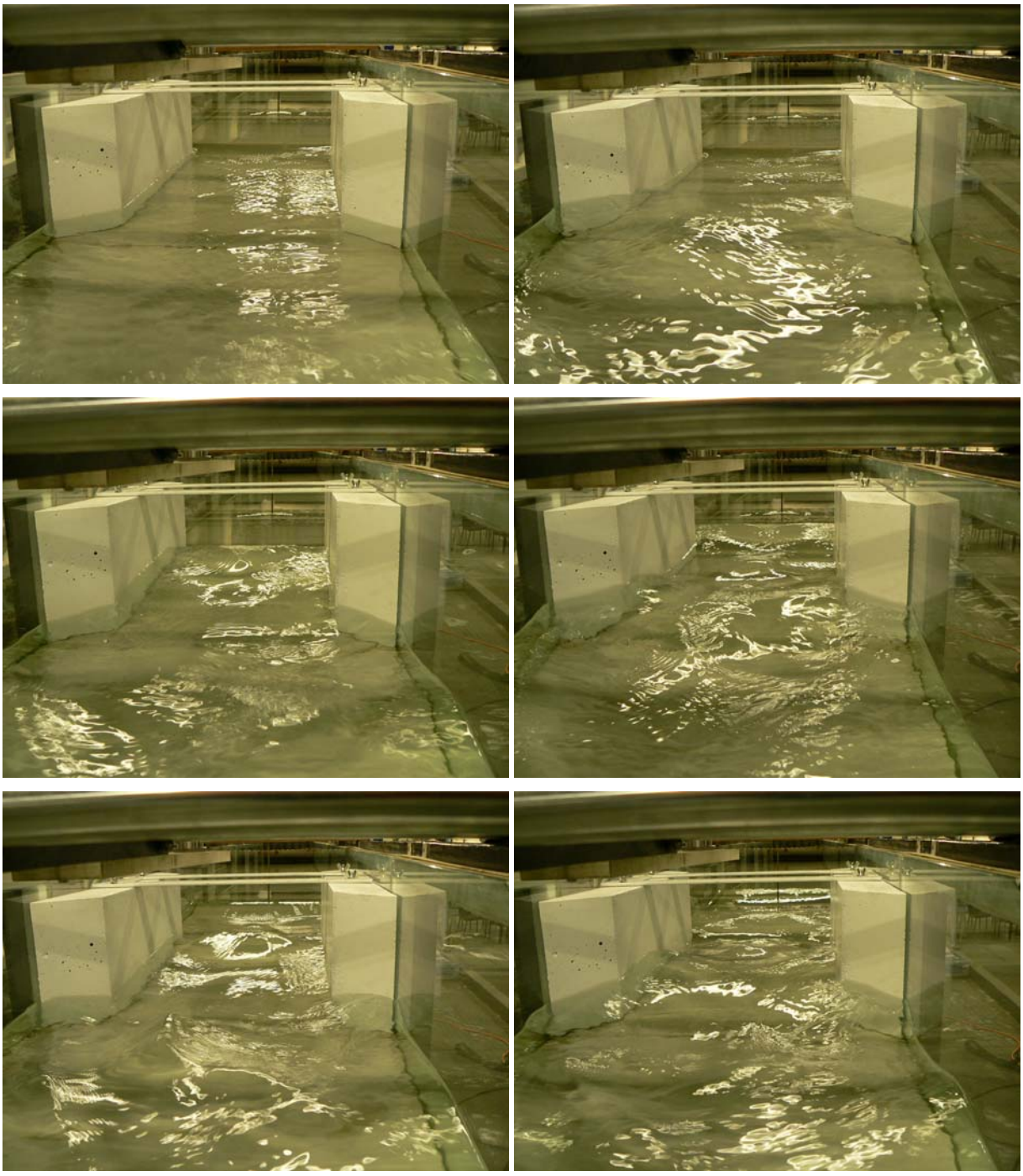

Fig. 3-2 - Undular tidal bore propagation in the constriction, looking upstream - Note the free-surface turbulence in the foreground caused by some reflection as well as the three-dimensional nature of the flow in the throat - From left to right, top to bottom: $t = t_o$, t_o+0.5 s, t_o+1 s, t_o+1.5 s, t_o+2 s, t_o+2.5 s, Shutter speed: 1/40 s - Run 090324_00, $Q = 0.0097$ m^3/s, $d_o = 0.0882$ mm (at $x = 3.6$ m), $Fr = 1.23$, $U = 0.885$ m/s

[3] That is, the upstream end of the channel constriction.

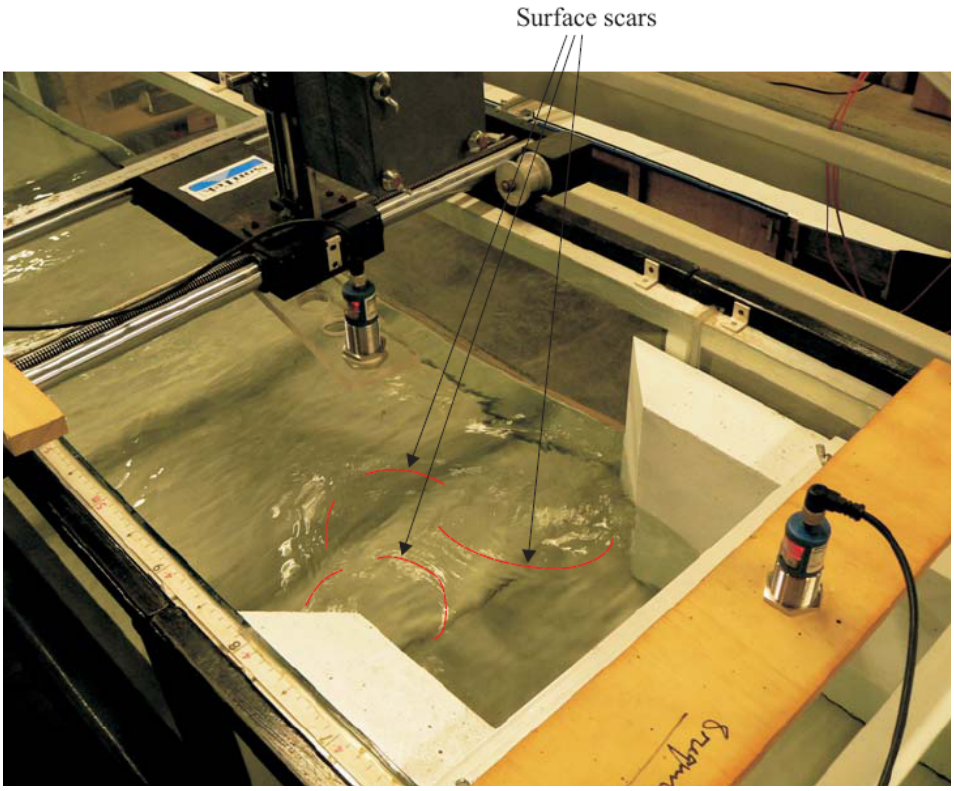

Fig. 3-3 - Undular tidal bore, looking at the first wave crest entering the constriction - Note the free-surface turbulence and scars next to the throat convergent - Shutter speed: 1/50 s - Run 090415_61, Q = 0.0089 m^3/s, d_o = 0.0845 mm (at x = 3.6 m), Fr = 1.16, U = 0.85 m/s

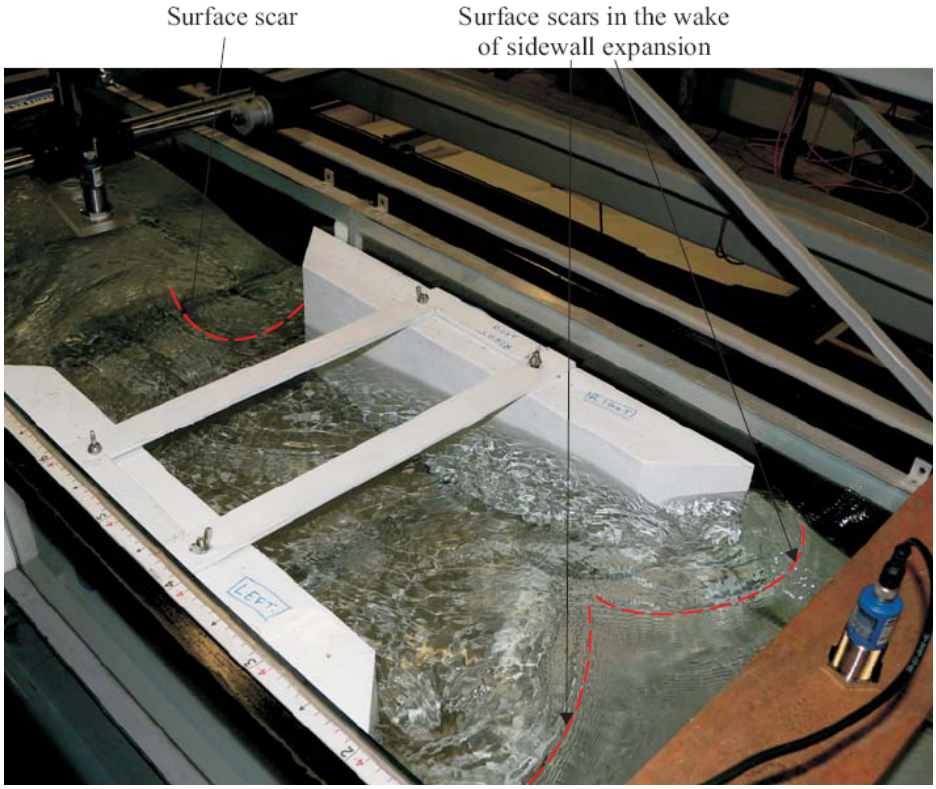

Fig. 3-4 - First wave crest of the undular bore (Fr = 1.15) exiting the channel constriction - Note the complicated turbulent pattern upstream of the channel constriction (right) as well as the surface scars in the throat and in the constriction divergent - Bore propagation from top left to bottom right, Shutter speed: 1/80 s - Run 090318_00, Q = 0.0232 m^3/s, d_o = 0.1552 mm (at x = 3.6 m), Fr = 1.15, U = 1.10 m/s

Altogether the propagation of the bore through the short channel constriction was associated with the development of large scale free-surface turbulence and some turbulent dissipation, while the tidal bore regained its quasi-two-dimensional flow pattern further upstream.

It is acknowledged that the sidewalls might adversely impact the development of large-scale structures in the present study. Herein the sidewalls acted as some planes of symmetry but would prevent the development large coherent structures reflected at the downstream end of a whole bridge pier. A study of such structures would require a wider channel with a complete pier on the flume centreline.

4. Free-surface properties of undular tidal bores

4.1 Presentation

In a tidal bore and hydraulic jump, the equation of conservation of momentum is applied across the jump front together with the equation of conservation of mass. When the rate of energy dissipation is negligible as in an undular tidal bore, there is a quasi-conservation of energy. Let us follow the tidal bore in the system of coordinates in translation with the undular bore front. The equations of conservation of momentum and energy may be rewritten as:

$$\frac{M}{d_c^2} = \frac{d_c}{d} + \frac{1}{2} \times \left(\frac{d}{d_c} \right)^2 = \text{cons tan t} \quad (4\text{-}1)$$

$$\frac{E}{d_c} = \frac{d}{d_c} + \frac{1}{2} \times \left(\frac{d_c}{d} \right)^2 = \text{cons tan t} \quad (4\text{-}2)$$

where M is the momentum function, E is similar to the energy per unit mass, also called the specific energy ([1]), d is the flow depth, and d_c is the critical flow depth. For a hydraulic jump in translation including a tidal bore, d_c equals:

$$d_c = \sqrt[3]{\frac{((V_o + U) \times d_o)^2}{g}} \quad (4\text{-}3)$$

where V_o is the initial flow velocity positive downstream, d_o is the initial flow depth, U is the tidal bore celerity positive upstream and g is the gravity acceleration (g = 9.80 m/s^2).

In tidal bores and hydraulic jumps, Equation (4-1) is always valid but Equation (4-2) is an approximation only applicable to small Froude numbers close to unity: e.g., an undular tidal bore. For an undular bore, Equations (4-1) and (4-2) may be considered as a parametric representation of the relationship between the dimensionless momentum M/d_c^2 and energy E/d_c (BENJAMIN and LIGHTHILL 1954, MONTES 1986). It is plotted in Figure 4-1. The function M-E has two branches intersecting at $M/d_c^2 = 1.5$ and $E/d_c = 1.5$ which corresponds to the minimum values that both functions could have in a fully-developed bore and jump with hydrostatic pressure distributions. The intersecting point relates to the critical flow conditions ($d = d_c$). The right branch of the curve M-E corresponds to the supercritical flow while the upper branch (or left branch) corresponds to a subcritical flow (Fig. 4-1). The domain of variation of the dimensionless momentum and energy is bounded by the two branches. The two lines represent the only possible relationship between M/d_c^2 and E/d_c in a tidal bore and hydraulic jump with horizontal streamlines ([2]) as long as both Equations (4-1) and (4-2) hold. The regions outside of the branches are not possible. Note that, in an undular bore, the pressure field is not hydrostatic. This limitation is discussed below.

---

[1] The M- and E-functions are commonly used in open channel hydraulics since BAKHMETEFF (1932), although the M-function was sometimes called "specific force", "specific momentum" or "force-plus-momentum" (JAEGER 1956, CHOW 1959, MONTES 1998). Their application to water waves is more recent (SERRE 1953, BENJAMIN and LIGHTHILL 1954, MONTES 1986).

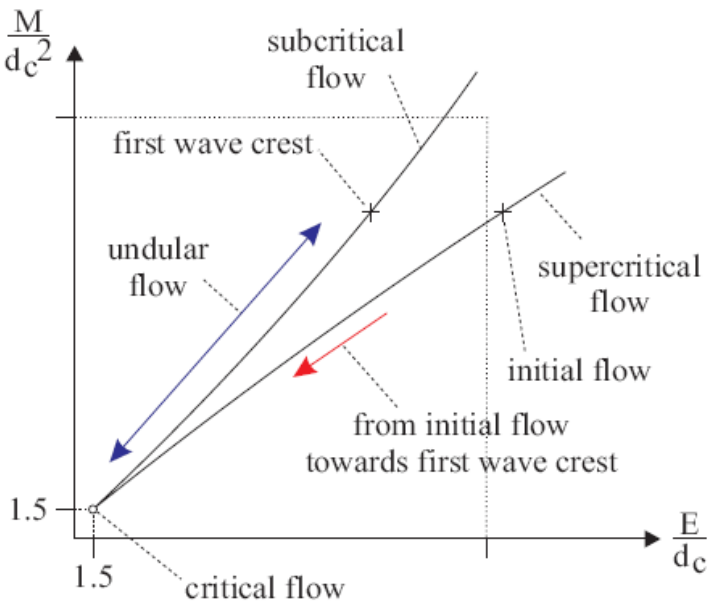

Fig. 4-1 - Definition sketch of the dimensionless relationship between the momentum and energy fluxes in undular bores and jumps with hydrostatic pressure distributions

Figure 4-2 shows some experimental results for two undular tidal bore flow conditions. The data include the initial flow conditions (symbol *) and the undular flow data between the first and fourth wave crests. The data justify the approximation of negligible energy losses (Eq. (4-2)): all data samples are located on the parameteric curve M-E. Further the quasi-totality of the undular flow data are on the subcritical flow branch of the M-E curve. Note a seemingly greater momentum function and specific energy at the first wave crest than in the initial flow. This is because Equations (4-1) and (4-2) are based upon the assumption of hydrostatic pressure distribution; but the free-surface curvature at the wave crest implies a pressure gradient less than hydrostatic, hence a smaller specific energy for example. Figure 4-1 represented the ideal case when there is conservation of momentum function and some slight energy dissipation across the bore front. In an undular tidal bore, the dissipation mechanisms are complicated with contributions by (a) some energy radiated into a train of quasi-periodic waves behind the bore front, (b) boundary friction at the bed and sides of the channel, (c) flow recirculation and separation regions, and (d) turbulent dissipation at the surface with some breaking at the first wave crest.

Considering the undular bore in the system of co-ordinates in translation with the bore front, the flow is quasi-steady and the free-surface profile is stationary. For an incompressible fluid, the equation of conservation of mass is:

$$\frac{\partial V_x}{\partial x} + \frac{\partial V_z}{\partial x} = 0 \qquad (4\text{-}4)$$

Since the fluid is incompressible, the stream function ψ exists and the velocity components equal $V_x = -\partial\psi/\partial z$ and $V_z = \partial\psi/\partial x$ for a two-dimensional flow. The condition of irrotational flow motion is a Laplace

---

[2] Figure 4-1 presents a definition sketch assuming hydrostatic pressure distributions.

equation in terms of the stream function ψ: $\Delta\psi = 0$, and the boundary conditions are:

(a) $\psi(z=0) = 0$ at the channel bed,

(b) $\psi(z=d) = -(V_o+U)\times d_o$ at the water free-surface where $(V_o+U)\times d_o$ represents the water flow rate per unit width in the quasi-steady flow analogy system of co-ordinates, and

(c) the Bernoulli principle:

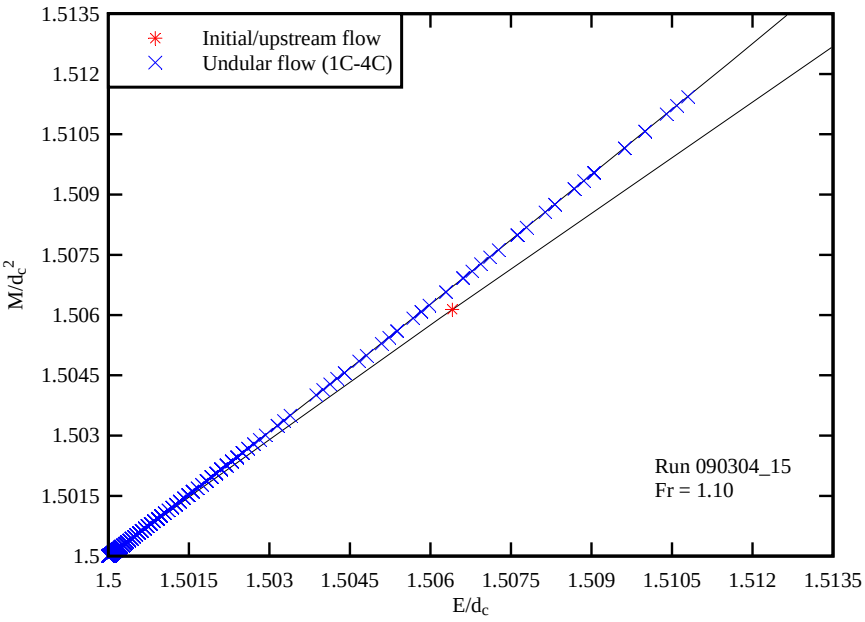

(A) Run 090304_15, Q = 0.0299 m^3/s, d_o = 0.2055 m, Fr = 1.10, U = 1.316 m/s, x = 5 m

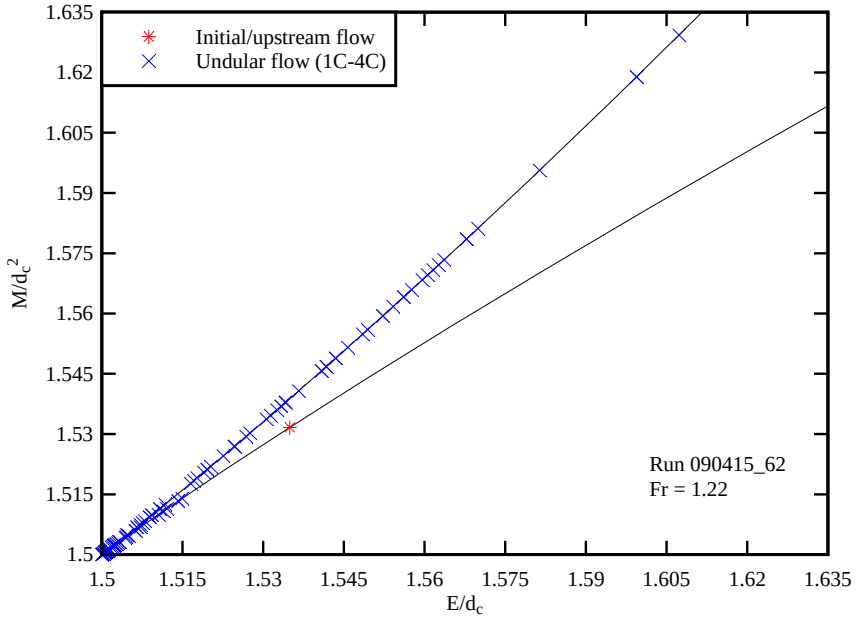

(B) Run 090415_62, Q = 0.0089 m^3/s, d_o = 0.0802 m, Fr = 1.22, U = 0.862 m/s, x = 5 m

Fig. 4-2 - Dimensionless relationship between the momentum and energy fluxes in undular tidal bores: comparison between Equations (3-T1) and (3-T2) and experimental data - Upstream flow conditions (symbol *) and undular flow data between the first and 4th wave crests

$$\frac{(V_x{}^2 + V_z{}^2)}{2} + g \times z + \frac{P}{\rho} = \text{cons tan t}$$

with z the vertical elevation (z = 0 at the bed), P the local pressure and ρ the fluid density. With the sign conventions that were selected, the flux $(V_o+U)\times d_o$ is positive for a tidal bore propagating upstream.

Using the continuity equation, the Navier-Stokes equation for an ideal fluid in the vertical z-direction yields:

$$V_x{}^2 \times \frac{\partial (V_z / V_x)}{\partial x} = -\frac{1}{\rho} \times \frac{\partial P}{\partial z} - g \times \cos\theta \tag{4-5}$$

where θ is the angle between the z-direction and the vertical. In the following, z is the vertical direction and cosθ = 1. When the streamline curvature is non negligible, the pressure gradient departs from the hydrostatic pressure gradient ($\partial P/\partial z = -\rho\times g$) and Equation (4-5) gives an expression for the pressure deviation caused by the free-surface curvature (MONTES 1998). Let us assume a linear vertical velocity distribution:

$$\frac{V_z}{V_z(z=d)} = \frac{z}{d} \tag{4-6}$$

with d the local flow depth. Since the free-surface is a streamline, the equation of conservation of mass implies that the vertical velocity component at the free-surface (z = d) equals:

$$\frac{V_z(z=d)}{V_x(z=d)} = \frac{\partial d}{\partial x} \tag{4-7}$$

After re-arranging, the variation of pressure with the surface curvature gives a differential equation in terms of the flow depth d and depth-averaged longitudinal velocity $\overline{V}$. For an ideal fluid in a horizontal channel, it yields:

$$\frac{\partial}{\partial x}\left(\overline{V}^2 \times d + \frac{1}{2} \times g \times d^2 + \frac{1}{3} \times \overline{V}^2 \times d \times \left(d \times \frac{\partial^2 d}{\partial x^2} - \left(\frac{\partial d}{\partial x}\right)^2\right)\right) = 0 \tag{4-8}$$

Note that a velocity correction coefficient was dropped in the uppermost left term for clarity. In the system of co-ordinates of the quasi-steady flow analogy, the integration of Equation (4-8) has a solution:

$$\left(\frac{\partial d}{\partial x}\right)^2 = 6 \times g \times \left(-M \times d - \frac{1}{3} \times d^3 + \frac{q}{g} - E \times d^2\right) = 0 \tag{4-9}$$

where M and E are respectively the momentum function and the specific energy. The M- and E-functions must be defined herein for the general case of a non hydrostatic pressure distribution and non-uniform velocity profile:

$$M = \int_0^d \left(\frac{P}{\rho \times g} + \frac{V_x{}^2}{2 \times g}\right) \times dz \tag{4-10}$$

$$E = \frac{1}{d} \times \int_0^d \left(z + \frac{P}{\rho \times g} + \frac{V_x{}^2 + V_z{}^2}{2 \times g}\right) \times dz \tag{4-11}$$

The periodic wave solution of Equation (4-9) is called a cnoidal wave function because it takes the form of the square of the Jacobian elliptic function cn. Some details of the cnoidal function are presented in Appendix D.

Free-surface profile of an undular tidal bore: experimental results

The undular tidal bore propagated upstream relatively slowly, and the bore consisted of first wave followed by a train of well-formed undulations (Fig. 4-3). The free-surface had a quasi-periodic shape. Figure 4-3 presents some typical water level data where the water depth at x = 5 m is plotted as a function of the time. The measurements illustrate the pseudo-periodic shape of the free-surface. In Figure 4-3, the data are compared with a sinusoidal curve and cnoidal wave function. Herein, each function was fitted for each half-wave length between a crest/trough and the adjacent trough/crest. Altogether there was a reasonable agreement between the data and the mathematical functions, although neither the linear wave theory nor the cnoidal wave equation captured the asymmetrical wave shape nor the fine details of the free-surface profile shape The undulation asymmetry was already noted in the stationary undular hydraulic jumps in terms of both the free-surface profile and the vertical distributions of pressure and velocity (DONNELLY and CHANSON 2005), and the asymmetry was also observed in undular tidal bores. The findings were consistent with a study of relatively large amplitude shallow water waves by LE MÉHAUTÉ et al. (1968) who concluded: "*none of the commonly used wave theories are in exceptional agreement with data*".

Noteworthy, the agreement between the free-surface data and cnoidal wave function was best achieved using the parameter of the elliptic function m > 0.5 between a wave crest and trough, while m < 0.5 between a wave trough and crest. For m = 0, the cnoidal wave function equals the sinusoidal profile and more generally the nonlinearity causes little departure from the linear wave theory for small values of m. As m increases, the crest becomes more peaky and the trough shallower. The present findings highlighted the asymmetry of the free-surface undulations of an undular tidal bore, with some differences in wave shape between a crest and the next trough, and between a trough and the next wave crest.

The flow properties immediately upstream and downstream of the tidal bore front must satisfy the continuity and momentum principles. The integral form of the equations of conservation of mass and momentum yields a dimensionless relationship between the flow properties in front of and behind the bore front called the Bélanger equation:

$$\frac{d_{conj}}{d_o} = \frac{1}{2}\left(\sqrt{1+8\times Fr^2}-1\right) \quad (4\text{-}12)$$

where d_{conj} is the conjugate flow depth, defined as the average water depth of the first wave length for an undular bore (Fig. 4-4). Experimental data are presented in Figure 4-5, where the ratio d_{conj}/d_o is plotted as a function of the tidal bore Froude number Fr. The data are compared with a number of field and laboratory studies whose details are given in Table 4-3. While the data trend was close to that predicted by the momentum principle (Eq. (4-12)), the results showed in average a lower experimental depth ratio for 1.05 < Fr < 2. Some factors may affect the results. For example, in an undular tidal bore, the estimate of the new flow depth was somewhat arbitrary. For all data shown in Figure 4-5, the conjugate depth was averaged between wave crest and trough. The averaging process assumed a symmetrical wave pattern (e.g. sinusoidal) that was not supported by the experimental data.

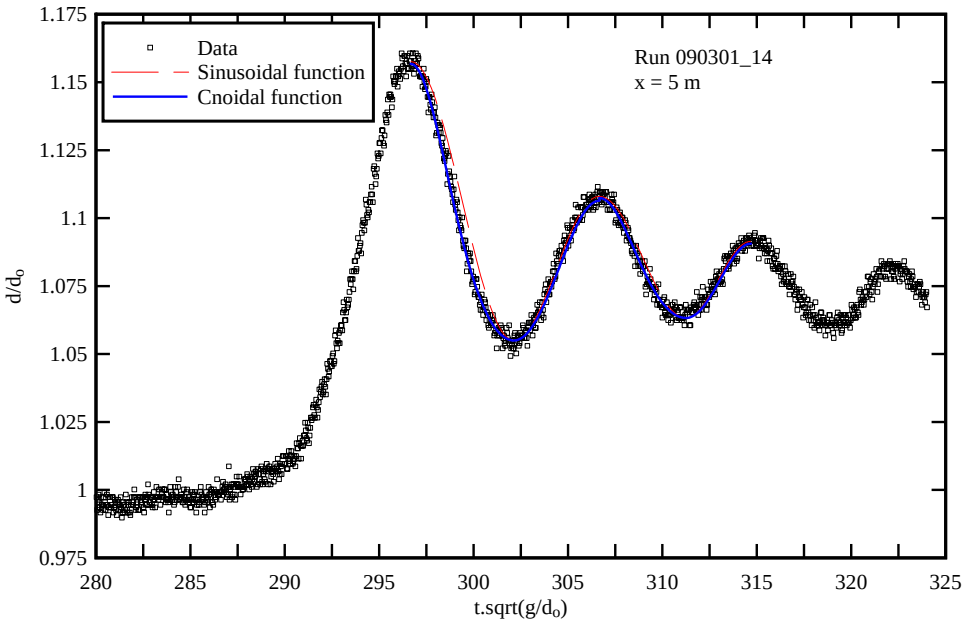

(A) Time-variation of the water depth at x = 5 m - Run 090304_14, Q = 0.0299 m^3/s, d_o = 0.2055 m (at x = 5 m), Fr = 1.10, U = 1.269 m/s

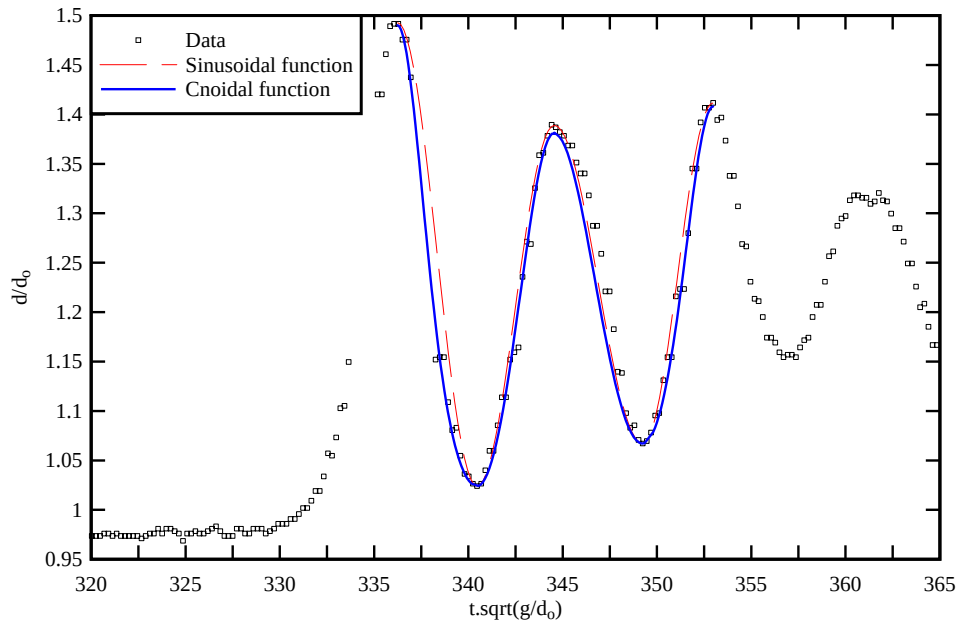

(B) Time-variation of the water depth at x = 5 m - Run 090415_62, Q = 0.0089 m^3/s, d_o = 0.0813 m (at x = 4.55 m), Fr = 1.22, U = 0.847 m/s

Fig. 4-3 - Dimensionless free-surface profile in an undular tidal bore - Comparison with the linear wave theory (sinusoidal wave) and Boussinesq equation solution (cnoidal wave)

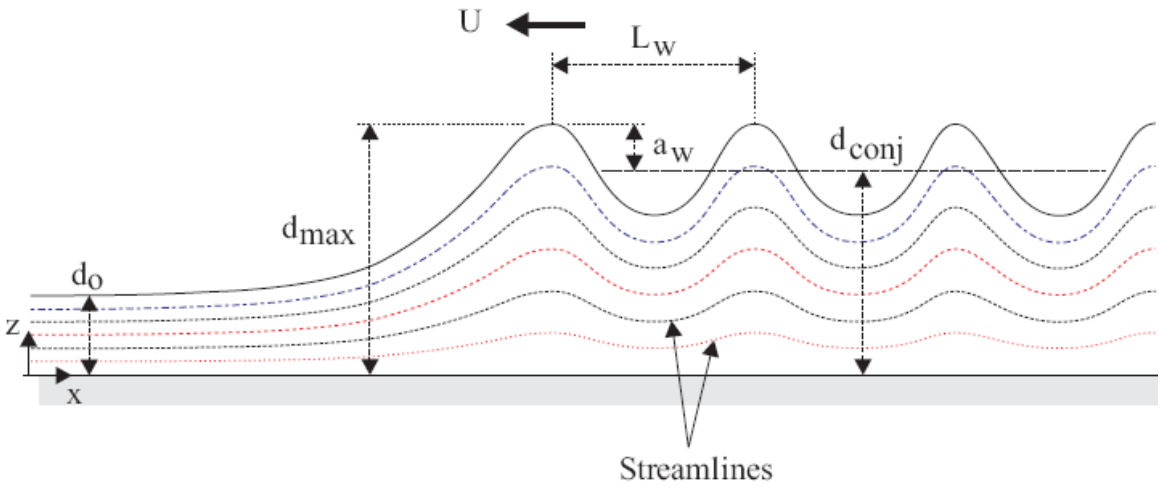

Fig. 4-4 - Sketch of an undular tidal bore- A small number of streamlines are included

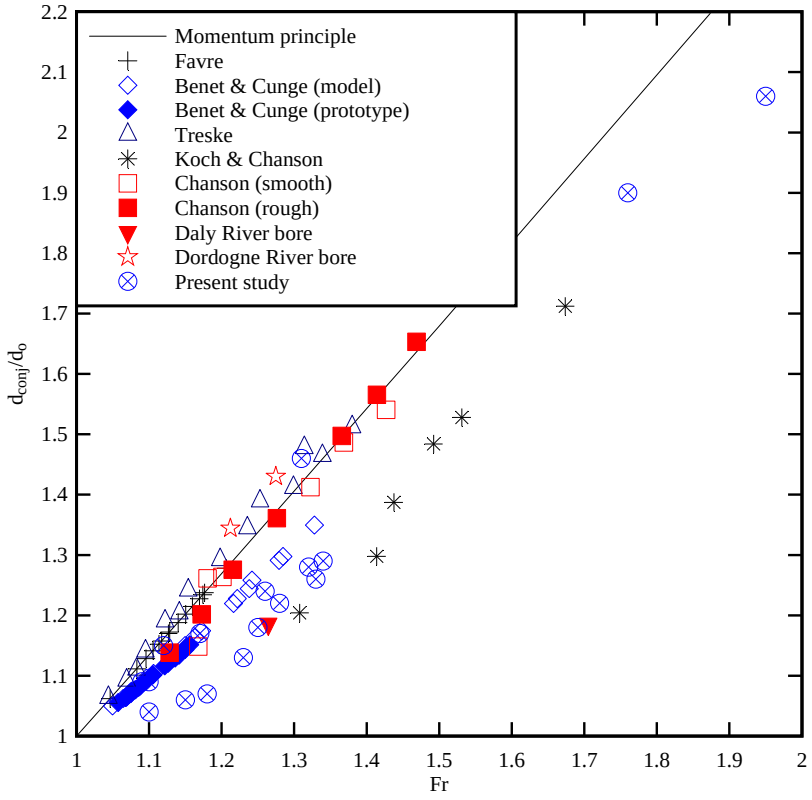

Fig. 4-5 - Ratio of flow depths d_2/d_1 across a tidal bore front - Comparison between the present data, the momentum principle (Eq. (4-12)), tidal bore data (NAVARRE 1995 [Dordogne], WOLANSKI et al. 2004 [Daly]), laboratory data (FAVRE 1935, BENET and CUNGE 1971, TRESKE 1994, KOCH and CHANSON 2008, CHANSON 2008a) and prototype data (BENET and CUNGE 1971) (Table 4-3)

For the undular, non-breaking bore, the maximum wave heights attained by the undulations are presented in Figure 4-6 and the data are compared with earlier studies. Herein the maximum wave height is that of the first wave crest (Fig. 4-4) and it is limited by breaking. The experimental data were compared with the calculations of PEREGRINE (1966), with the onset of wave breaking in tidal bores (d_{conj}/d_o-1 > 0.4, or Fr > 1.3 to 1.4, Table 3-2), and with the maximum height of a solitary wave. The present experimental data were in general agreement with earlier results including the solitary wave theory.

The dimensionless wave amplitude and steepness are presented in Figures 4-7 and 4-8. The data were compared with both field and laboratory observations (Table 4-3). The measurements were compared also with the analytical solutions of LEMOINE (1948) and ANDERSEN (1979) respectively based upon the linear wave theory and the Boussinesq equations. For a bore Froude number slightly larger than unity, the wave amplitude a_w/d_o and wave steepness a_w/L_w increased with an increasing bore Froude number Fr. However, both the wave amplitude and steepness showed a maximum followed by a sharp decrease immediately before the disappearance of free-surface undulations. It is believed that the flow conditions associated with the maximum wave amplitude and steepness took place shortly before the appearance of small wave breaking at the first wave crest for Fr ~ 1.3 to 1.4. Note, in Figure 4-8, that the undular bore data are compared with some stationary hydraulic jump data.

The pressure and velocity fields are affected by the free-surface curvature in an undular tidal bore. The free-surface is a streamline (Fig. 4-4) and a simple flow net analysis shows that the pressure gradient must be greater than hydrostatic beneath wave trough and less than hydrostatic beneath wave crest (e.g. ROUSE 1938,1959, PEREGRINE 1966). This was also observed in stationary undular hydraulic jumps (CHANSON and MONTES 1995, MONTES and CHANSON 1998). The pressure redistributions between wave crests and troughs, and troughs and crests, are associated with a significant velocity redistribution between the upstream/initial flow cross section and the first wave crest, and between subsequent crests and troughs. The maximum velocity amplitudes are observed at crests and the minimum velocities at wave troughs, while the velocity distributions are not symmetrical on either side of crest and trough (KOCH and CHANSON 2008).

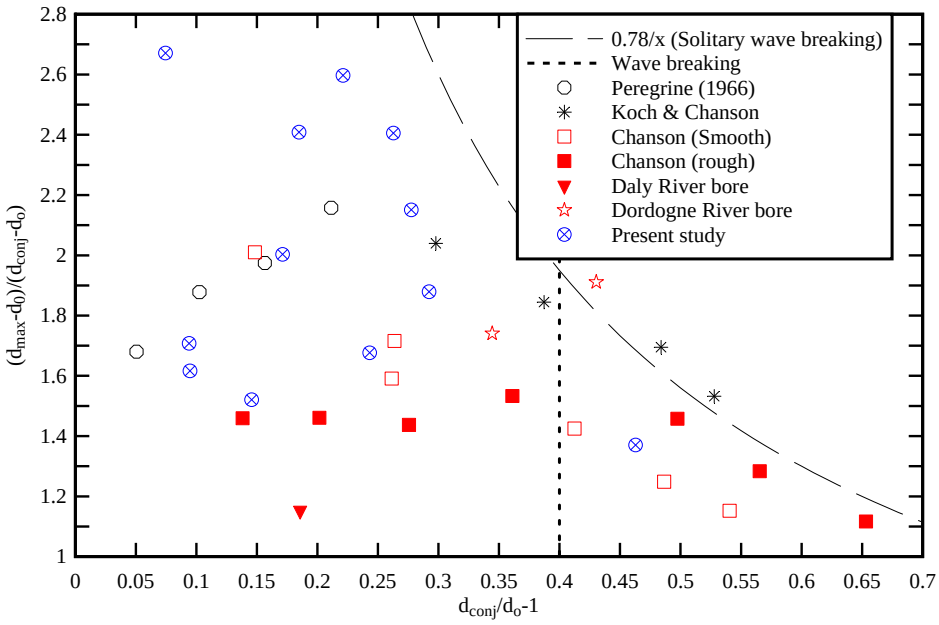

Fig. 4-6 - Maximum wave height of undular tidal bores - Comparison between the present study, experimental data (NAVARRE 1995, WOLANSKI et al. 2004, KOCH and CHANSON 2008, CHANSON 2008a), calculations (PEREGRINE 1966) and maximum solitary wave height

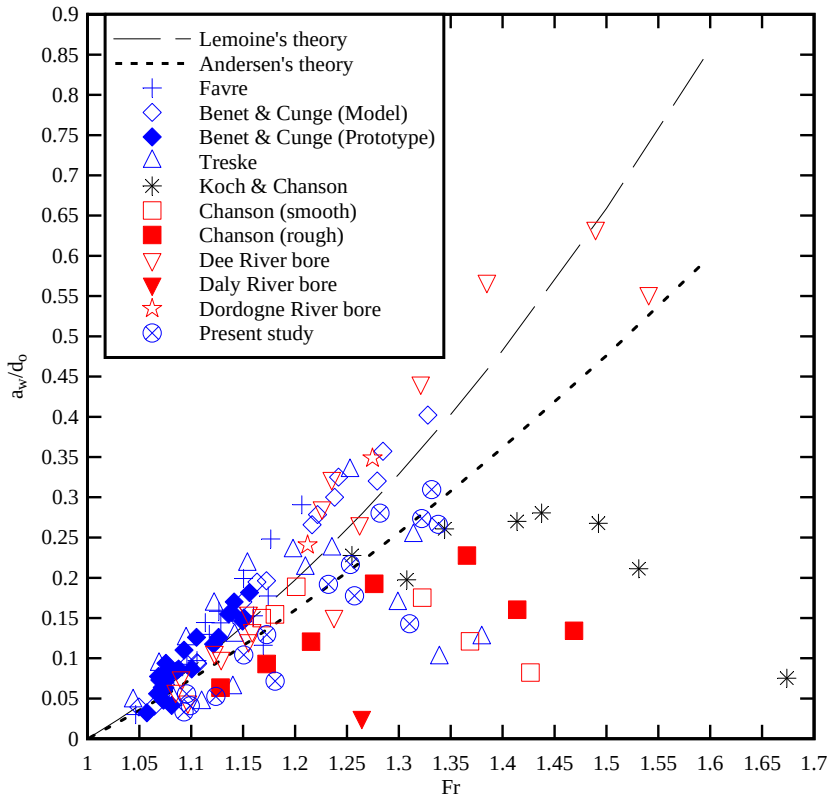

Fig. 4-7 - Dimensionless wave amplitude a_w/d_o in undular bores - Data: Present study, FAVRE (1935), BENET and CUNGE (1971), TRESKE (1994), KOCH and CHANSON (2008), CHANSON (2008a), LEWIS (1972) [Dee River tidal bore], NAVARRE (1995) [Dordogne River], WOLANSKI et al. [Daly River tidal bore]

Table 4-3 - Past experimental investigations of tidal bores and positive surges

Reference	Initial flow V_o m/s	d_o m	Surge direction	Channel geometry	Remarks
(1)	(2)	(3)	(4)	(5)	(6)
Laboratory experiments					
FAVRE (1935)	0	0.106 to 0.206	U/S	Rectangular (B = 0.42 m) $\theta = 0^o$	Flume length : 73.8 m.
	$\neq 0$	0.109 to 0.265	U/S	Rectangular (B = 0.42 m) $\theta = 0.017^o$	
BENET & CUNGE (1971)	0 to 0.198	0.057 to 0.138	D/S	Trapezoidal (base width : 0.172 m, sideslope: 2H:1V) $\theta = 0.021^o$	Flume length: 32.5 m.
TRESKE (1994)		0.08 to 0.16	U/S	Rectangular (B = 1 m) $\theta = 0.001^o$	Flume length: 100 m. Concrete channel.
		0.04 to 0.16	U/S, D/S	Trapezoidal (base width : 1.24 m, sideslope: 3H:1V) $\theta = 0^o$	Flume length: 124 m. Concrete channel.
CHANSON (1995)	0.4 to 1.2	0.02 to 0.15	U/S	Rectangular (B = 0.25 m) $\theta = 0.19$ to 0.54^o, glass bed	Flume length: 20 m.
HORNUNG et al. (1995)	0	--	D/S	Rectangular $\theta = 0^o$	Flume length: 24 m.
KOCH & CHANSON (2008, 2009)	1.0	0.079	+U/S	Rectangular (B = 0.50 m) $\theta = 0^o$, PVC invert	Flume length: 12 m.
CHANSON (2008a)	0.83	0.137	U/S	Rectangular (B = 0.50 m) $\theta = 0^o$, PVC invert	Flume length: 12 m.
	0.83	0.142	U/S	Rectangular (W = 0.50 m) $\theta = 0^o$, rough screen invert	
Prototype experiments					
BENET & CUNGE (1971)	0.59 to 1.08	6.61 to 9.16	U/S	Trapezoidal (base width : 9 m, sideslope: 2H:1V) $\theta = 0.006$ to 0.0086^o	Oraison power plant intake channel.
	1.51 to 2.31	5.62 to 7.53	U/S	Trapezoidal (base width : 8.6 m, sideslope: 2H:1V)	Jouques-Saint Estève intake channel.
Tidal bores					
LEWIS (1972)	0 to +0.2	0.9 to 1.4	U/S	Dee River near Saltney Ferry footbridge. Trapezoidal channel	Field experiments between March and September 1972.
NAVARRE (1995)	0.65 to 0.7	1.12 to 1.15	U/S	Dordogne River at Port de Saint Pardon. Width ~ 290 m	Field experiments on 25 & 26 April 1990.
WOLANSKI et al. (2004)	0.15	1.5 to 4	U/S	Daly River. Width ~ 140 m	Field experiments in July and September 2002, and on 2 July 2003.

Notes: d_o: initial water depth; V_o: initial flow velocity; θ: bed slope angle with the horizontal; Bore direction: U/S = propagating upstream; D/S = propagating downstream; (--) : information not available.

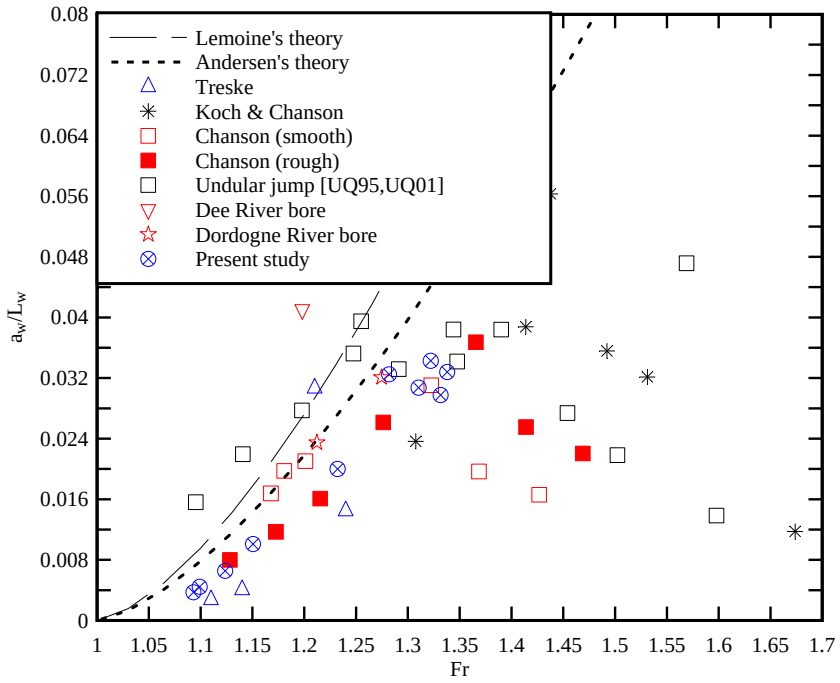

Fig. 4-8 - Wave steepness a_w/L_w in undular bores - Data: Present study, TRESKE (1994), KOCH and CHANSON (2008), CHANSON (2008a), LEWIS (1972) [Dee River tidal bore], NAVARRE (1995) [Dordogne River] - Comparison with stationary undular hydraulic jump data: CHANSON (1995,2005) [UQ95,UQ01]

4.2 Effects of bridge pier and channel constriction

The channel constriction had a significant effect on the undular tidal bore propagation and its free-surface profile as illustrated in Figure 4-9. Figure 4-9 shows some time-series of the dimensionless flow depth d/d_o on the channel centreline at several longitudinal locations when an experiment was repeated with the channel constriction (Fig. 4-9A) and without (Fig. 4-9B). Further comparative graphs are presented in Appendix F.

The comparative analysis of the data showed first the energetic and somehow chaotic wave motion in the throat of the channel constriction: i.e., at x = 4.55 m in Figure 4-9A. The centreline data were consistent with the visual observations (section 3.2), and tended to show a greater maximum wave height in the constriction throat. Second, some key differences were seen in the free-surface profiles at x = 5 m and x= 4 m. These highlighted some effects of the channel contraction and expansion respectively on the tidal bore propagation. Visually, some wave reflection process was observed downstream of the constriction (i.e. x < 4.9 m) (section 3.2). While at x = 4 m, the rapid channel expansion induced a rapid change in free-surface profile. Third, the data in the throat (x = 4.55 m) showed some form of secondary peak possibly caused by some reflection effect on the walls.

Potential energy

The wave energy of the free-surface undulations is a combination of (a) the potential energy due to the water the elevation above the mean water level, and (b) the kinetic energy due to the fluid motion.

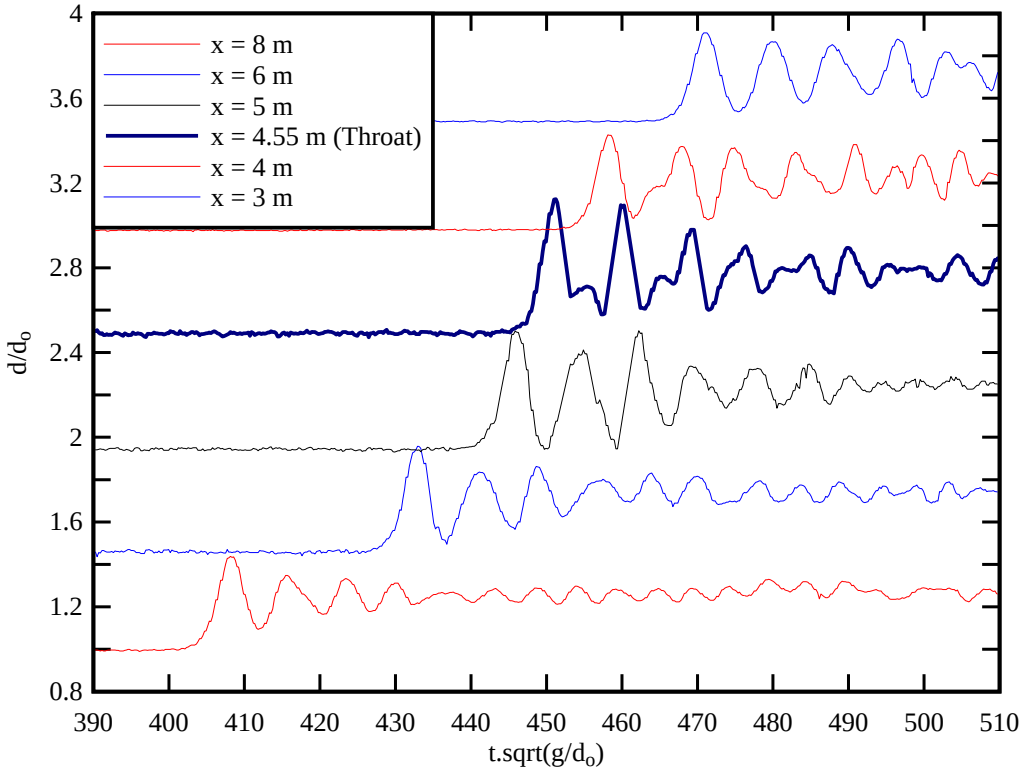

(A) Run 090417_61, Q = 0.0089 m^3/s, d_o = 0.0845 m, Fr = 1.16, U = 0.847 m/s, Channel constriction

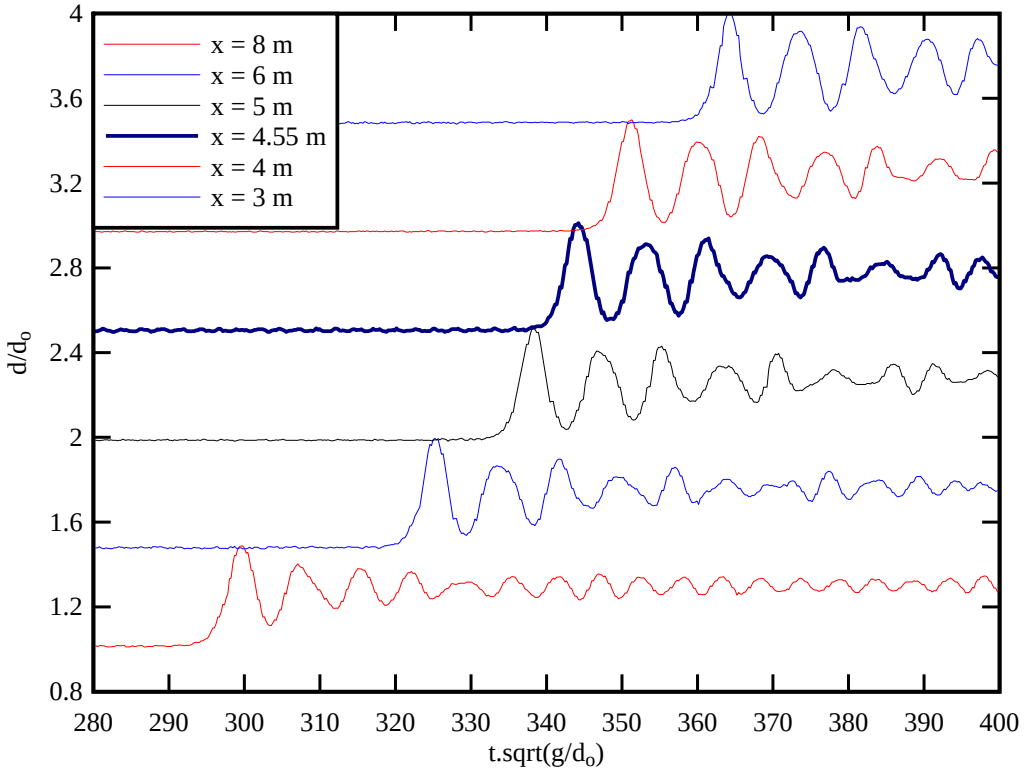

(B) Run 090417_62, Q = 0.0089 m^3/s, d_o = 0.0802 m, Fr = 1.22, U = 0.862 m/s, No channel constriction

Fig. 4-9 - Dimensionless time-variations of the flow depth during the propagation of an undular tidal bore with and without bridge pier model: Q = 0.0089 m^3/s, d_o = 0.08 m, Fr = 1.16-1.22, U = 0.8 m/s - Each curve was offset vertically by 0.5

Over one wave length, the potential energy is equal to the integral of the weight of water above the mean water level times the distance to the centroid:

$$\text{P.E.} = \int_0^{L_w} \frac{1}{2} \times \rho \times g \times \eta^2 \times B \times dx \qquad (4\text{-}13)$$

where η is the water elevation relative to the mean water level over the wave length L_w and B is the channel width ([3]) (LIGGETT 1994). The kinetic energy over a wave length is:

$$\text{K.E.} = \int_0^{L_w} \int_0^{\bar{d}+\eta} \frac{1}{2} \times \rho \times (V_x^2 + V_z^2) \times B \times dz \times dx \qquad (4\text{-}14)$$

where $\bar{d}$ is the mean water depth over the wave length L_w. For linear waves, the potential energy and kinetic energy equal respectively (LIGGETT 1994):

$$\text{P.E.} = \frac{1}{4} \times \rho \times g \times a_w^2 \times L_w \times B \qquad (4\text{-}15a)$$

$$\text{K.E.} = \frac{1}{4} \times \rho \times g \times a_w^2 \times L_w \times B \qquad (4\text{-}15b)$$

Hence the total energy per unit area is:

$$\text{T.E.} = \frac{1}{4} \times \rho \times g \times a_w^2 \qquad (4\text{-}16)$$

In an undular tidal bore, the wave shape is non-linear, and Equations (5-15) and (4-16) are not valid. In fact, the velocity distributions are complex and the kinetic energy could not be estimated. Instead the potential energy was calculated herein and used as a surrogate of the total energy. Since the water elevation was recorded as a function of time at a fixed location, the potential energy over a wave period T may be deduced using the Taylor hypothesis:

$$\text{P.E.} = \int_0^{T} \frac{1}{2} \times \rho \times g \times \eta^2 \times U \times B \times dt \qquad (4\text{-}17)$$

where U is the bore celerity. Note that the water elevation η was calculated relative to the average water level over the wave length L_w ([4]). Fig. 4-10 illustrates the integration process. The potential energy per unit surface area is then:

$$E_p = \frac{\text{P.E.}}{U \times T \times B} = \frac{1}{T} \times \int_0^{T} \frac{1}{2} \times \rho \times g \times \eta^2 \times dt \qquad (4\text{-}18)$$

Typical experimental results are presented in Figure 4-11, where the dimensionless potential energy per unit area $E_p/(0.5 \times \rho \times g \times d_o^2)$ is plotted as a function of the dimensionless distance x/d_o. Figure 4-11A presents some data with the channel constriction and Figure 4-11B shows some experimental results without the channel constriction. The data showed typically an increasing potential energy with increasing distance from

---

[3] Equation (4-13) implies a two-dimensional wave propagation.

[4] Defined herein from a wave crest to the next wave crest.

the gate ($x/d_o \approx 135$ in Figure 4-11) up to x = 6 m ($x/d_o \approx 75$ in Figure 4-11). This corresponded to the formation and development of the bore, and the visual observations suggested that the tidal bore profile was fully-developed and nearly invariant for x < 6 m. For x < 6 m, the potential energy of the undulations were thereafter quasi-constant in absence of channel constriction. The data highlighted further a greater potential energy per unit area in the first wave length than in the subsequent wave lengths. This is illustrated in Figure 4-11B.

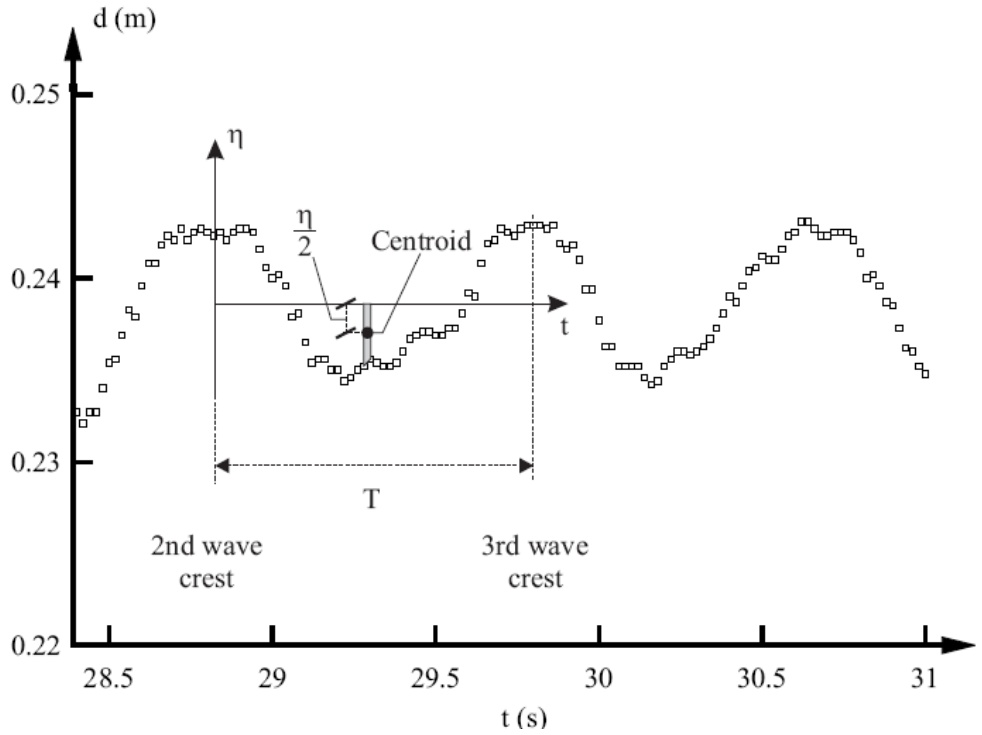

Fig. 4-10 - Potential energy integration along the second wave length - Experimental data: Run 090417_63, x = 5 m, Q = 0.0190 m^3/s, d_o = 0.212 m at x = 3.6 m, Fr = 1.04, U = 1.32 m/s

In presence of the channel constriction, the experimental data showed a marked increase in potential energy in the constriction throat: e.g., for $47.3 < x/d_o < 54.8$ in Figure 4-11A. The data indicated also a larger potential energy per surface area immediately upstream of the convergent and downstream of the divergent. This trend is clearly seen in Figure 4-11A for the first three wave lengths. It corresponded to some effects of the bore reflection on the convergent as well as of the divergent of the channel constriction.

After the channel constriction, the data suggested a lesser potential energy of the free-surface undulations than in the experiments without constriction: e.g., for $x/d_o < 40$ in Figure 4-11A, E_p was about 1/3rd smaller after the bore propagation through the channel constriction than for the same bore in a prismatic rectangular channel without constriction (Fig. 4-11B).

Another quantitative information is the total potential energy per surface area of the tidal bore estimated as:

$$(E_p)_{bore} = \frac{1}{T} \times \int_0^T \frac{1}{2} \times \rho \times g \times (d - d_o)^2 \times dt \qquad (4\text{-}19)$$

In the present study, the potential energy of the undulations represented up to 30% of the total potential

energy of the tidal bore, and this ratio decreased with an increasing wave length number (Fig. 4-12). The largest ratio of potential energy of the undulations to the total potential energy of the bore was observed for Fr ≈ 1.3 which corresponded to the onset of wave breaking at the first wave crest. Typical data are presented in Figure 4-12.

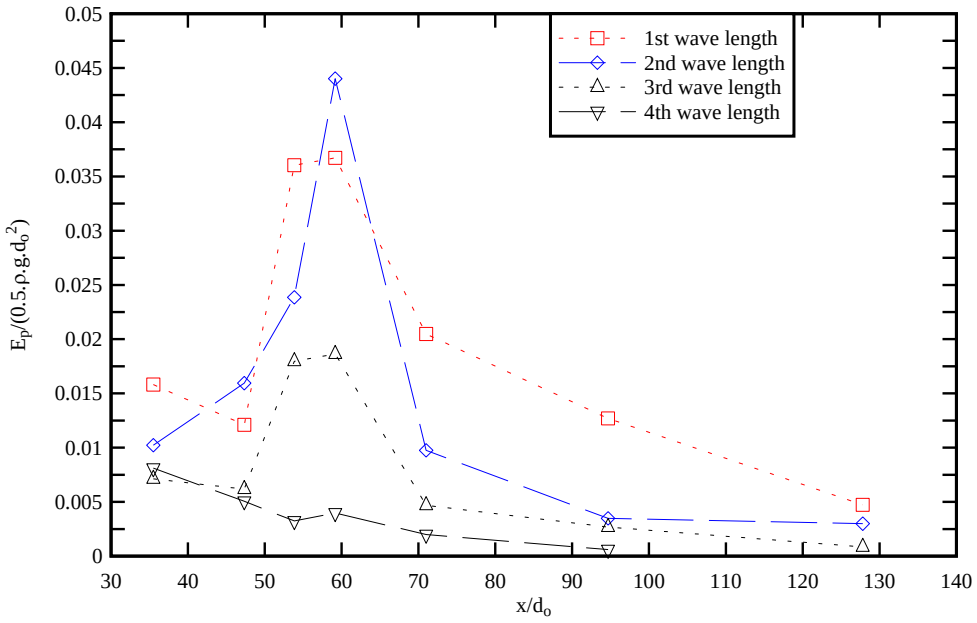

(A) With channel constriction ($47.3 < x/d_o < 54.8$) - Experimental data: Run 090415_61, Q = 0.089 m^3/s, d_o = 0.0845 m at x = 3.6 m, Fr = 1.16, U = 0.847 m/s

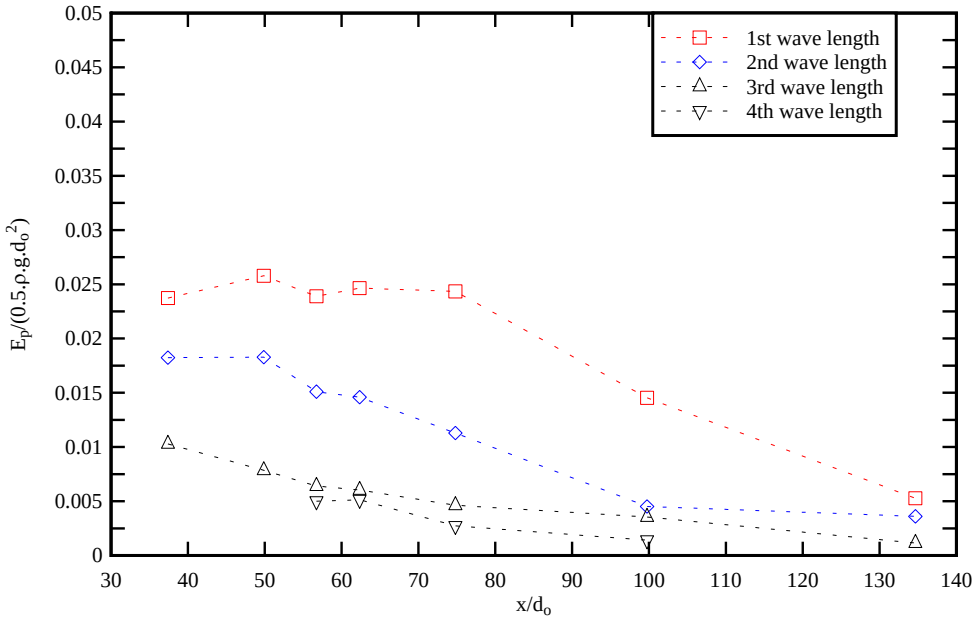

(B) No constriction - Experimental data: Run 090415_62, Q = 0.089 m^3/s, d_o = 0.0802 m at x = 3.6 m, Fr = 1.22, U = 0.862 m/s

Fig. 4-11 - Dimensionless potential energy per surface area in an undular bore with and without channel constriction - Experimental data: Q = 0.0089m^3/s, d_o = 0.08 m at x = 3.6 m, Fr = 1.2, U = 0.85 m/s

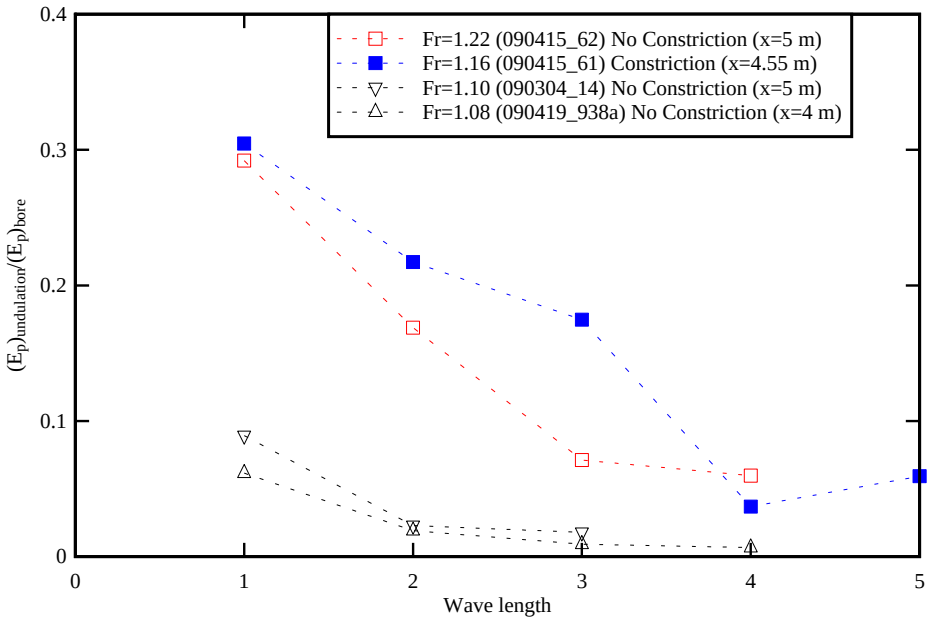

Fig. 4-12 - Ratio of the potential energy of the undulations to the bore potential energy as a function of the wave length number

5. Unsteady velocity measurements in undular tidal bores

5.1 Presentation

Three series of experiments were conducted, all performed with an identical initial flow rate Q = 0.019 m^3/s, but different initial flow depths, during which turbulent velocity measurements were performed using an acoustic Doppler velocimeter (ADV) (Table 5-1). The flow conditions yielded the generation of an undular (non-breaking) tidal bore propagating upstream against an initially subcritical flow motion. The turbulent velocity measurements were conducted at x = 4 m, 4.55 m and 5 m located respectively upstream, in the middle and downstream of the channel constriction. Herein the words "upstream" and "downstream" are defined in terms of the initially steady flow conditions. Note that the velocity measurements were recorded at vertical elevations $z/d_o < 0.76$ for the ADV sampling volume and receivers to remain underwater prior to and during the tidal bore passage. Some movies of the experiments are available in the form of a digital appendix (Appendix B).

A key feature of the present study was the repetition of identical experiments with and without the channel constriction, keeping the same identical initial flow conditions (Table 5-1).

Table 5-1 - Detailed turbulence measurements beneath tidal bores

Run	d_o	V_o	U	Fr	Tidal bore	Bed	S_o	x_{ADV}	F
	m	m/s	m/s					m	Hz
(1)	(2)	(3)	(4)	(5)	(6)	(7)	(8)	(9)	(10)
KOCH and CHANSON (2005)									
Run 050519	0.0790	1.016	0.235	1.43	Undular	Smooth PVC	0	5.0	50
Run 050530	0.0785	1.020	0.541	1.78	Breaking				
CHANSON (2008a)									
Run 080422	0.1385	0.830	0.553	1.17	Undular	Smooth PVC	0	5.0	200
Run 080416	0.1388	0.832	0.903	1.50	Breaking				
Run 080430	0.1412	0.826	0.551	1.20	Undular	Rough screens	0	5.0	200
Run 080428	0.1415	0.824	0.892	1.46	Undular/Breaking				
Run 080424	0.0701	1.641	0.034	2.02	Breaking & Decelerating	Smooth PVC	0.0145	5.0	200
Present study									
090424_901-902	0.115	0.331	1.05	1.16	Undular	Smooth PVC	0	5.0	200
090424_903-904					with channel			4.55 (*)	
090424_905-906					constriction			4.0	
090427_911-912	0.170	0.223	1.21	1.10	Undular	Smooth PVC	0	5.0	200
090427_913-914					with channel			4.55 (*)	
090427_915-916					constriction			5.0	
090427_921-927	0.165	0.230	1.21	1.13	No Constriction			4.0	
090429_931-932	0.199	0.189	1.32	1.08	Undular	Smooth PVC	0	5.0	200
090429_933-934					with channel			4.55 (*)	
090429_935-936					constriction			4.0	
090429_938-939					No Constriction			4.0	

Notes: d_o: initial flow depth; F; sampling frequency; Fr: surge Froude number; S_o: bed slope ($S_o = \sin\theta$); U:

surge front celerity positive upstream; V_o: initial flow velocity positive downstream; x_{ADV}: ADV longitudinal sampling location; (*): measurements in the throat; all steady flow properties were recorded at x = 3.6 m (present study) and 5 m (earlier studies).

5.2 Turbulent velocity measurements

The velocity measurements showed that the undular tidal bore passage was associated with some deceleration of the flow. The longitudinal velocity component V_x decreased when the first wave crest passed above the sampling volume as illustrated in Figure 5-1. Figure 5-1 presents the dimensionless instantaneous flow depth d/d_o and instantaneous velocity components V_x/V_o, V_y/V_o and V_z/V_o at two vertical elevation z/d_o for an experiment in the prismatic rectangular channel, where d is the flow depth, d_o is the initial flow depth measured at x = 3.6 m, V_x is the longitudinal velocity component positive downstream, V_y is the transverse velocity component positive towards the left bank, V_z is the vertical velocity component positive upwards and V_o is the initial flow velocity at x = 3.6 m: $V_o = Q/(d_o \times B)$. In Figure 5-1, the data were collected on the channel centreline at x = 4 m.

The undular bore was characterised by a smooth first wave crest followed by a series of free-surface undulations, and no breaking roller was observed. When the undular bore front passed above the sampling volume, a relatively gentle longitudinal flow deceleration was observed at all vertical elevations (Fig. 5-1). The longitudinal velocity component was minimum beneath the first wave crest and it oscillated afterwards with the same period as the surface undulations and out of phase (by π) as previously observed by KOCH and CHANSON (2008) and CHANSON (2008a) in laboratory and WOLANSKI et al. (2004) in the Daly River. The longitudinal velocities were maximum beneath the wave troughs and minimum below the wave crests at all sampling elevations (Fig. 5-1). Close to the free-surface, the vertical velocity data presented also some oscillating pattern. The basic flow net theory predicts these redistributions in longitudinal and vertical velocity components since the free-surface is a streamline (ROUSE 1938, MONTES and CHANSON 1998, CHANSON 2009).

It is noteworthy that the experiments were conducted at a relatively high sampling rate. Yet the fast sampling acquisition did not provide a greater level of details on the bore front passage than the earlier studies of HORNUNG et al. (1995) and KOCH and CHANSON (2008). The reason is unclear: it might be a physical feature of the shock, although it could be linked with some limitations of the acoustic Doppler velocimetry including the non-negligible sampling volume (about 42 mm^3 ([1])).

[1] herein a volume of about 6 mm diameter and 1.5 mm height.

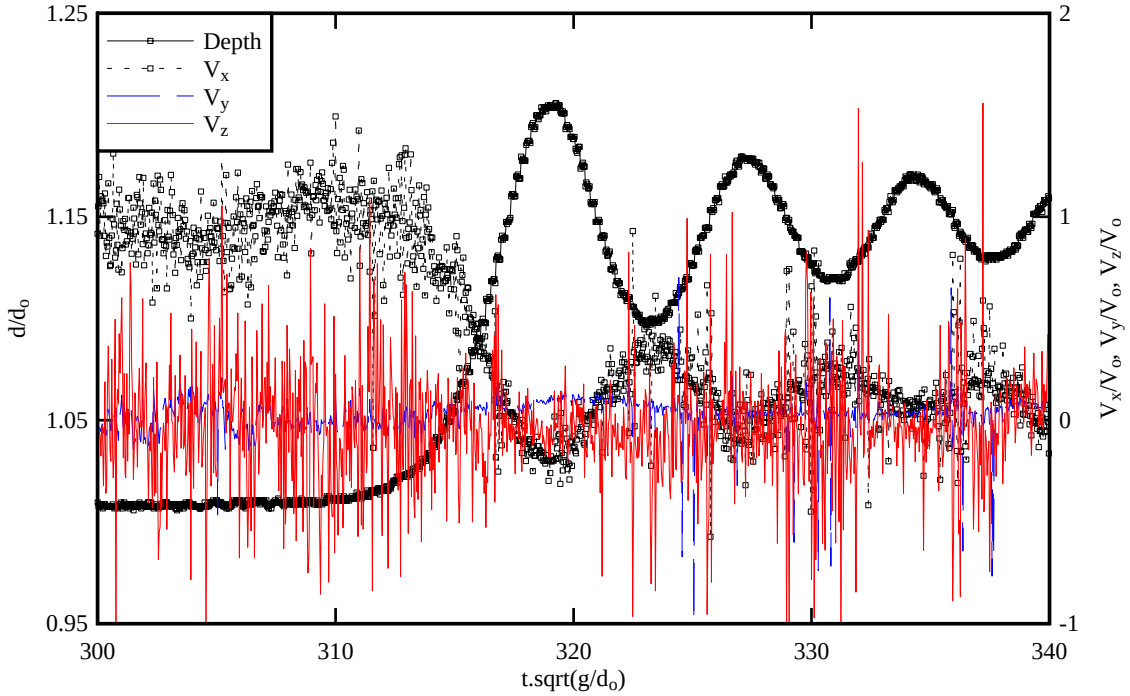

(A) z/d_o = 0.182, Run 090429_938a

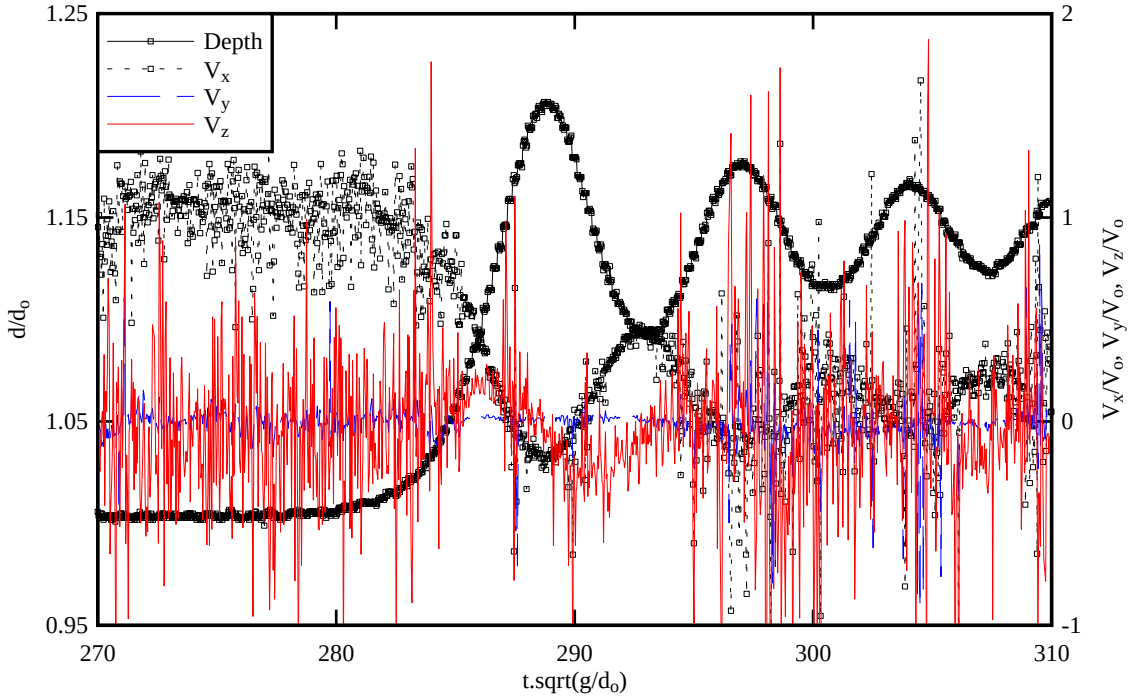

(B) z/d_o = 0.73, Run 090429_939a

Fig. 5-1 - Dimensionless water depth and instantaneous velocity components in an undular bore propagating upstream in a prismatic rectangular channel at x = 4 m - Run 090429_938-939, d_o = 0.1989 m at x = 3.6 m, V_o = 0.189 m/s, U = 1.32 m/s, Fr = 1.08 (For interpretation of the references to colour in this figure legend, the reader is referred to the web version of this report.)

5.3 Undular bore propagation through a channel constriction

In presence of the channel constriction, the initially steady flow was characterised by some flow separation downstream of the constriction divergent. Some flow visualisations showed a flow pattern sketched in Figure 5-2 with a jet flow region along the channel centreline. In the steady flows, the measurements showed some larger centreline velocities downstream of the channel constriction than upstream (Fig. 5-3 and 5-4).

Figures 5-3 and 5-4 present some typical dimensionless instantaneous flow depth d/d_o and instantaneous velocity components V_x/V_o, V_y/V_o and V_z/V_o for some experiments with the channel constriction. In one figure, the data were collected at the same vertical elevation z/d_o and at three longitudinal locations: x = 5 m downstream of the constriction, x = 4.55 m, in the throat of the constriction and x = 4 m upstream of the constriction. All the data were recorded on the channel centreline and the three sampling locations are drawn to scale in Figure 5-2. Note that, in Figure 5-4, the data were performed with the same identical flow conditions to those presented in Figure 5-1, but for the presence of the channel constriction.

The velocity measurements suggested small to moderate effects of the channel constriction on the unsteady turbulent velocity field. The finding was somehow deceiving since a significant impact of the constriction was observed visually (section 3.2) and measured in terms of the free-surface profile (section 4.2). However the data sets suggested some energetic turbulent events beneath the first and subsequent wave lengths. These were best seen by some sudden and rapid fluctuations of the transverse velocity data V_y/V_o as highlighted in Figure 5-5. Some fluctuations of the horizontal and vertical velocity components were observed also. Note that a careful signal analysis was conducted manually in each case to ascertain that these turbulence patches were not ADV erroneous signals. Figure 5-5 illustrates some typical examples.

Such vigorous turbulent events were also observed in the prismatic rectangular channel, in both the present and past studies (KOCH and CHANSON 2008, CHANSON 2008a). KOCH and CHANSON (2008) reported: "*maximum normal and tangential stresses were observed immediately upstream of and at wave crests*". However the present study suggested some more intense occurrence in presence of the channel constriction.

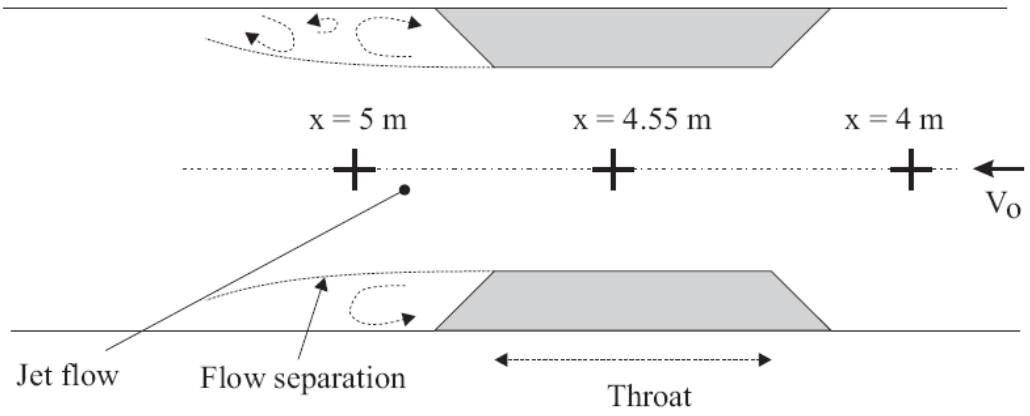

Fig. 5-2 - Sketch of the steady flow pattern downstream of the channel constriction

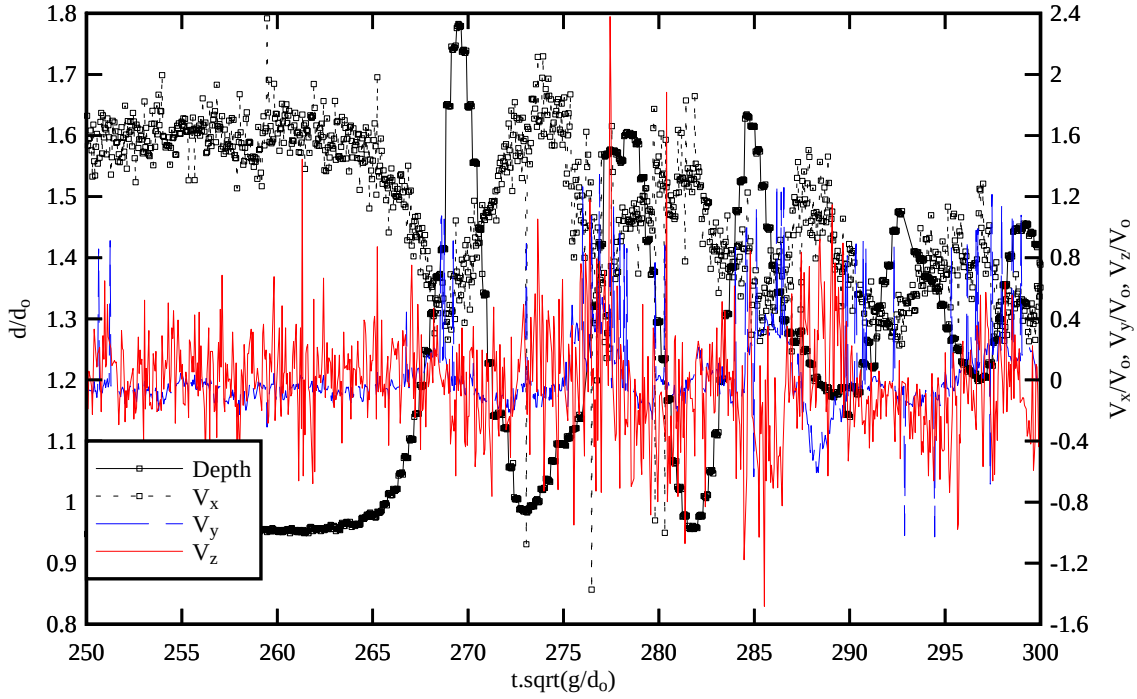

(A) Downstream of constriction: x = 5 m, z/d$_o$ = 0.312, Run 090424_901c

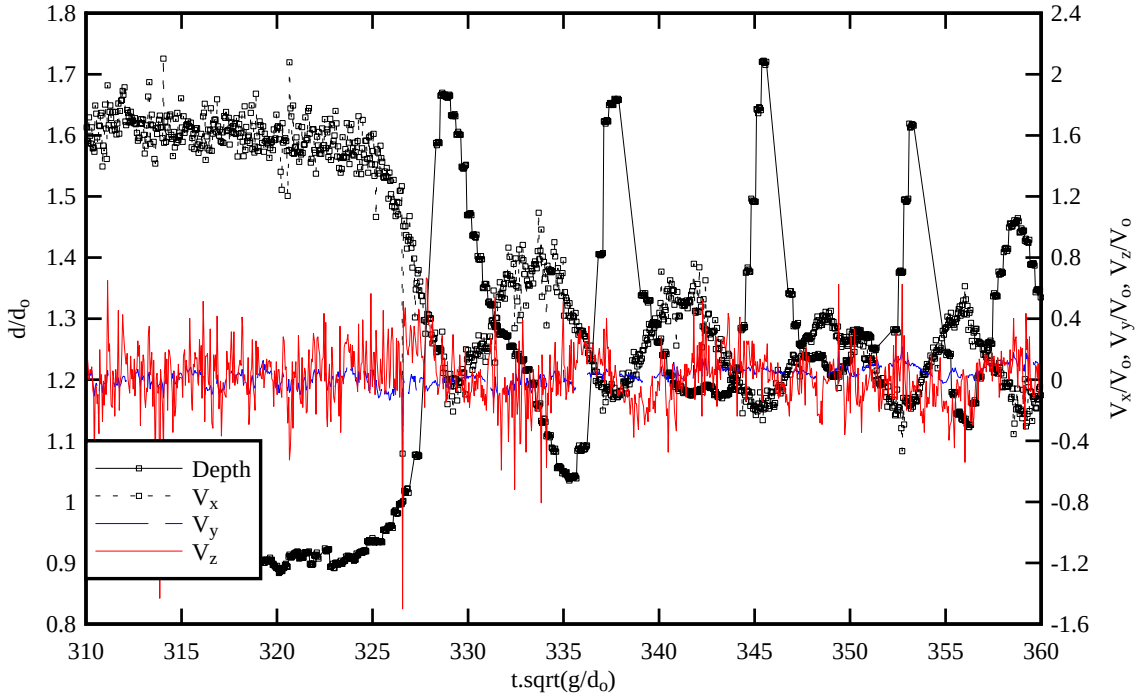

(B) In the constriction throat: x = 4.55 m, z/d$_o$ = 0.312, Run 090424_903

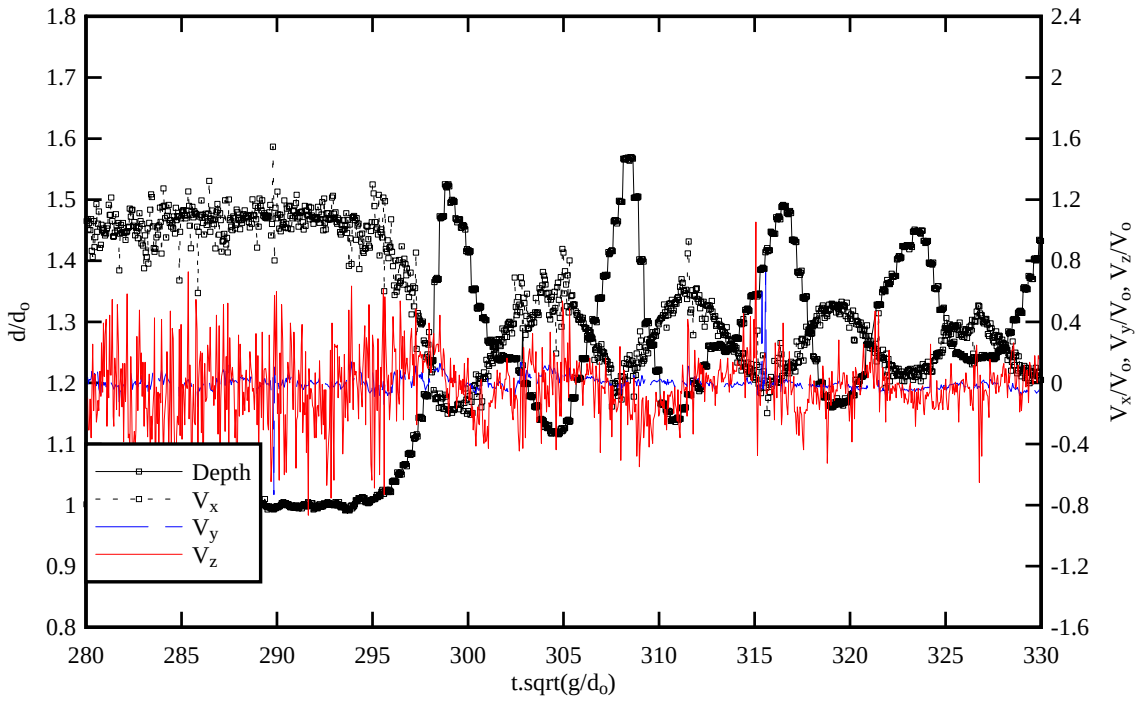

(C) Upstream of the constriction: x = 4 m, z/d_o = 0.316, Run 090424_905

Fig. 5-3 - Dimensionless water depth and instantaneous velocity components in an undular bore propagating upstream in a channel with channel constriction - Run 090424_901-906, d_o = 0.1147 m at x = 3.6 m, V_o = 0.3313 m/s, U = 1.05 m/s, Fr = 1.16 (For interpretation of the references to colour in this figure legend, the reader is referred to the web version of this report.)

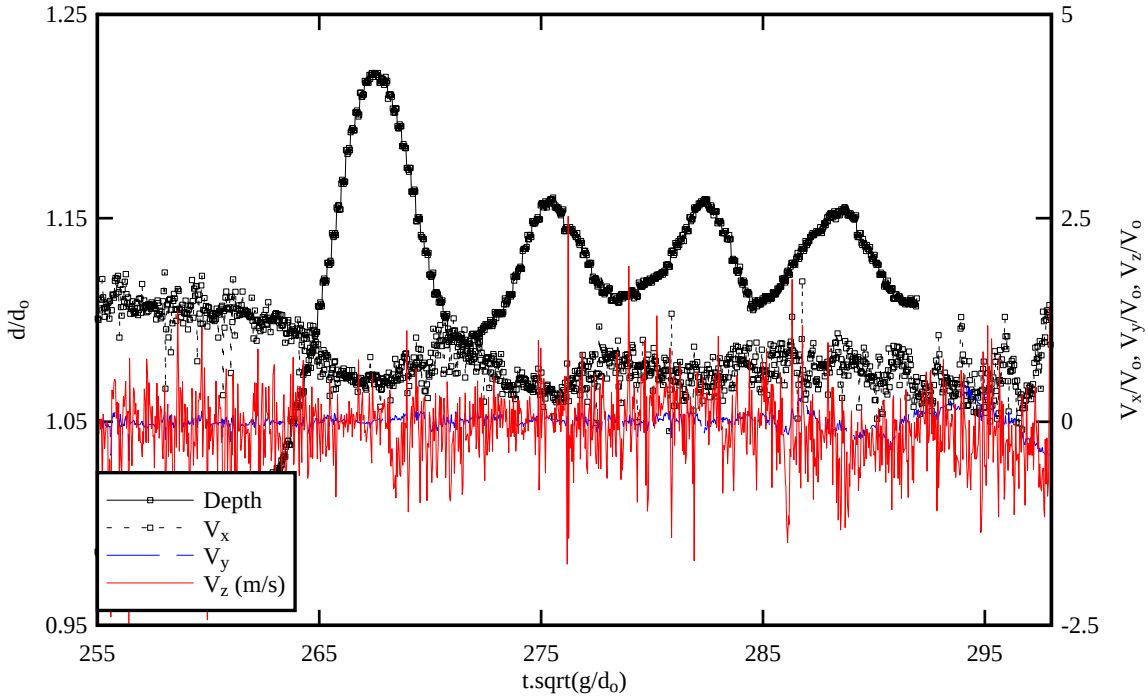

(A) Downstream of constriction: x = 5 m, z/d_o = 0.180, Run 090429_931

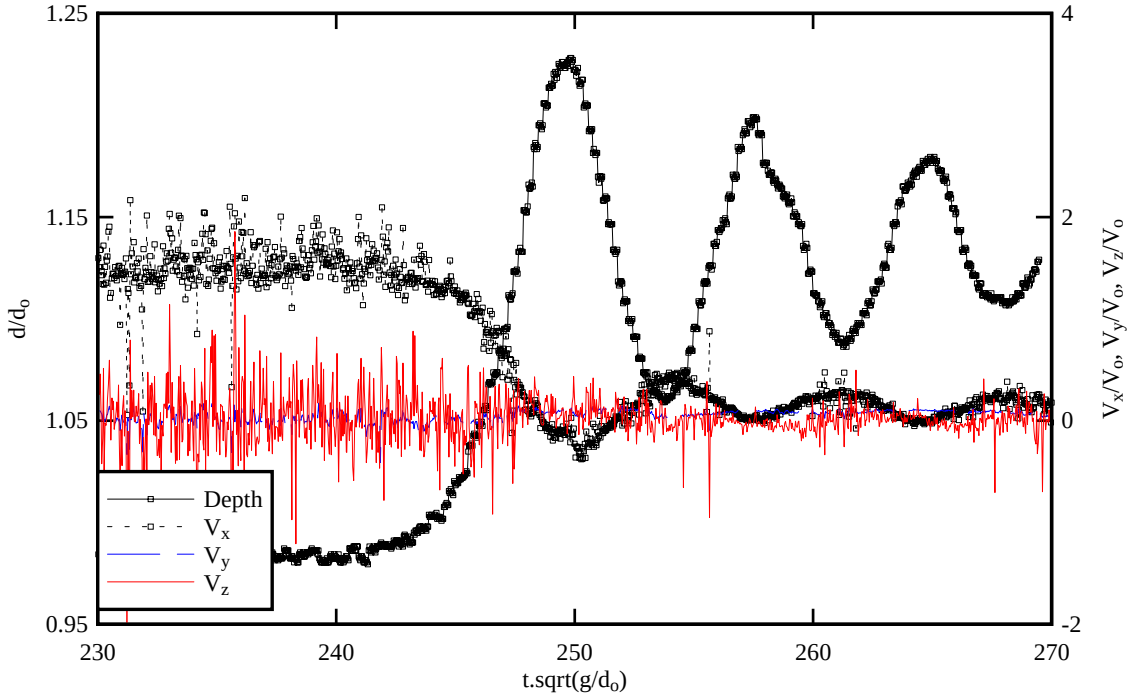

(B) In the constriction throat: x = 4.55 m, z/d_o = 0.180, Run 090429_933

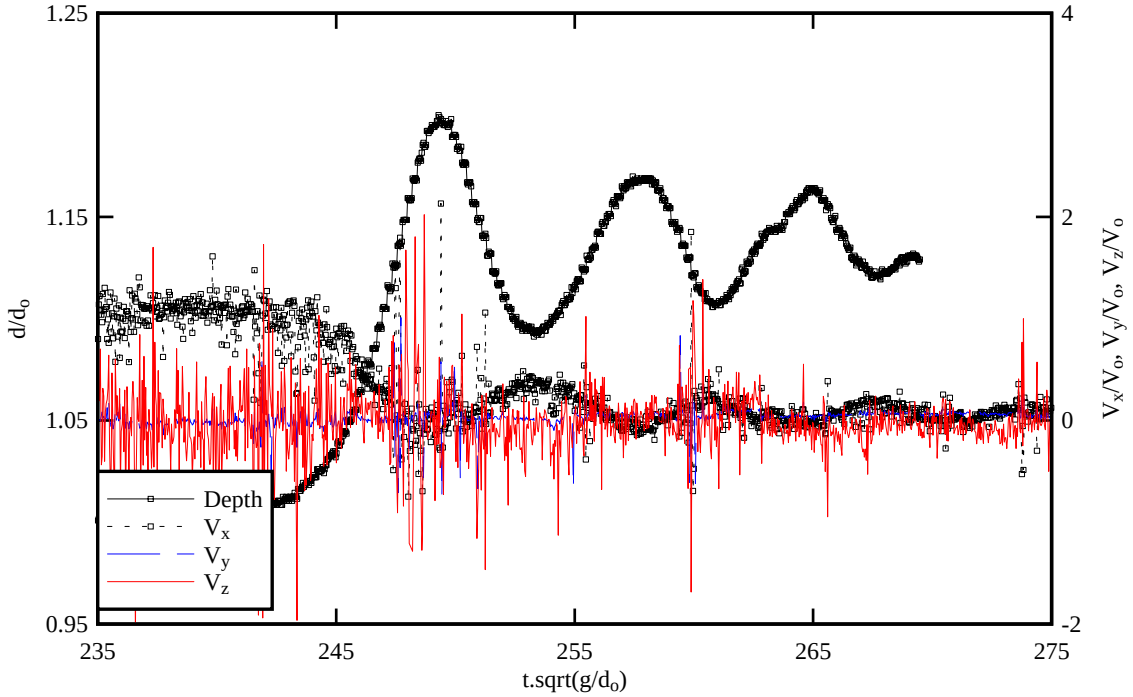

(C) Upstream of the constriction: x = 4 m, z/d_o = 0.182, Run 090429_935

Fig. 5-4 - Dimensionless water depth and instantaneous velocity components in an undular bore propagating upstream in a channel with channel constriction - Run 090429_931-936, d_o = 0.1989 m at x = 3.6 m, V_o = 0.189 m/s, U = 1.32 m/s, Fr = 1.08 (For interpretation of the references to colour in this figure legend, the reader is referred to the web version of this report.)

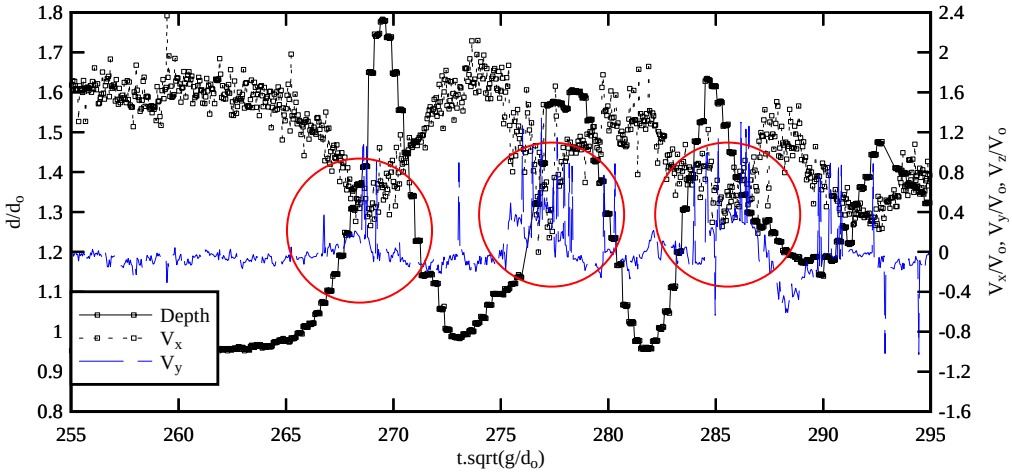

(A) Downstream of constriction: x = 5 m, z/d$_o$ = 0.312, Run 090424_901c, d$_o$ = 0.1147 m at x = 3.6 m, V$_o$ = 0.3313 m/s, U = 1.05 m/s, Fr = 1.16

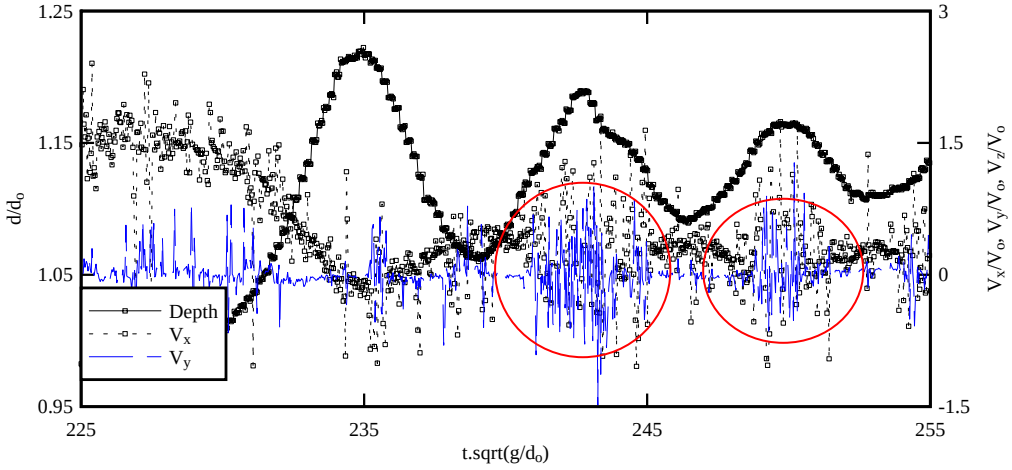

(B) In the constriction throat: x = 4.55 m, z/d$_o$ = 0.73, Run 090429_934, d$_o$ = 0.1989 m at x = 3.6 m, V$_o$ = 0.189 m/s, U = 1.32 m/s, Fr = 1.08

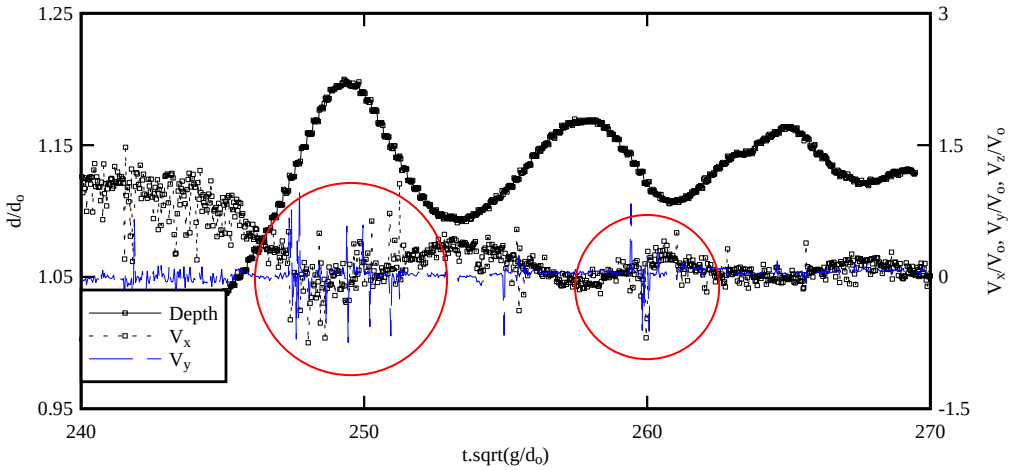

(C) Upstream of the constriction: x = 4 m, z/d$_o$ = 0.182, Run 090429_935, d$_o$ = 0.1989 m at x = 3.6 m, V$_o$ = 0.189 m/s, U = 1.32 m/s, Fr = 1.08

Fig. 5-5 - Turbulent events behind tidal bores in a channel with channel constriction: dimensionless water depth and instantaneous longitudinal and transverse velocity component (For interpretation of the references

to colour in this figure legend, the reader is referred to the web version of this report.)

5.4 Discussion

It is argued herein that the energetic turbulent events illustrated in Figure 5-5 were some form of macro-turbulence advected upstream behind the tidal bore that were likely induced by secondary motion. The evidences of advected turbulent "patches" behind a tidal bore were documented in the field. In the Mersey River (UK) and Rio Mearim (Brazil), the salinity measurements during and after tidal bore events showed sharp jumps in salinity and temperature several minutes after the bore passage with a delay depending upon the sampling site location and depth (DAVIES 1988, KJERFVE and FERREIRA 1993). In the Daly River (Australia) and the northern Branch of the Changjiang River Estuary, some major re-suspension of sediments occurred several minutes after the passage of the tidal bore (CHEN 2003, WOLANSKI et al. 2004). In these rivers, the delayed jumps in salinity, temperature and suspended sediment concentration implied some turbulent advection process in the wake of the tidal bore front. The delays were caused by an upstream advection speed slower than the tidal bore celerity U.

An unusual observation was recorded in the Daly River (Australia) where a period of very strong turbulence was observed about twenty minutes after the bore passage that lasted for about three minutes: "*about 20 min after the passage of the undular bore, a 3-min-duration patch of macro-turbulence was observed. Horizontal eddies with peak velocity V of about 0.5 m/s were imbedded within a prevailing tidal current of about 0.7 m/s. This unsteady motion was sufficiently energetic to topple moorings that had survived much higher, quasi-steady currents of 1.8 m/s (Wolanski et al., 2001). Both clockwise and counterclockwise rotating eddies were observed. Since these eddies lasted typically 10 s, their horizontal dimensions were about 7 m in depth of about 3 m. These eddies were associated with water level fluctuations not exceeding 1 cm*" (WOLANSKI et al. 2004). The sampling location was located about 50 km upstream of the river mouth. The anecdote suggested the upstream advection of a "cloud" of turbulence and vorticity behind the tidal bore for possibly a considerable distance. The advection speed of the turbulence boils was slower than the tidal bore celerity, explaining the 20 minutes delay.

In the present study, the instantaneous velocity data showed some large fluctuations in transverse velocities V_y on the channel centreline. The findings implied the existence of transient secondary currents behind the bore front that were associated with some unsteady transverse shear pattern. These intense turbulent events were observed at several longitudinal locations highlighting the upstream advection process. While these turbulent bursts might be linked with the undular shape of the bore, the experimental study of KOCH and CHANSON (2009) presented some evidences of turbulence "patches" behind both undular and breaking bores, and HORNUNG et al. (1995) showed that the vorticity production rate was proportional to $(Fr - 1)^3$. These two studies implied that the vorticity "clouds" were a feature of both non-breaking and breaking bores, and this was supported by some recent numerical results with breaking tidal bores (FURUYAMA and CHANSON 2008, LUBIN et al. 2009). The present results suggested further that some turbulence clouds could be linked with the non-prismatic channel shape, and hence with some secondary current motion.

The secondary currents are currents that develop in the plane normal to the local axis of the main flow. In a

prismatic channel, the vorticity profiles at the sidewall and on the invert interact next to the corner (Fig. 5-6, Inset). In the regions of high wall shear stress effects as in the channel corner, the local production of turbulent kinetic energy is greater than the local dissipation. Conversely the local production is lesser than the dissipation in regions of low wall shear stresses. As a result, there exists a mean flow in the y-z-plane that corresponds to the secondary current sketched in Figure 5-6. This secondary motion is driven by the Reynolds stress gradients (HINZE 1967, BRADSHAW 1971). Secondary currents may also occur in the regions of transition from smooth to rough boundaries when the boundary roughness is not uniform as shown by HINZE (1973). Considering a tidal bore propagating upstream in a prismatic rectangular channel, it induced some intense turbulent mixing, and it hypothesised that some strong turbulent kinetic energy production caused by secondary motion next to the step corners took place beneath the wave troughs, as sketched in Figure 5-6. The turbulent events interacted with the mean flow and some energetic "clouds" of turbulence were advected within the main flow behind the bore.

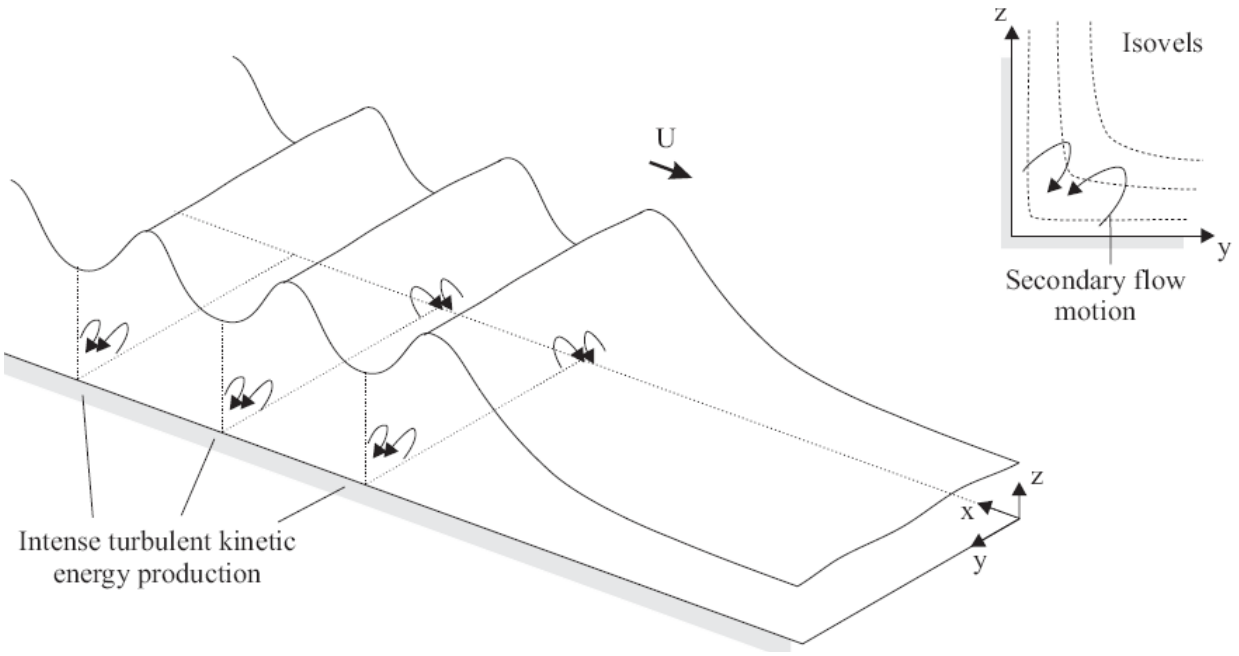

Fig. 5-6 - Secondary currents in an undular bore propagating in a prismatic channel - Inset: secondary flow motion in a corner

When the channel is not prismatic, there is a change in mean flow direction and the streamline curvature induces some longitudinal component of mean vorticity. Some vorticity may be generated by the invisicid flow motion and some complicated secondary currents may develop (THORNE and HEY 1979, XIE 1998, TREVETHAN et al. 2008). In some geometries, the effects of secondary currents are so strong that the main flow is forced to follow some change (XIE 1998). In the present study, the tidal propagation in the channel constriction was associated with the development of large scale vortical structures next to the free-surface at the throat intake and in the divergent section (section 3.2). It is suggested that the free-surface boil structures illustrated the intense production of turbulent kinetic energy and vorticity next to the sidewall contraction and expansion when the bore front entered and exited respectively the constriction. The macro-scale

turbulence was advected behind the bore front, contributing to the energetic turbulent velocity fluctuation periods observed on the channel centreline (Fig. 5-5). The proposed mechanism would be consistent with the surface "*clockwise and counterclockwise rotating eddies*", "*quasi two dimensional, rotating around a vertical axis*", observed in the Daly River by WOLANSKI et al. (2004) about 20 minutes after the tidal bore passage (Fig. 5-7).

Some transient fronts were also observed behind some tidal bores and they can induce further secondary currents and vertical circulation. Figure 5-8 illustrates two examples of transient fronts in the Baie du Mont Saint Michel; in each case, the transient front arrived a couple of minutes after the bore front and lasted several minutes. The transient front was basically a zone of marked local gradients that highlihgted some singularity in terms of one or more parameters (DYER 1997). Secondary flows associated with such fronts can lead to enhanced scalar concentrations of larvae and pollutants, and enhanced sediment transport. Their presence influenced the horizontal dispersion and residual circulation in the flood flow.

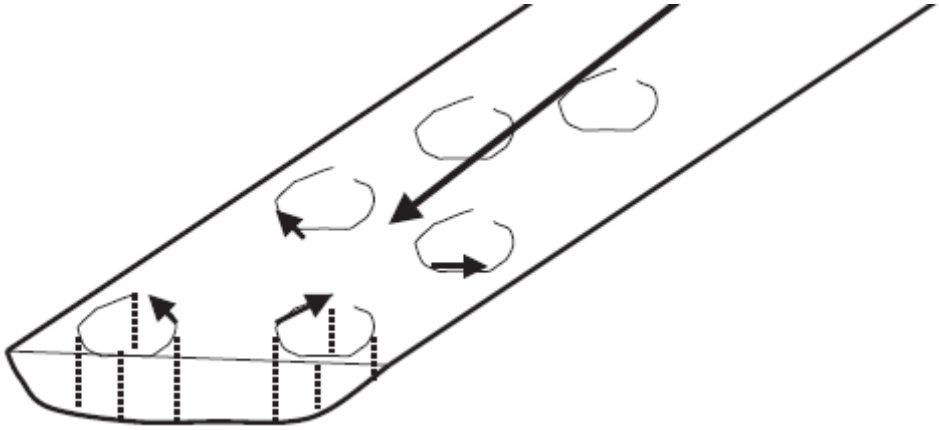

Fig. 5-7 - Surface macro-scale turbulence advected upstream behind the tidal bore of the Daly River and observed 20 minutes after the bore passage (after WOLANSKI et al. 2004, Fig. 1b)

Fig. 5-8 - Transient fronts behind tidal bores in the Baie du Mont Saint Michel (France)
(Left) in the Sélune River on 3 August 2008 about 3 minutes after the tidal bore, viewed from the left bank; (Right) in the Sée-Sélune River main channel on 14 October 2008 about 10 minutes after the tidal bore, viewed from the right bank at Pointe du Grouin du Sud

6. Conclusion

A tidal bore is a positive surge characterised by a sudden change in flow that increases the depth. Tidal bores are observed in estuaries when the tidal flow turns to rising, the tidal range exceeds 4 to 6 m, the estuarine bathymetry is funnel-shaped to amplify the tidal wave and the freshwater level is low (Fig. 6-1). Herein a new experimental investigation was conducted in a large rectangular channel (12 m long, 0.5 m wide). Some detailed velocity measurements were performed in the undular tidal bores with a high temporal and spatial resolution (200 Hz, sampling volume: 6×6×1.5 mm^3) while the free-surface elevations were recorded using non-intrusive acoustic displacement meters. The experiments were designed to study the effects of a short channel constriction on the undular tidal bores. The constriction had a simple shape that was a 1/20 scale model of the Pont Aubaud on the Sélune River in the Baie du Mont Saint Michel (Fig. 6-2). The experiments are illustrated by a series of five movies available in the form of a digital appendix (App. B) at the University of Queensland institutional open access repository UQeSpace {http://espace.library.uq.edu.au/}.

In the prismatic channel ([1]), an undular (non-breaking) bore was observed for surge Froude number Fr less than 1.5. The wave front consisted of a first wave followed by a train of well-defined free-surface undulations. For Fr < 1.2, the undulations were smooth and quasi-two dimensional. For 1.2 < Fr < 1.3, some cross-waves developed in front of the first wave crest and the shock waves propagated across the channel width. For 1.3 < Fr < 1.5, some breaking was seen at the first wave crest. For tidal bore Froude numbers greater than 1.5, a breaking bore was observed with a marked roller, although some surface upward curvature ahead of the roller was observed.

The free-surface properties of undular tidal bores were carefully documented. Following BENJAMIN and LIGHTHILL (1954) and MONTES (1986), the analysis of the parametric relationship between momentum function and specific energy showed that the undular flow properties were restricted to the subcritical, upper branch of the M-E diagram. The analysis indicated further that the effects of streamline curvature could not be ignored. The free-surface undulation profiles exhibited a quasi-periodic shape that followed closely a sinusoidal function and cnoidal wave function. Both field measurements and laboratory observations demonstrated however that neither the linear wave theory nor the Boussinesq equation theory captured the fine details of the free-surface profiles. Both field and laboratory data highlighted some asymmetrical wave shape for example. The data showed that the dimensionless undular wave height and wave steepness increased with increasing Froude number for 1 < Fr < 1.3 until an upper limit. The upper values were obtained for the flow conditions corresponding to the apparition of some small breaking at the first wave crest. An analysis of the potential energy showed further that the potential energy of the free-surface undulations represented up to 30% of the potential energy of the tidal bore.

The presence of a channel constriction had a major impact on the free-surface properties. In the channel throat, the wave motion was three-dimensional, pseudo-chaotic and energetic. Some shock reflection in the channel convergent was associated with the development of large-scale vortical structures at the free-surface.

[1] That is, in absence of the channel constriction.

In the divergent section, some large free-surface scars were observed highlighting some intense turbulence production in the wake of the sidewall expansion. The undular tidal bore lost nearly one third of its potential energy per surface area as it propagated through the channel constriction. While no information was recorded in terms of the kinetic energy, the present findings demonstrated some significant impact of the simple channel constriction comparable to a set of bridge piers.

The detailed instantaneous velocity measurements showed a marked effect of the tidal bore passage in a prismatic channel. The streamwise velocities were characterised by some flow deceleration at all vertical elevations, and some large fluctuations of all velocity components were recorded beneath the bore and undulations. The velocity measurements showed some small to moderate effects of the channel constriction on the unsteady turbulent velocity field. However the velocity data sets suggested the upstream advection of energetic events and vorticity "clouds" behind the bore front in both channel configurations: prismatic and with constriction. This was seen in particular by some sudden and rapid fluctuations of the transverse velocity data V_y/V_o. It is suggested herein that these energetic turbulent events were some form of macro-turbulence advected upstream behind the bore. When the tidal bore propagated upstream in a prismatic channel, it induced some strong turbulent mixing and intense secondary motion. It is hypothesised that some strong turbulent kinetic energy was produced next to the step corners beneath the wave troughs. In presence of a channel constriction, some strong macro-scale turbulence was produced additionally as the tidal bore propagated through the constriction, and some intense vorticity was generated and later advected behind the bore front. The proposed mechanisms were consistent with some field observations in the Daly River tidal bore in 2003.

(A) Undular tidal bore of the Garonne River at Arcins (France) on 6 July 2008 - Shutter speed: 1/20 s

(B) Tidal bore of the Sélune River in the Baie du Mont Saint Michel (France) passing Roche Torin on 19 September 2008 - Note the "wavy" transverse profile of the undular tidal bore (propagation from left to right) - Shutter speed: 1/800 s

Fig. 6-1 - Photographs of undular tidal bores

Fig. 6-2 - Propagation of the Sélune River tidal bore beneath the Pont Aubault, Pontaubault (France) on 31

August 2008 at 20:35 - View from the left bank; note the kayaker riding the first wave of the undular tidal bore

7. Acknowledgements

The author thanks Dr Dominique MOUAZÉ (University of Caen, France) for their detailed review of the report and most valuable comments. He acknowledges the technical assistance of Graham ILLIDGE and Clive BOOTH (The University of Queensland).

Appendix A - Photographs of the experimental facilities and of the experiments

A.1 Presentation

Detailed experimental measurements were conducted for a range of flow conditions that are summarised in Table A-1. Some photographs of the experimental facility are presented in the next paragraphs. A series of short movies were taken during some key experiments and presented in Appendix B.

Table A-1 - Detailed turbulence measurements beneath positive surge fronts

Reference	S_o	Q	d_o	Gate opening h	Surge type at x = 5 m	U	Fr	Remarks
		m^3/s	m	m		m/s		
(1)	(2)	(3)	(4)	(5)	(6)	(7)	(8)	(9)
Present study								Smooth bed. L = 12 m, B = 0.5 m.
Series 1	0	0.0089 to 0.0511	0.056 to 0.212	0 to 0.07	Undular to breaking	0.67 to 1.37	1.04 to 1.95	Free-surface measurements. Runs 090122_01 to 090423_803
Series 2a	0	0.0190	0.115	0	Undular	1.05	1.16	Turbulence measurements. Runs 090424_901-906
Series 2b	0	0.0190	0.165 to 0.170	0	Undular	1.2 to 1.25	1.10 to 1.13	Turbulence measurements. Runs 090427_911-927.
Series 2c	0	0.0188	0.199	0	Undular	1.2 to 1.3	1.08	Turbulence measurements. Runs 090429_930-939.

Notes: d_o: initial depth measured at x = 5 m (in absence of construction) or x = 3.6 m (with constriction); Fr: surge Froude number ($Fr = (V_o + U)/\sqrt{g \times d_o}$); Q: initial steady flow rate; U: surge front celerity measured at x = 5 m; ($^+$) at 5.2 m upstream of the gate; (*) measured above the screens.

A.2 Photographs of the channel and experimental setup

(A) View from upstream with the intake reservoir on the centre right (dark grey) - Note the smaller 0.25 m wide channel (in light blue) in the background

(B) View from downstream with the channel downstream section, the tainter and radial gates and dropshaft (on the left) downstream of the radial gate

(C) Looking upstream with the main flow direction from right to left

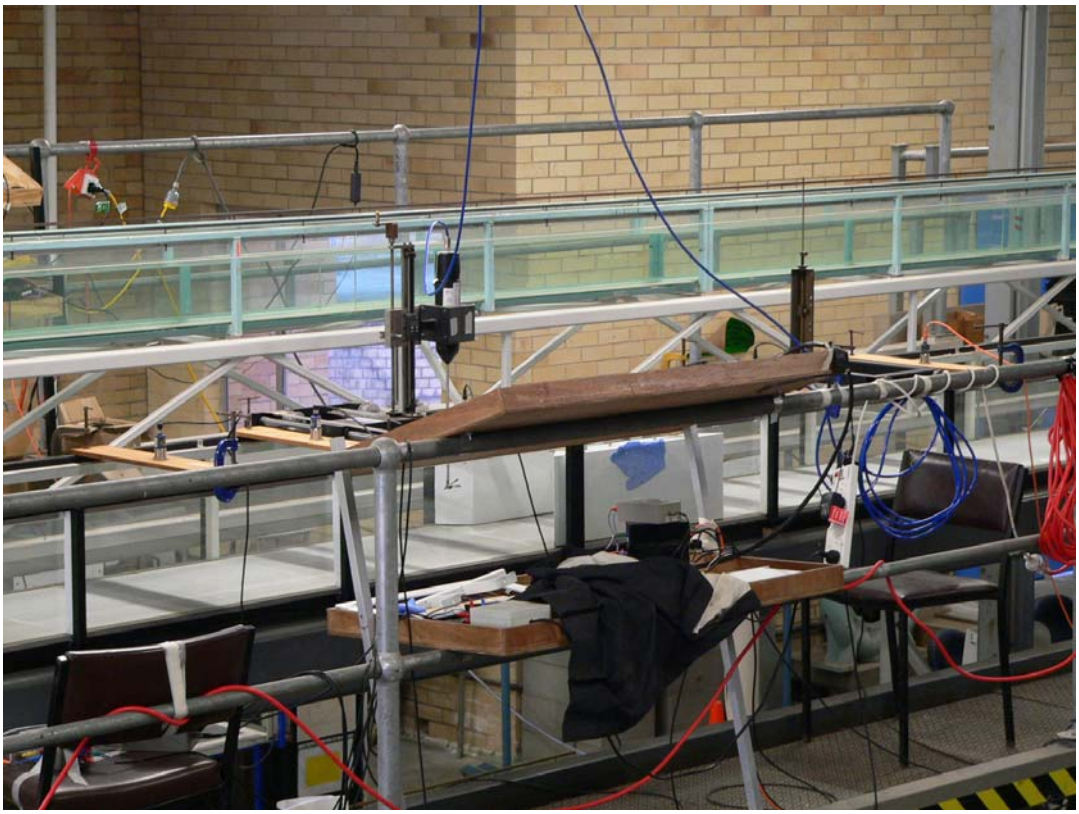

(D) Measurement section - The ADV was mounted at x = 5 m and the channel constriction was installed (white painted mortar)

Fig. A-1 - General views of the experimental channel

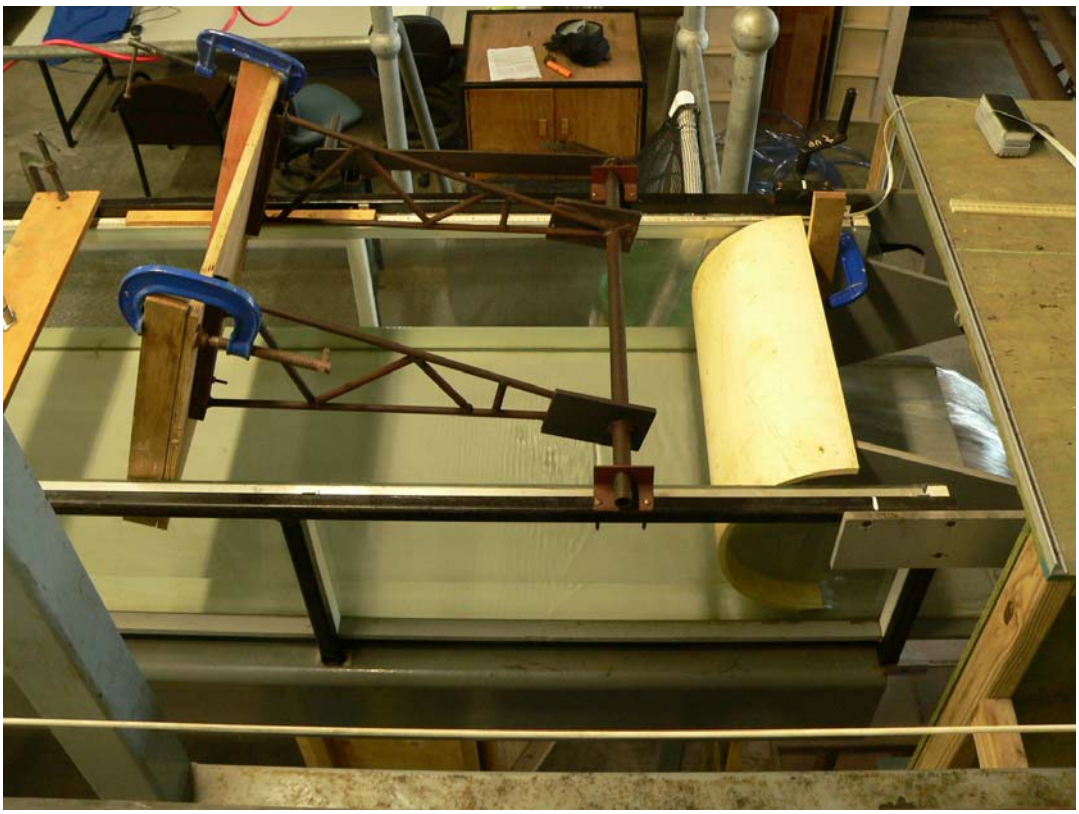

(A) Details of the radial gate located at x = 11.9 m (on the right) - The tainter gate (left) was fully opened - Flow direction from left to right

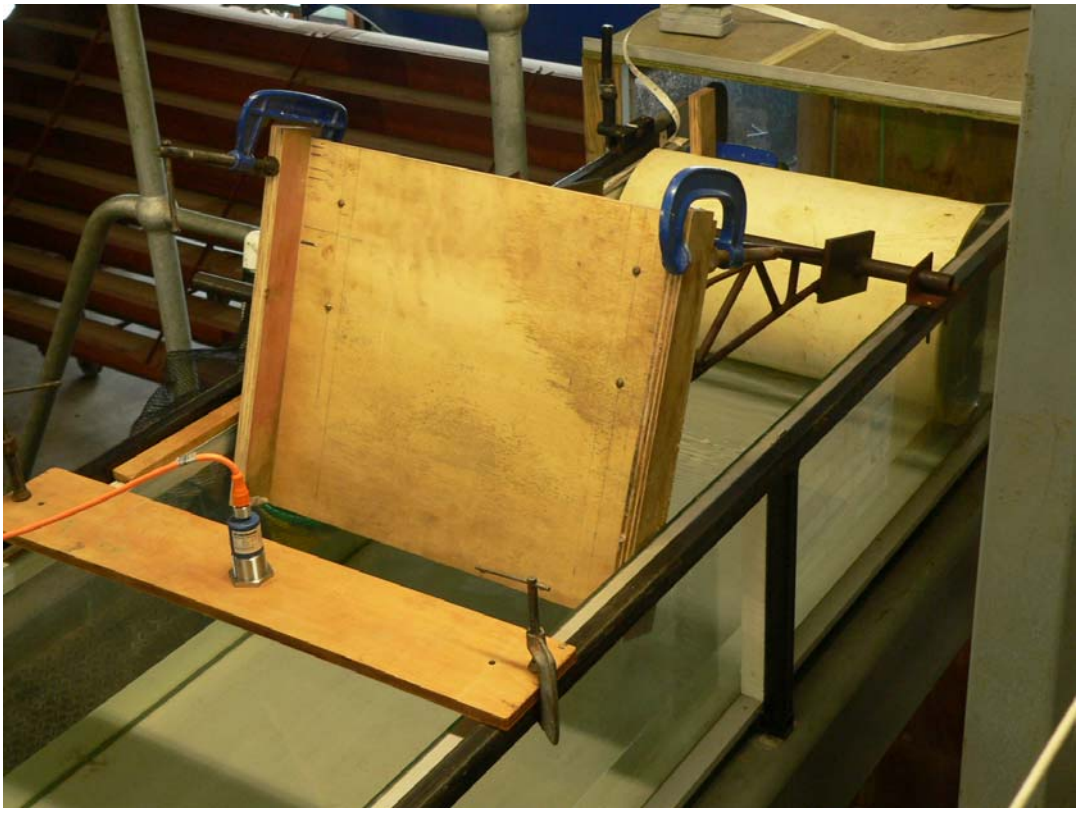

(B) Details of the fast-closing tainter gate located at x = 11.15 m - Steady flow direction from bottom left to top right - The tainter gate was fully opened - Note the Mic+35 acoustic displacement meter on the foreground (left) located at x = 10.8 m, and the radial gate in the background (right)

Fig. A-2 - Details of the radial and tainter gates at the channel downstream end - Run 090415_61, Q =

0.00895 m^3/s, d_o = 0.0845 m (x=3.6 m), Fr_o = 0.23

Fig. A-3 - Acoustic Doppler velocimeter (ADV) sampling at x = 5 m - Note the four receiver side-looking ADV head sampling at z = 0.0654 m and the Mic+25 acoustic displacement sensor recording the water elevation immediately above the ADV sampling volume - Steady flow direction from right to left - Run 090417_66, Q = 0.0190 m^3/s, d_o = 0.1147 m (x = 3.6 m), Fr_o = 0.31

(A) Details of the two half-sections

(B) Looking upstream with the acoustic displacement sensors in the foreground and background

Fig. A-4 - Details of the channel constriction - Steady flow direction from right to left

A.3 Experimental observation of the tidal bore generation process

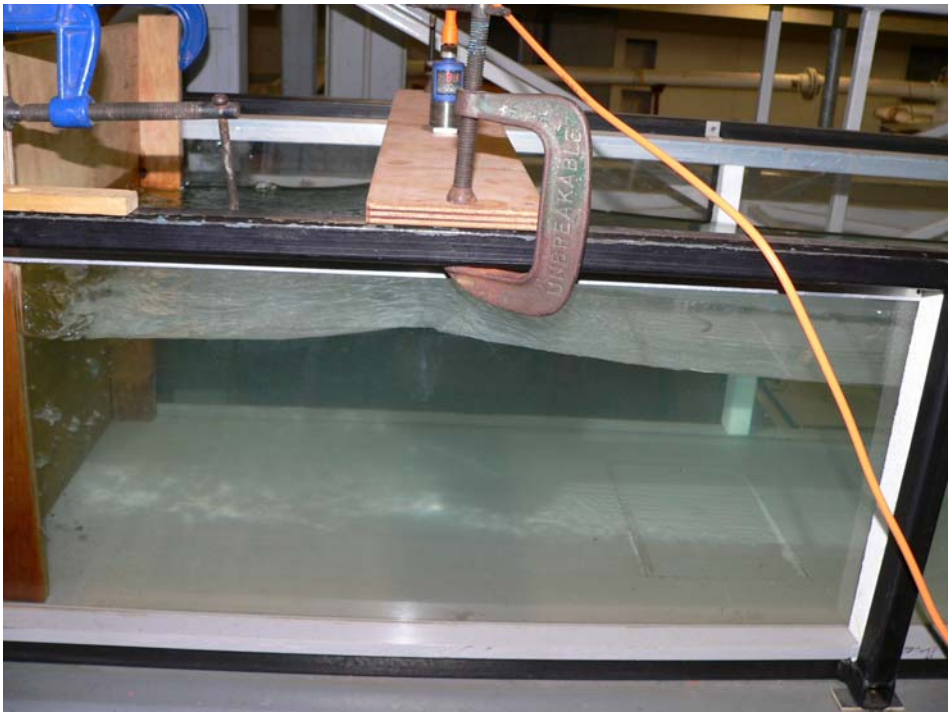

(A) Run 090429_936a, Q = 0.0188 m^3/s, d_o = 0.1989 m at x=3.6 m, Fr_o = 0.14, Bore Froude number: Fr = 1.08 (Shutter speed: 1/80 s) - Note the closed tainter gate on the far left and the Mic+35 acoustic displacement sensor located at x = 10.8 m immediately above the bore front

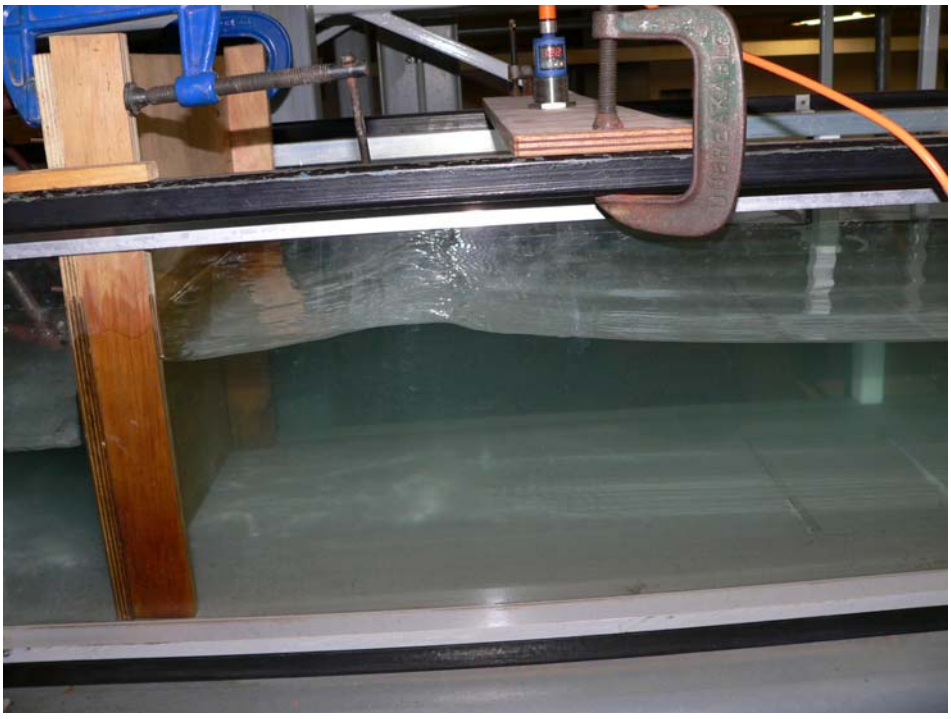

(B) Run 090427_922a, Q = 0.0190 m^3/s, d_o = 0.165 m at x=3.6 m, Fr_o = 0.18, Bore Froude number: Fr = 1.13 (Shutter speed: 1/80 s) - Note the closed tainter gate on the far left and the Mic+35 acoustic displacement sensor

Fig. A-5 - Undular tidal bore generation by the rapid closure of the tainter gate - Initially steady flow propagation from right to left and tidal bore propagation from left to right

A.4 Experimental observations in a prismatic rectangular channel

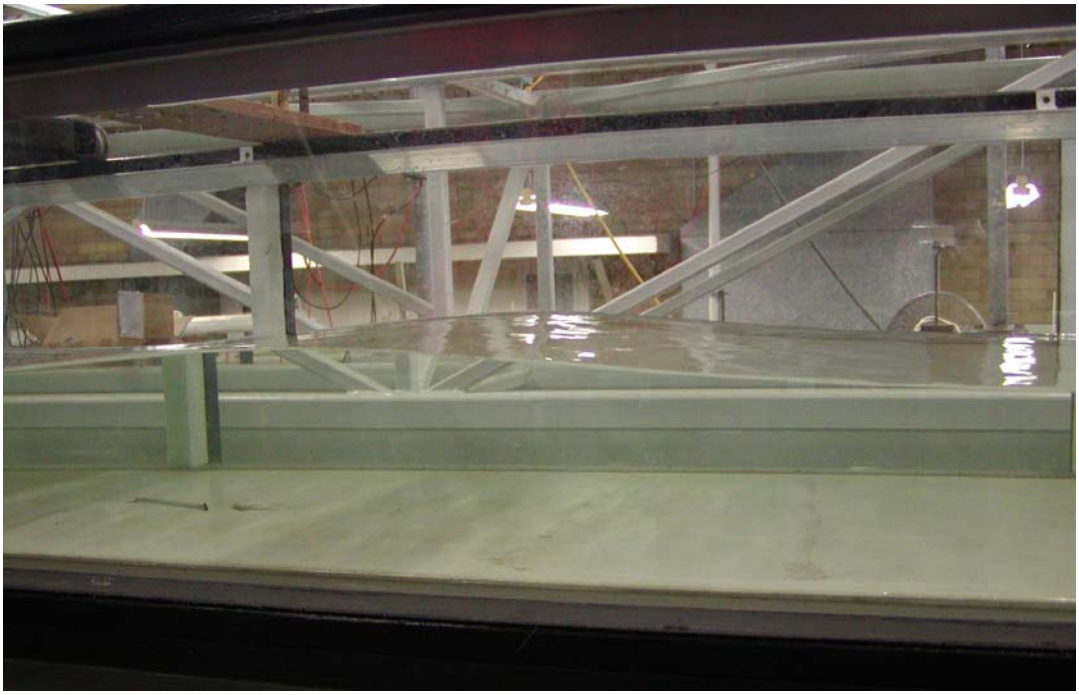

(A) Gentle undular bore (no cross-wave) passing x = 3.5 to 4 m - Run 090305_22, Q = 0.019 m^3/s, d_o = 0.1015 mm (at x = 4.8 m), Fr = 1.150, U = 0.781 m/s, Shutter speed: 1/40 s (Filename: P1010009.jpg)

(B) Steep undular bore passing x = 4.5 to 4.8 m - Run 090305_21, Q = 0.019 m^3/s, d_o = 0.1015 mm (at x = 4.8 m), Fr = 1.338, U = 0.917 m/s, Shutter speed: 1/40 s (Filename: P1010007.jpg)

Fig. A-6 - Photographs of undular bores for Q= 0.019 m^3/s, d_o = 0.1015 mm (at x = 4.8 m) - Bore propagation from left to right (unless otherwise indicated)

Fig. A-7 - Undular tidal bore with cross-waves passing x = 4.7 m - Bore propagation from left to right - Run 090306_32, Q = 0.0283 m^3/s, d_o = 0.1025 mm (at x = 4.8 m), Fr = 1.332, U = 0.792 m/s, Shutter speed: 1/40 s (Filename: P1010014.jpg)

A.5 Experimental observations in a rectangular channel with a channel constriction

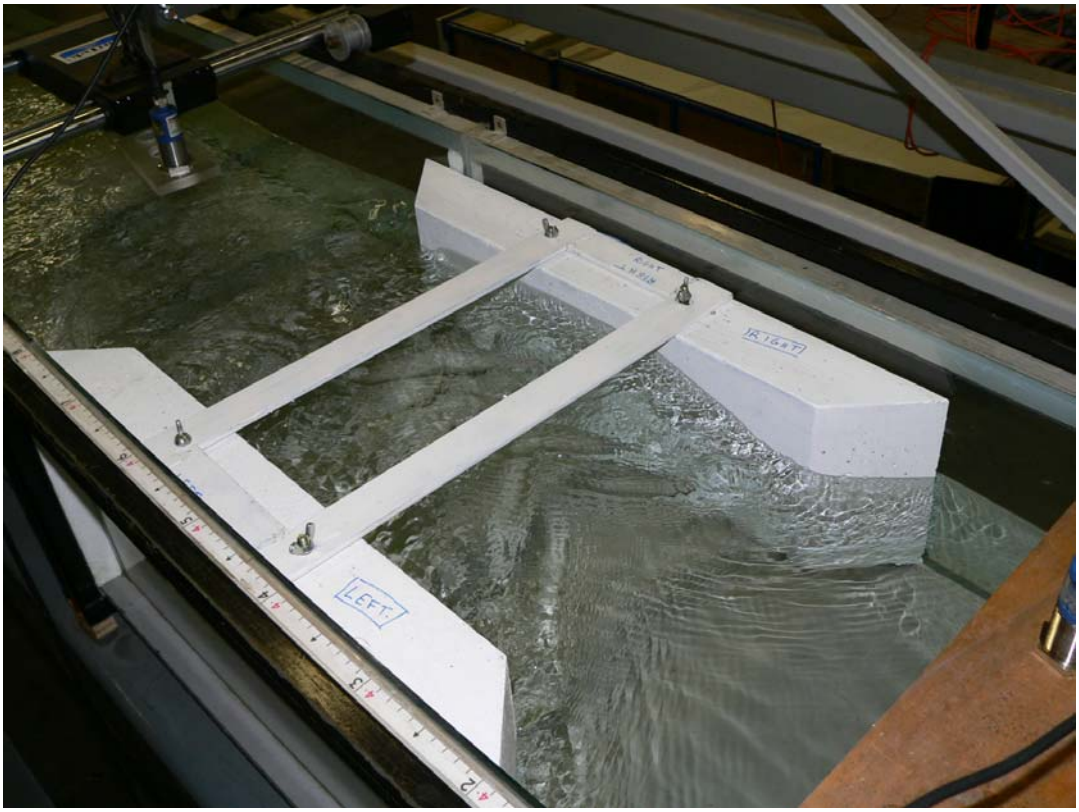

(A) First wave crest between the channel constriction - Shutter speed: 1/80 s (Filename: P11300846.jpg)

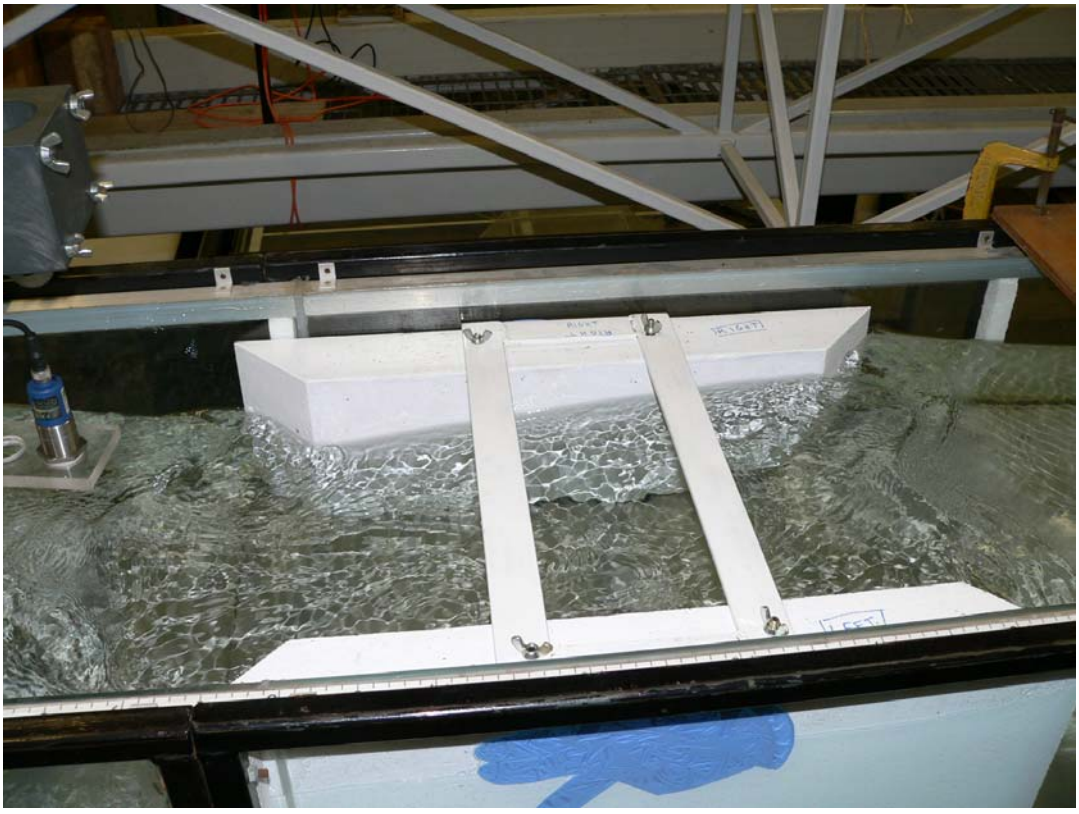

(B) First wave crest exiting the channel constriction - Shutter speed: 1/80 s (Filename: P11300848.jpg)

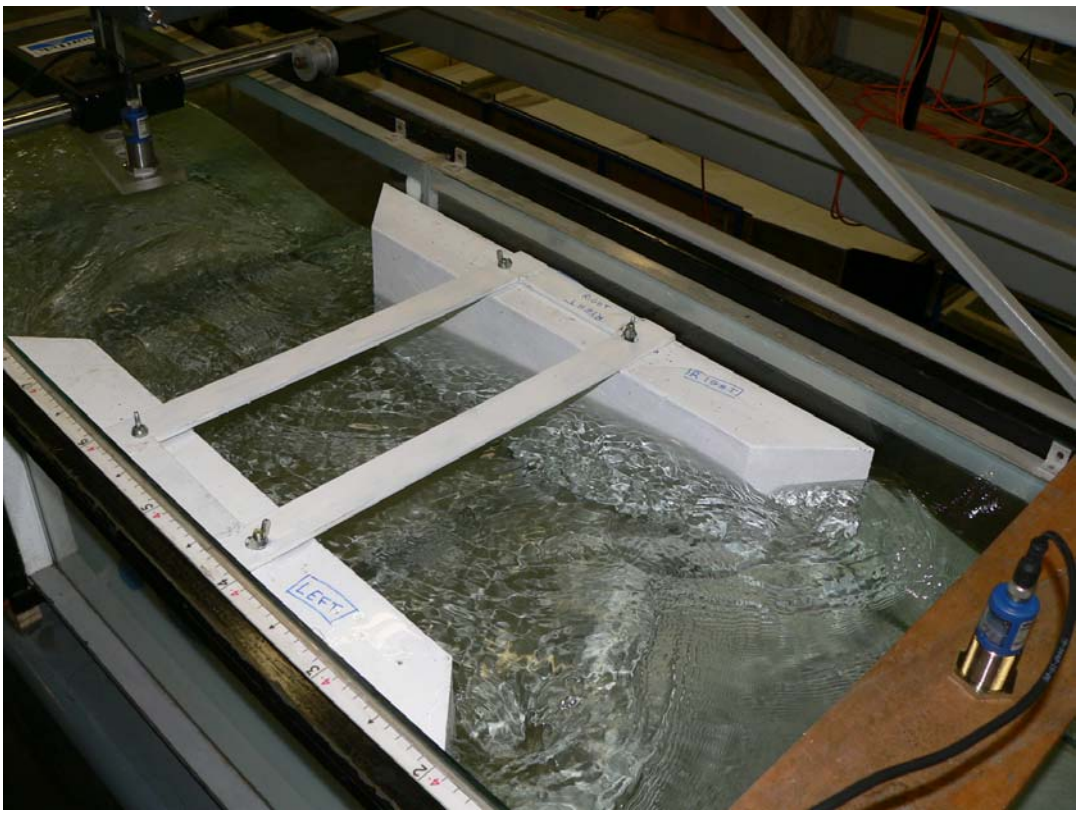

(C) First wave crest exiting the channel constriction - Note the complicated turbulent pattern upstream of the channel constriction (right) - Shutter speed: 1/80 s (Filename: P11300852.jpg)

Fig. A-8 - Undular tidal bore passage between the channel constriction - Bore propagation from left to right - Run 090318_00, Q = 0.0232 m^3/s, d_o = 0.1552 mm (at x = 3.6 m), Fr = 1.15, U = 1.10 m/s

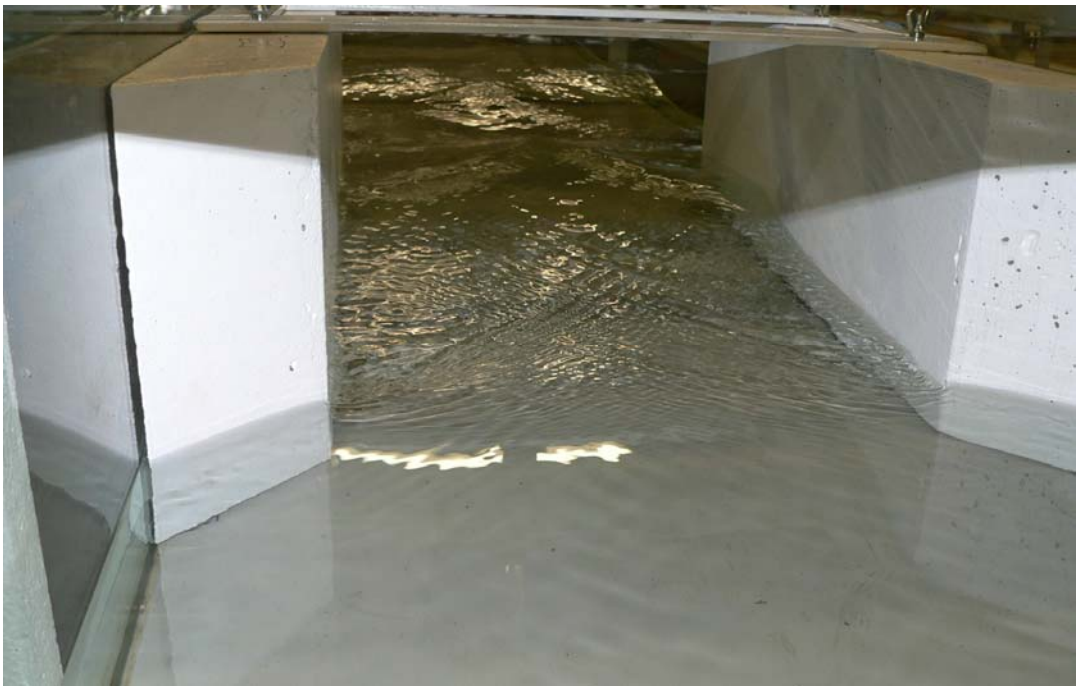

Fig. A-9 - Undular tidal bore propagation, looking downstream with the first wave crest in the constriction throat - Shutter speed: 1/80 s - Run 090324_00, Q = 0.0097 m^3/s, d_o = 0.0882 mm (at x = 3.6 m), Fr = 1.23, U = 0.885 m/s (Filenames: 1140030.jpg)

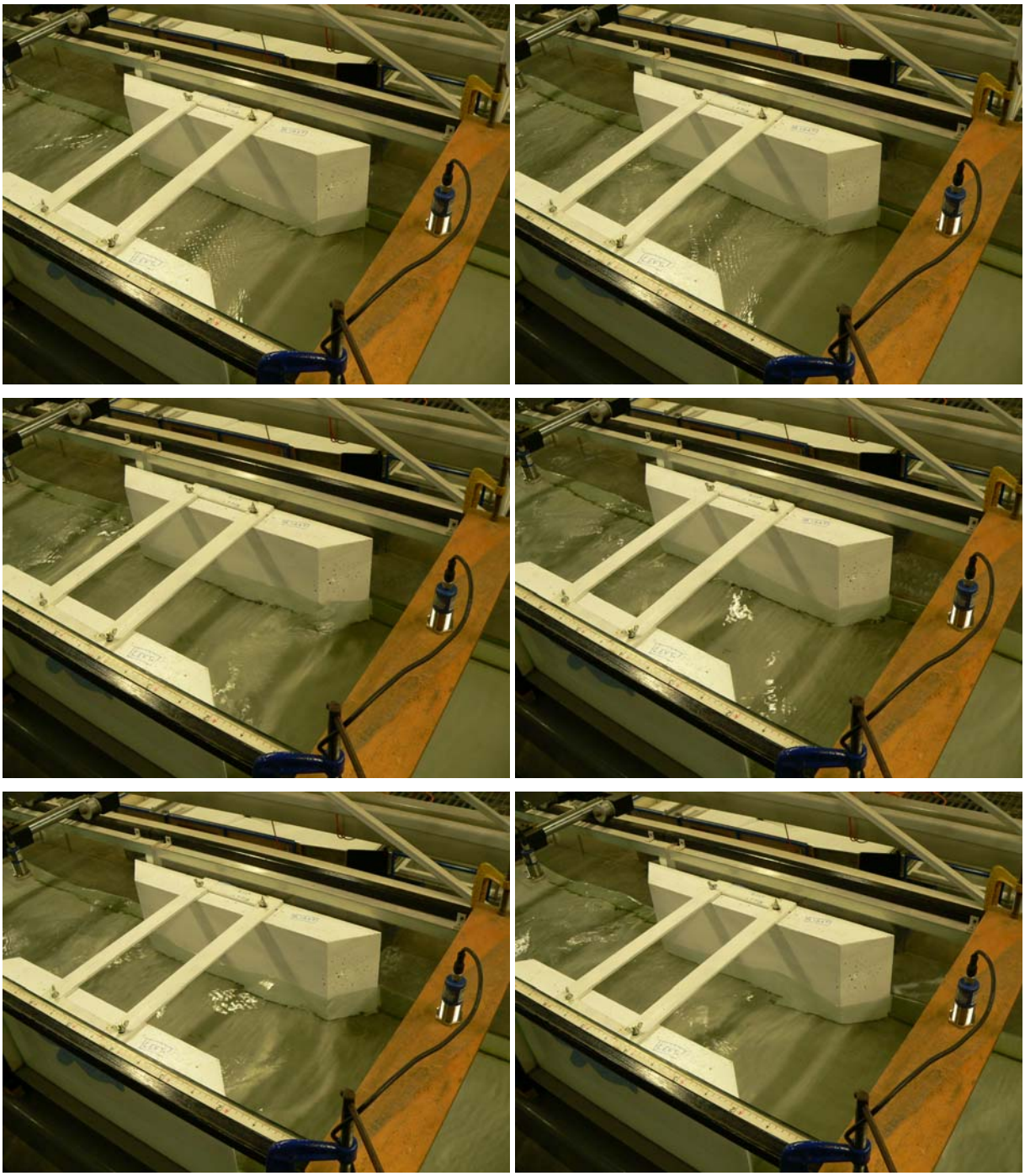

Fig. A-10 - Undular tidal bore propagation from left to right between the channel constriction - From left to right, top to bottom: $t = t_o$, t_o+0.5 s, t_o+1 s, t_o+1.5 s, t_o+2 s, t_o+2.5 s, Shutter speed: 1/40 to 1/50 s - Run 090324_00, Q = 0.0097 m^3/s, d_o = 0.0882 mm (at x = 3.6 m), Fr = 1.23, U = 0.885 m/s (Filenames: 1140022.jpg to 1140027.jpg)

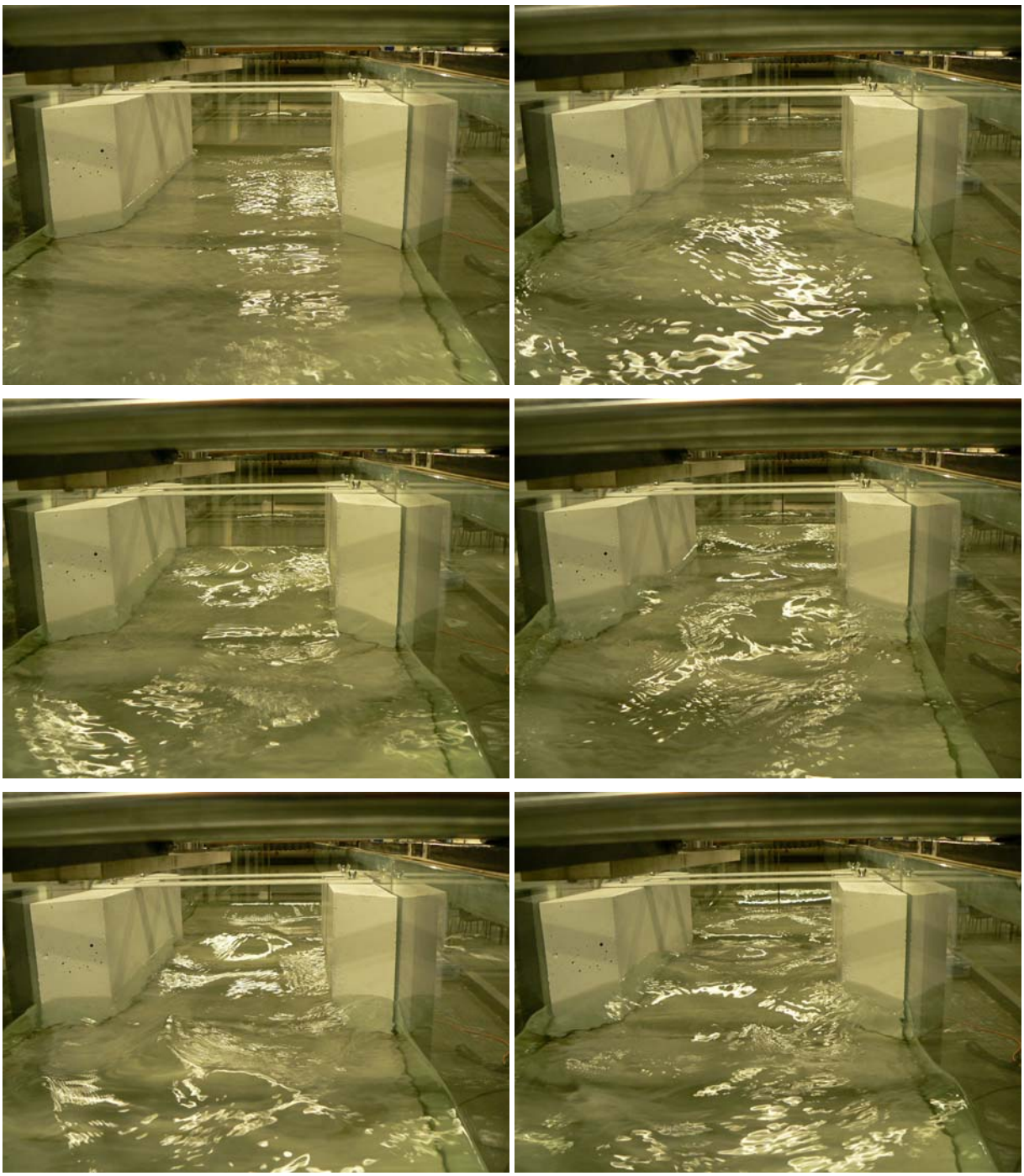

Fig. A-11 - Undular tidal bore, looking upstream at the propagation between the constriction - Note the free-surface turbulence in the foreground caused by some reflection as well as the three-dimensional nature of the flow in the throat - From left to right, top to bottom: $t = t_o$, t_o+0.5 s, t_o+1 s, t_o+1.5 s, t_o+2 s, t_o+2.5 s, Shutter speed: 1/40 s - Run 090324_00, Q = 0.0097 m^3/s, d_o = 0.0882 mm (at x = 3.6 m), Fr = 1.23, U = 0.885 m/s (Filenames: 1140033.jpg to 1140038.jpg)

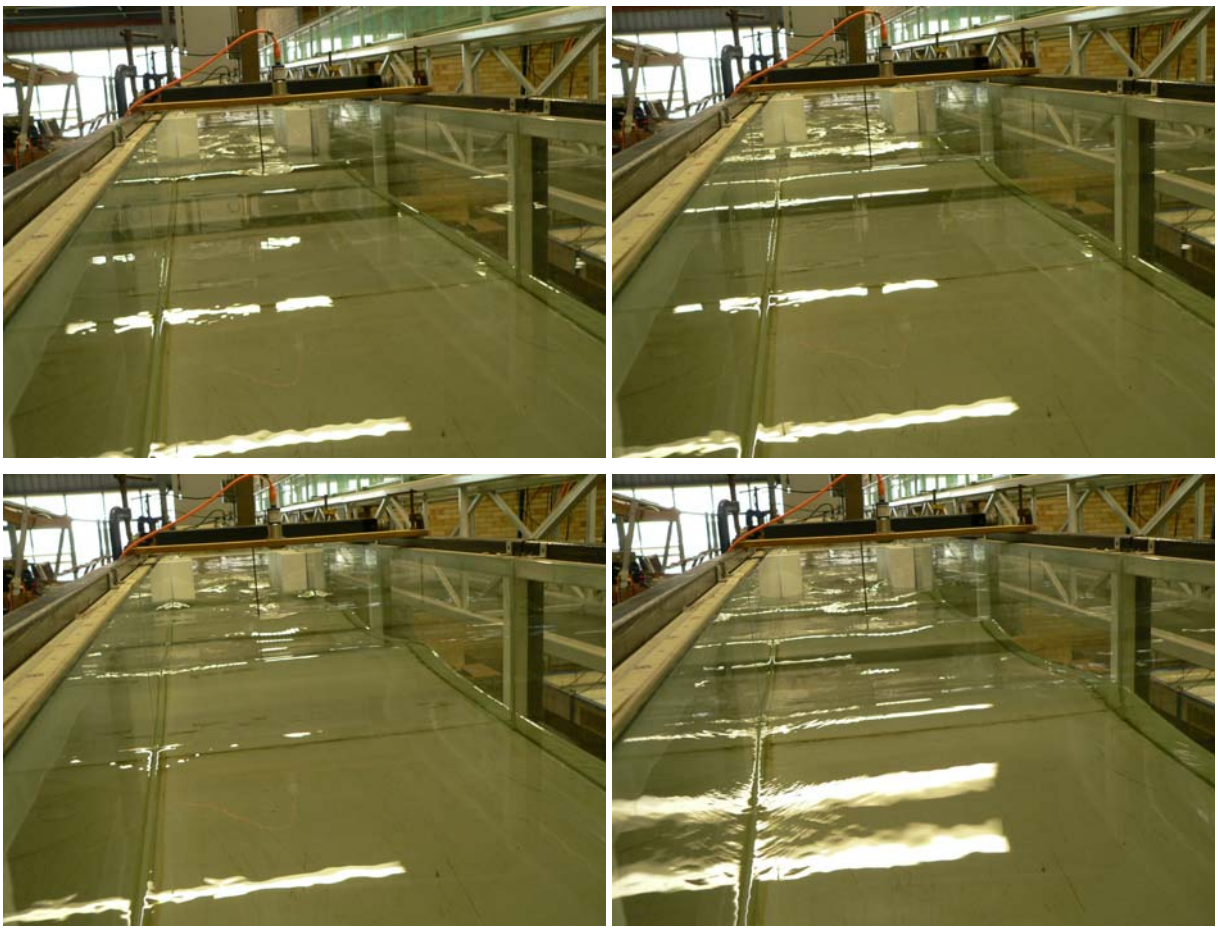

Fig. A-12 - Undular tidal bore, looking downstream at the propagation after the constriction - From left to right, top to bottom: $t = t_o$, t_o+0.5 s, t_o+1 s, t_o+1.5 s, Shutter speed: 1/50 s - Run 090415_61, Q = 0.0089 m^3/s, d_o = 0.0845 mm (at x = 3.6 m), Fr = 1.16, U = 0.85 m/s (Filenames: 1140198.jpg to 1140201.jpg)

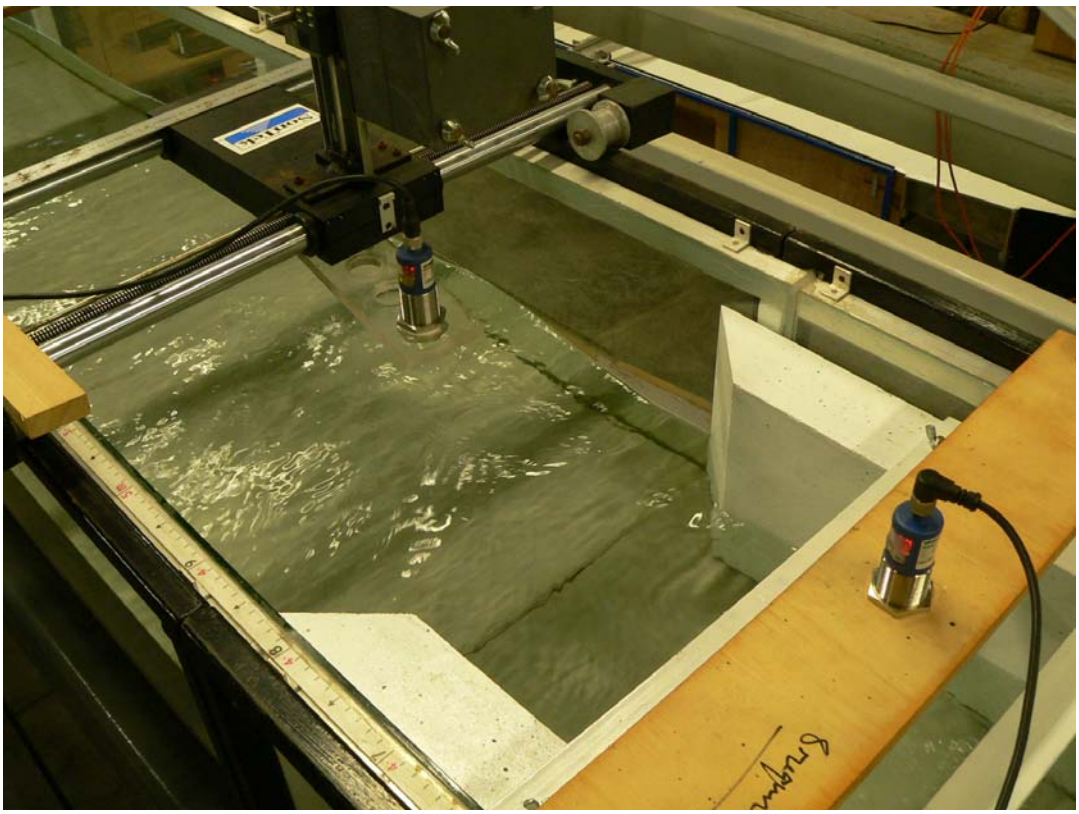

(A) First wave crest immediately before the constriction: t = t_o - Shutter speed: 1/50 s (Filename: 1140227.jpg)

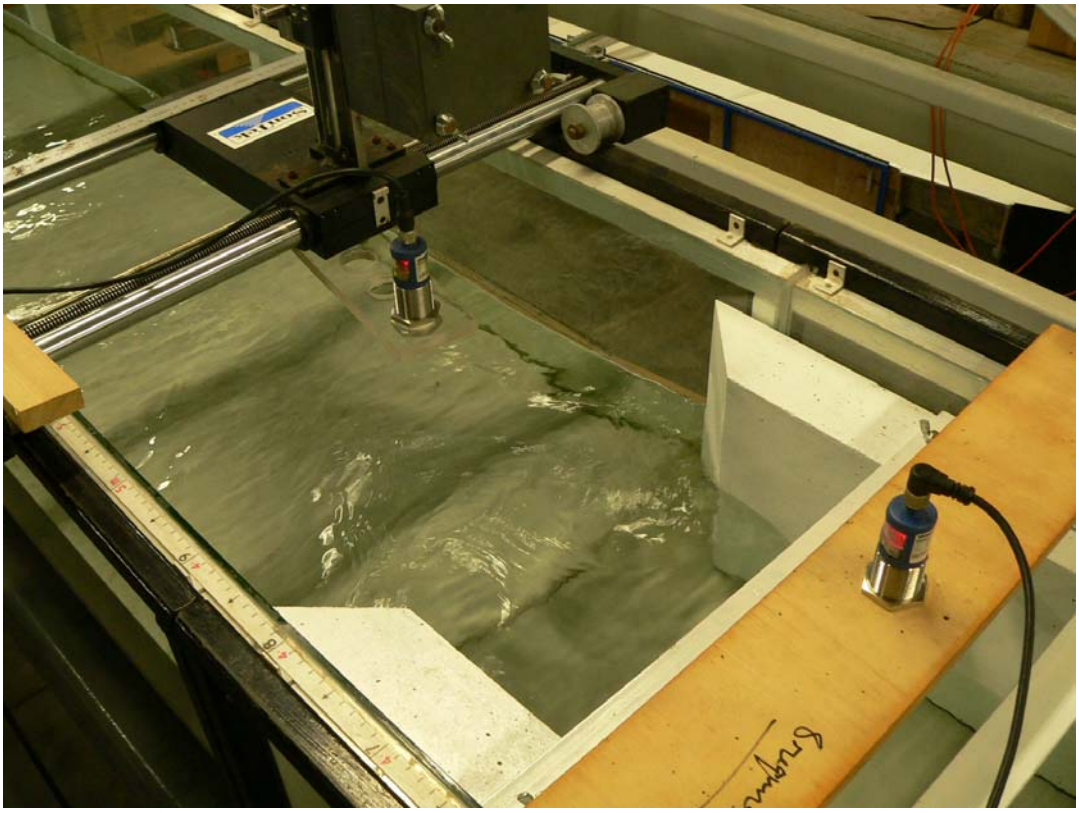

(B) First wave crest entering the constriction: t = t_o + 0.5 s- Note the free-surface turbulence and scars next to the throat start - Shutter speed: 1/50 s (Filename: 1140228.jpg)

Fig. A-13 - Undular tidal bore, looking at the first wave crest entering the constriction - Run 090415_61, Q = 0.0089 m^3/s, d_o = 0.0845 mm (at x = 3.6 m), Fr = 1.16, U = 0.85 m/s

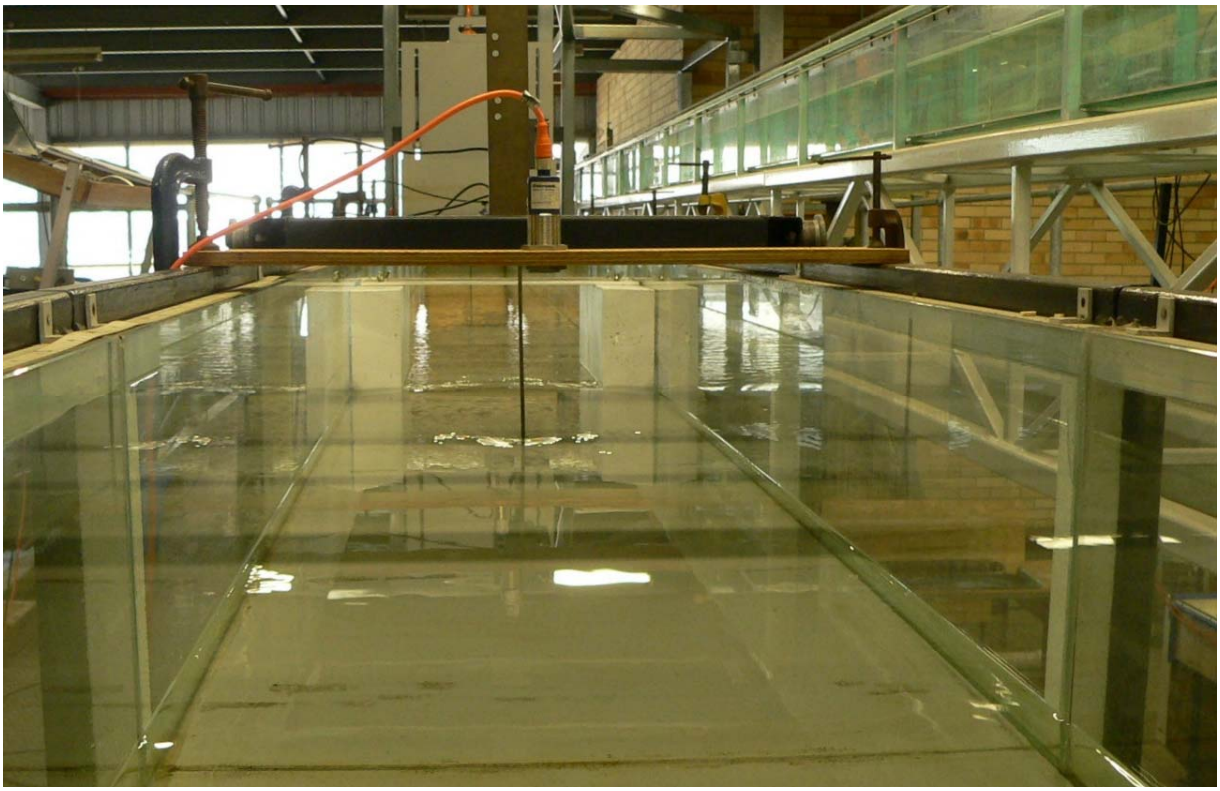

Fig. A-14 - Undular tidal bore, looking downstream at the bore exiting the constriction throat - Shutter speed: 1/40 s - Run 090415_61, Q = 0.0089 m^3/s, d_o = 0.0845 mm (at x = 3.6 m), Fr = 1.16, U = 0.85 m/s (Filename: 1140233.jpg)

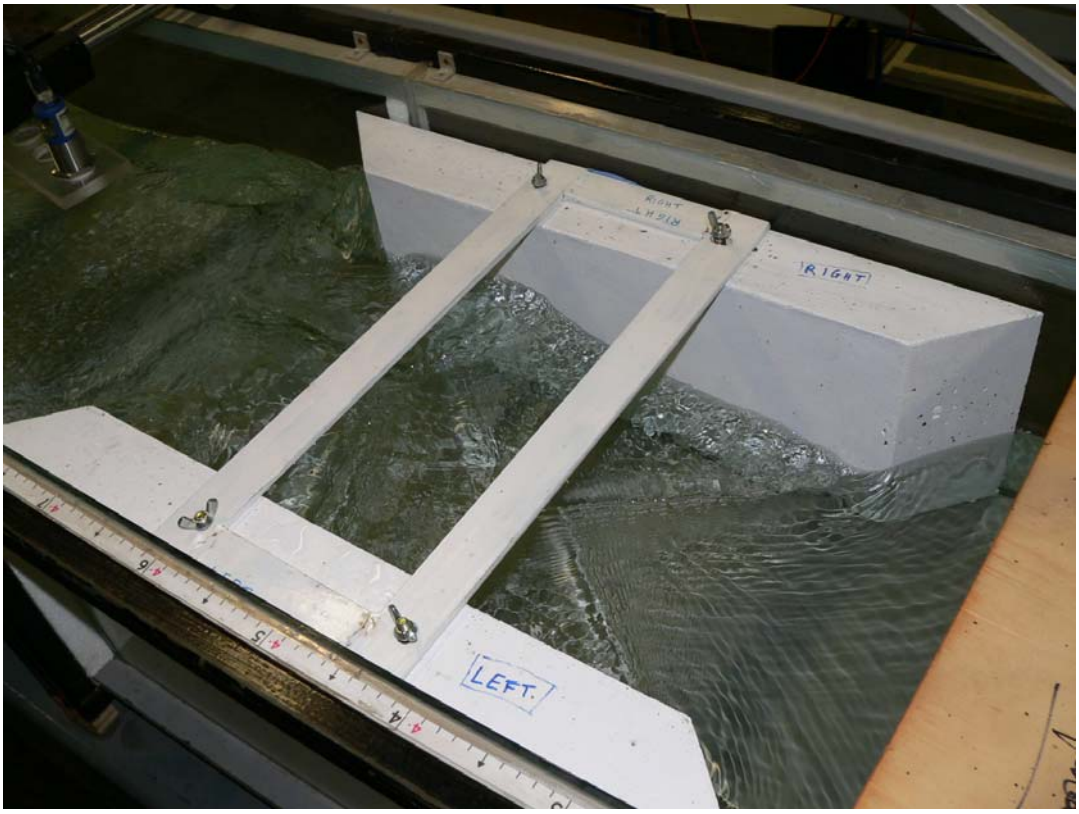

Fig. A-15 - Undular tidal bore entering the constriction throat - Note the steady flow cross-waves at the upstream end of the throat - Shutter speed: 1/80 s - Run 090417_65, Q = 0.0193 m^3/s, d_o = 0.117 mm (at x =

3.6 m), Fr = 1.14, U = 0.89 m/s (Filename: 1140310.jpg)

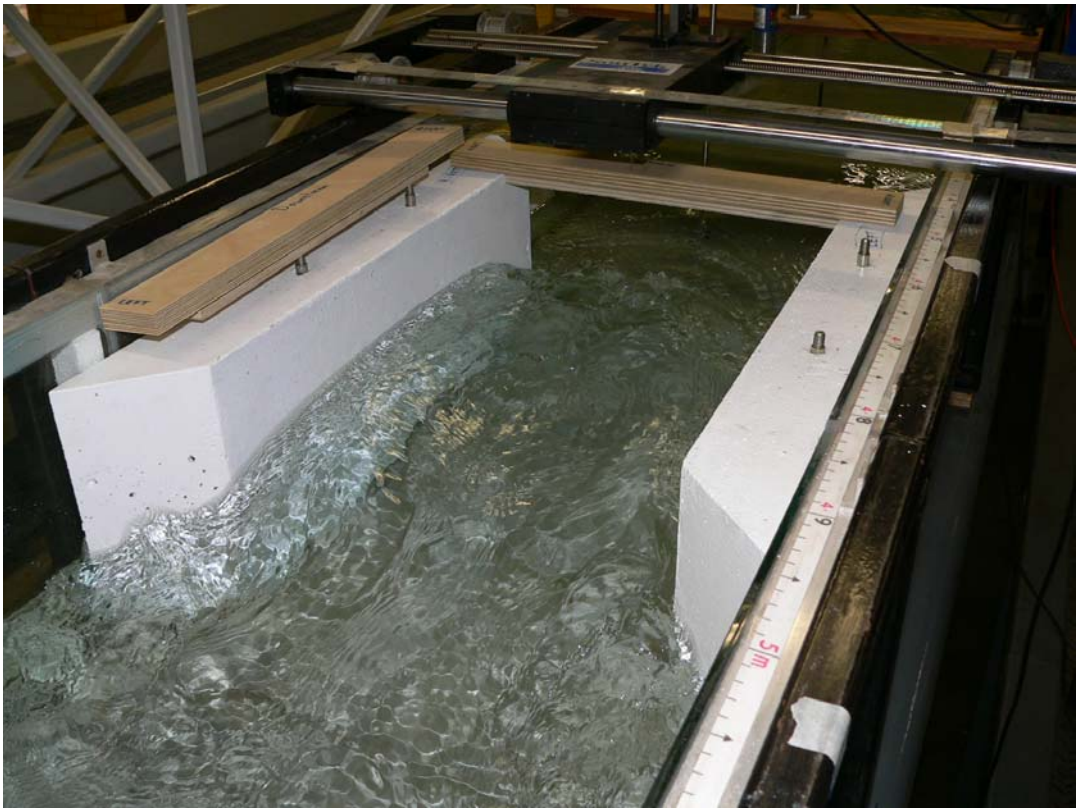

(A) Note the bore surface turbulence in the throat - Shutter speed: 1/80 s (Filename: 1140335.jpg)

(B) Details of the surface turbulence and scars - Shutter speed: 1/80 s (Filename: 1140338.jpg)

Fig. A-16 - Propagation of the first wave crest in the constriction throat - Run 090424_901, Q = 0.019 m^3/s, d_o = 0.1147 mm (at x = 3.6 m), Fr = 1.16, U = 0.90 m/s

(A) Bore propagation from bottom left to upper right - Shutter speed: 1/80 s (Filename: 1140364.jpg)

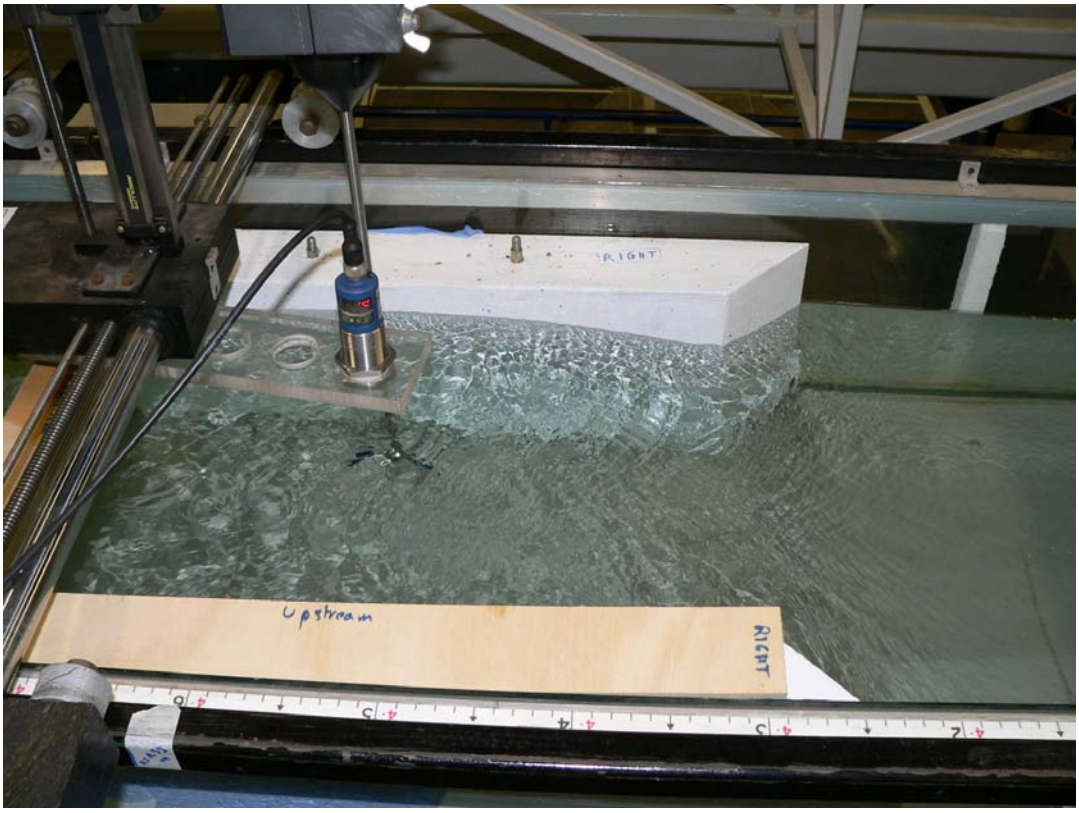

(B) Bore propagation from left to right - Shutter speed: 1/80 s (Filename: 1140382.jpg)

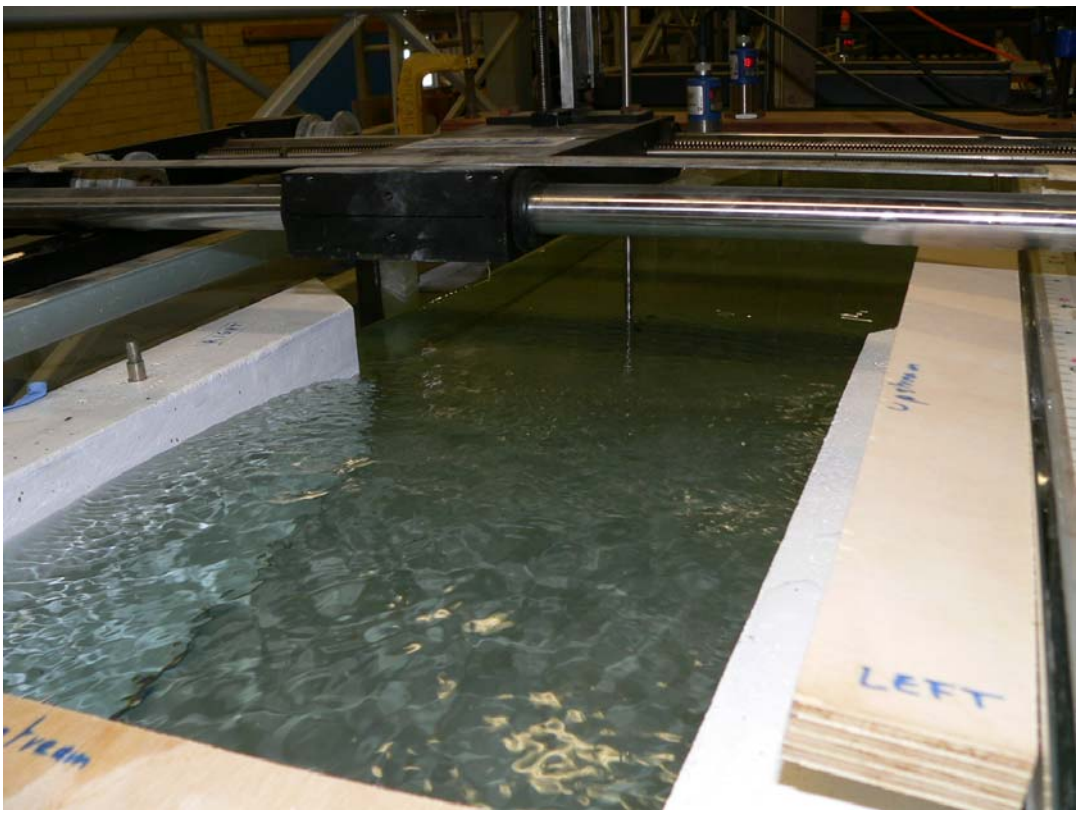

(C) Looking upstream - Shutter speed: 1/80 s (Filename: 1140384.jpg)

Fig. A-17 - Propagation of the first wave crest in the constriction throat - Run 090427_911a, Q = 0.019 m^3/s, d_o = 0.1703 mm (at x = 3.6 m), Fr = 1.10, U = 1.203 m/s

Appendix B - Movies of the experiments

B.1 Introduction

Detailed experimental measurements were conducted, and some photographs of the experimental facility are presented in Appendix A. A series of short movies were further taken during some key experiments. The movie files are deposited with the digital record of the publication at the institutional open access repository of the University of Queensland: {http://espace.library.uq.edu.au/}. They are listed as part of the technical report deposit at {http://espace.library.uq.edu.au/list/author_id/193/}. The list of the movies is detailed in section B.2, including the filenames, file format, and a description of each video.

B.2 List of movies

Filename	Format	Description
P1010015.mov	Quicktime	Two-dimensional undular wave (Fr = 1.17) - Duration: 3 s. Run 090309_41, Q= 0.040 m^3/s, d_o = 0.179 m, S_o = 0, Fr = 1.17, U = 1.136 m/s.
P1130854.mov	Quicktime	Two-dimensional undular wave (Fr = 1.15) propagating (from right to left) between constriction - Duration: 9 s. Run 090318_00, Q= 0.0232 m^3/s, d_o = 0.155 m, S_o = 0, Fr = 1.15, U = 1.11 m/s.
P1140031.mov	Quicktime	Two-dimensional undular wave (Fr = 1.23) propagating between constriction, looking downstream - Duration: 6 s. Run 090324_00, Q= 0.0097 m^3/s, d_o = 0.0828 m, S_o = 0, Fr = 1.23, U = 0.885 m/s.
P1140032.mov	Quicktime	Two-dimensional undular wave (Fr = 1.23) propagating between constriction, looking upstream - Duration: 5 s. Run 090324_00, Q= 0.0097 m^3/s, d_o = 0.0828 m, S_o = 0, Fr = 1.23, U = 0.885 m/s.
P1140315.mov	Quicktime	Two-dimensional undular wave (Fr = 1.15) propagating (from left to right) between a half-constriction - Duration: 6 s. Run 090417_66, Q= 0.0193 m^3/s, d_o = 0.1145 m, S_o = 0, Fr = 1.15, U = 0.88 m/s.

B.3 Movie files

The movies files of Appendix B are available in the institutional open access repository of the University of Queensland (Brisbane, Australia) and they are deposited at UQeSpace {http://espace.library.uq.edu.au/}. The Digital Files are a series of Quicktime™ movies. The deposited movie files (Section B.2) were converted to Flash video for video streaming.

At request, the writer may provide the Quicktime™ movies as a single compressed file (Filename Movie_File.7z). The file was prepared with 7-zip version 4.23. The software 7-zip is an open source

software. Most of the source code is under the GNU LGPL license. The unRAR code is under a mixed license: GNU LGPL + unRAR restrictions. The software 7-zip may be freely downloaded from {www.7-zip.org}.

CHANSON, H. (2009). "An Experimental Study of Tidal Bore Propagation: the Impact of Bridge Piers and Channel Constriction." *Hydraulic Model Report No. CH74/08*, School of Civil Engineering, The University of Queensland, Brisbane, Australia, 110 pages & 5 movie files (ISBN 9781864999600).

Further details on the report including the digital appendix may be obtained from Prof. Hubert CHANSON {h.chanson@uq.edu.au}.

Appendix C - Undular tidal bore free-surface measurements

C.1 Presentation

The new experiments were performed in a 12 m long, 0.5 m wide flume at the University of Queensland. The flume was made of a smooth PVC bed and glass walls, and the slope was horizontal for all the experiments. The unsteady water depths were measured with a series of acoustic displacement meters. A Microsonic™ Mic+35/IU/TC unit was located immediately upstream of the tainter gate and a further 6 acoustic displacement meters Microsonic™ Mic+25/IU/TC were spaced along the channel at x = 10.8 m (Mic+35), 8.0 m, 6.0 m, 5.0 m, 4.55 m, 4.0 m, and 3.0 m, where x is the longitudinal distance from the channel upstream end. The sensors were located above the channel centreline

The experimental setup was selected to generate an initially steady, subcritical flow for a given initial flow rate Q. At the downstream end of the flume (x = 11.9 m), a radial gate controlled the initially-steady subcritical flow; the gate opening remained unchanged for all the duration of an experiment. The tidal bore was generated by the rapid partial (or complete) closure of the downstream tainter gate located at x = 11.15 m. After closure, the bore propagated upstream and each experiment was stopped when the bore front reached the intake structure to avoid wave reflection interference.

For some experiments, two half-channel constrictions were introduced between x = 4.88 m and 4.21 m (Fig. C-1). Both sides were identical and made of mortar. The convergent and divergent shapes were sloped at 1:1 roughly. For an experiment (Run 090417_66), one half-channel constriction only was installed and the free-surface measurements were performed on the channel centreline.

Typical free-surface measurement results are presented in the next section. Figure C-2 introduces the basic notations. The section C.2.1 presents a series of experiments without the channel constriction. The section C.2.2 details the experiments with the channel constriction as well as the repeated experiments with the same, identical flow conditions but without the channel constriction.

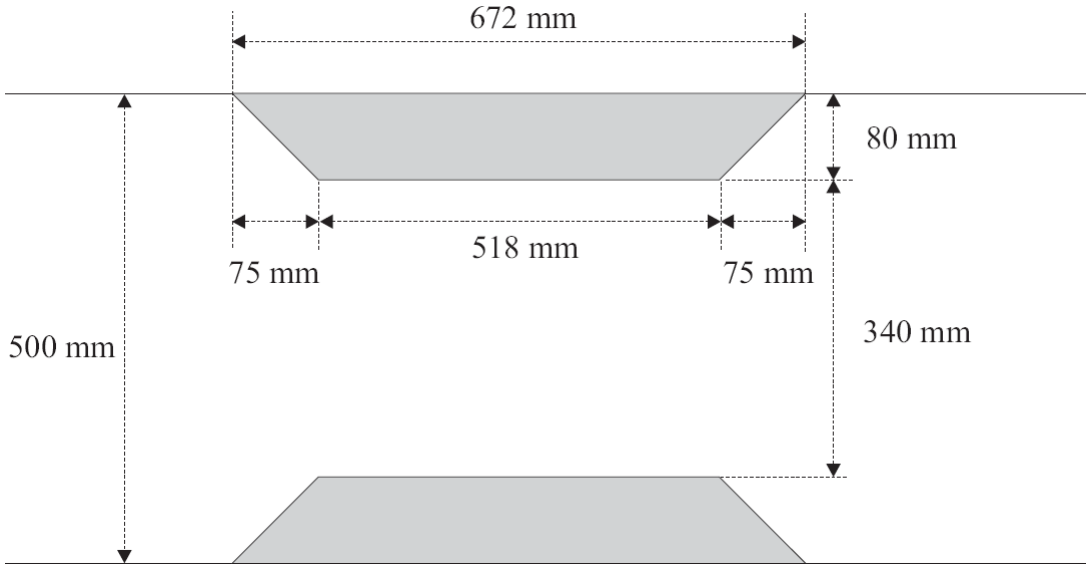

Fig. C-1 - Dimensioned drawing of the channel constriction - View in elevation

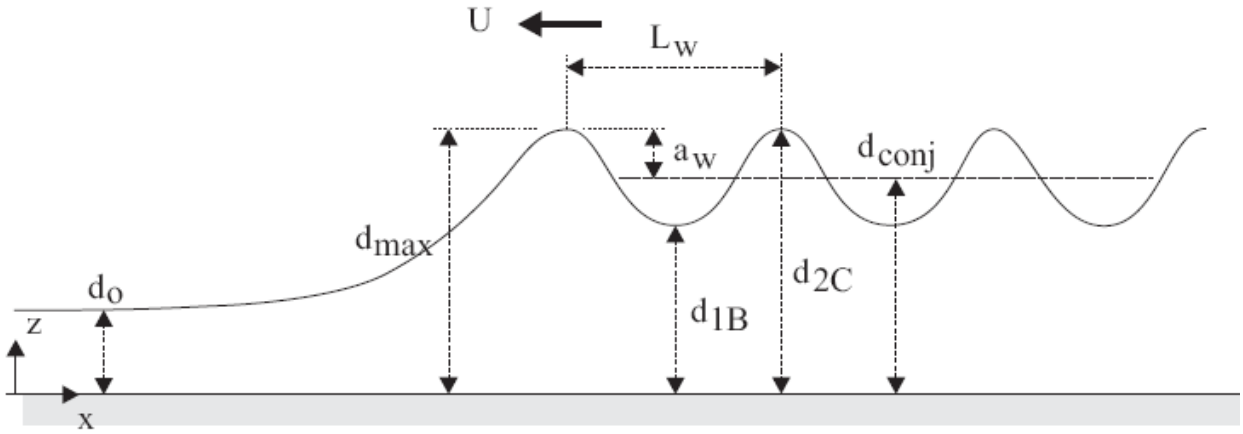

Fig. C-2 - Definition of an undular tidal bore

Notation

a_w amplitude (m) of the first wave crest; measured at x = 5 m;

d_{conj} conjugate flow depth (m); for an undular bore, average depth of the first wave length;

d_{max} water depth (m) of the first wave crest; measured at x = 5 m;

d_o initial steady flow depth (m); measured at x = 5 m;

Fr bore Froude number;

h tainter gate opening (m) after rapid closure;

L_w wave length (m) of the first wave crest; measured at x = 5 m;

Q initial steady flow rate (m^3/s);

T wave period (s) of the first wave crest; measured at x = 5 m;

U bore celerity (m/s) positive upstream; measured at x = 5 m;

x longitudinal distance (m) from the channel upstream distance;

C.2 Experimental results

C.2.1 Flow properties in a prismatic rectangular channel

Run	Q	d_o	Radial gate	h	Surge type	U	Fr
	m^3/s	m	m	m		m/s	
(1)	(2)	(3)	(4)	(5)	(6)	(7)	(8)
090122_01	0.0217	0.0558	Open	0	Breaking	0.654	1.95
090122_02	0.0511	0.1105	Open	0	Breaking	0.909	1.76
090304_11	0.0298	0.2063	0.030	0	Undular	1.351	1.17
090304_12	0.0298	0.2038	0.030	0	Undular	1.408	1.18
090304_13	0.0298	0.205	0.030	Partially open	Undular	1.274	1.09
090304_14	0.0298	0.2055	0.030	Partially open	Undular	1.316	1.10
090304_15	0.0298	0.204	0.030	Small opening	Undular	1.250	1.12
090305_21	0.0190	0.1005	0.030	0	Undular (almost breaking)	0.917	1.34
090305_22	0.0190	0.1015	0.030	0.034	Undular - very gentle	0.781	1.15
090305_23	0.0190	0.1015	0.030	0.009	Undular - slight cross-waves	0.922	1.28
090305_24	0.0190	0.1015	0.030	0	Undular - almost breaking	0.948	1.32
090305_25	0.0190	0.1015	0.050	0.021	Undular bore - gentle bore	0.881	1.23
090306_31	0.0285	0.105	0.050	0	Undular/breaking	0.683	1.31
090306_32	0.0285	0.1025	0.050	0.031	Undular with shock waves	0.792	1.33
090306_33	0.0285	0.102	0.050	0.051	Undular - Gentle bore	0.680	1.18
090306_34	0.0285	0.1013	0.050	0.041	Undular - Very slight cross-waves	0.719	1.25
090309_41	0.0399	0.179	0.050	0.031	Undular - no cross-waves	1.136	1.17
090309_42	0.0399	0.18	0.050	0.011	Undular - with cross-waves	1.316	1.26
090306_43	0.0399	0.18	0.050	0.061	Undular - no cross-waves	1.022	1.10

Run	d_o	U	Fr	d_{conj}	d_{max}	a_w	T	L_w
	m	m/s		m	m	m	s	m
(1)	(3)	(7)	(8)	(9)	(10)	(11)	(12)	(13)
090122_01	0.0558	0.654	1.95	0.115	--	--	--	--
090122_02	0.1105	0.909	1.76	0.210	--	--	--	--
090304_11	0.2063	1.351	1.17	0.206	--	--	1.13	1.527
090304_12	0.2038	1.408	1.18	0.204	--	--	1.08	1.528
090304_13	0.205	1.274	1.09	0.429	0.24	0.0068	1.44	1.834
090304_14	0.2055	1.316	1.10	0.430	0.24	0.0084	1.44	1.895
090304_15	0.204	1.250	1.12	0.438	0.25	0.0107	1.31	1.638
090305_21	0.1005	0.917	1.34	0.230	0.16	0.0268	0.89	0.817
090305_22	0.1015	0.781	1.15	0.209	0.12	*0.0106*	1.34	1.047
090305_23	0.1015	0.922	1.28	0.225	0.16	0.0285	0.95	0.876
090305_24	0.1015	0.948	1.32	0.231	0.16	0.0278	0.86	0.810
090305_25	0.1015	0.881	1.23	0.216	0.14	*0.0195*	1.11	0.974
090306_31	0.105	0.683	1.31	0.259	0.17	0.0150	0.72	0.488
090306_32	0.1025	0.792	1.33	0.232	0.17	0.0317	1.35	1.067
090306_33	0.102	0.680	1.18	0.212	*0.12*	*0.0073*	0.01	0.010
090306_34	0.1013	0.719	1.25	0.221	0.15	0.0219	0.04	0.032
090309_41	0.179	1.136	1.17	0.389	0.24	0.0232	0.05	0.053
090309_42	0.18	1.316	1.26	0.404	*0.25*	*0.0320*	0.06	0.084
090306_43	0.18	1.022	1.10	0.367	0.20	0.0101	0.02	0.021

Notes: *Italic data*: suspicious data; (--): data not available; unless indicated, all the data were measured at x =

5 m.

C.2.2 Flow properties in a rectangular channel with channel constriction

Run	Q	d_o	Radial gate	h	Surge type	U	Fr
	m^3/s	m	m	m		m/s	
(1)	(2)	(3)	(4)	(5)	(6)	(7)	(8)
090318_00	0.0232	0.1552	0.030	0	Undular	--	--
090318_51	0.0232	0.1538	0.030	0	Undular	1.110	1.15
090323_00	0.0175	0.1937	0.015	0	Undular- gentle, no cross-wave	--	--
090323_52	0.0175	0.1855	0.015	0	Undular- gentle, no cross-wave	1.210	1.04
090323_53	0.0175	0.1872	0.015	0	Undular (gentle, no cross-wave)	1.256	1.07
090324_00	0.0097	0.0828	0.015	0	Undular (gentle, no cross-wave)	--	--
090324_54	0.0097	0.0837	0.015	0	Undular (gentle, no cross-wave)	0.885	1.23
090415_61	0.0089	0.0845	0.015	0	Undular. Gentle. No shock waves	0.847	1.16
090415_62	0.0089	0.0802	0.015	0	Undular. Gentle. No shock waves	0.862	1.22
090417_63	0.019	0.212	0.015	0	Undular. Gentle. No shock waves	1.316	1.04
090417_64	0.019	0.191	0.015	0	Undular. Gentle. No shock waves	1.316	1.11
090417_65	0.0193	0.117	0.030	0	Undular. Gentle. No shock waves	0.893	1.14
090417_66	0.0193	0.1145	0.030	0	Undular. Gentle. No shock waves	0.877	1.15
090417_67	0.0193	0.1122	0.030	0	Undular. Gentle. No shock waves	1.000	1.28
090423_803	0.0194	0.1163	0.030	0	Undular. Gentle. No shock waves	1.000	1.25
090424_901a	0.019	0.1147	0.030	0	Undular. Gentle. No shock waves	0.899	1.16
090427_911a	0.019	0.1703	0.020	0	Undular. Gentle. No shock waves	1.203	1.10
090427_921a	0.019	0.1651	0.020	0	Undular. Gentle. No shock waves	1.212	1.13
090429_931a	0.0188	0.1989	0.017	0	Undular. Gentle. No shock waves	1.322	1.08
090429_938a	0.0188	0.1989	0.017	0	Undular. Gentle. No shock waves	1.322	1.08

Run	d_o	U	Fr	d_{conj}	d_{max}	a_w	T	L_w	x	Configuration
	m	m/s		m	m	m	s	m	m	
(1)	(3)	(7)	(8)	(9)	(10)	(11)	(12)	(13)	(14)	(15)
090318_00	0.1552	--	--	--	--	--	--	--	5.00	Bridge piers
090318_51	0.1538	1.11	1.15	0.182	0.219	0.0291	0.99	1.102	5.00	Bridge piers
				--	--	--	0.99	1.099	4.55	
				0.189	0.216	0.0214	1.05	1.166	4.00	
090323_00	0.1937	--	--	--	--	--	--	--	5.00	Bridge piers
090323_52	0.1855	1.21	1.04	0.202	0.217	0.0087	1.09	1.319	5.00	Bridge piers
				--	--	--	1.09	1.319	4.55	
				0.201	0.213	0.0087	1.11	1.343	4.00	
090323_53	0.1872	1.26	1.07	0.205	0.221	0.0102	1.11	1.394	5.00	Bridge piers
				--	--	--	1.08	1.351	4.55	
				0.204	0.216	0.0094	1.13	1.420	4.00	
090324_00	0.0828	--	--	--	--	--	--	--	5.00	Bridge piers
090324_54	0.0837	0.88	1.23	0.092	0.119	0.0228	0.74	0.655	5.00	Bridge piers
				--	--	--	0.86	0.757	4.55	
				0.094	0.111	0.0151	0.87	0.770	4.00	
090415_61	0.0845	0.85	1.16	0.101	0.127	0.0216	0.84	0.712	5.00	Bridge piers
				0.114	*0.137*	0.0224	0.86	0.729	4.55	
				0.103	*0.120*	0.0154	0.88	0.746	4.00	
090415_62	0.0802	0.86	1.22	0.100	0.121	0.0168	0.74	0.638	5.00	No pier
				0.101	0.121	0.0162	0.82	0.707	4.55	
				0.099	0.120	0.0173	0.78	0.672	4.00	
090417_63	0.2120	1.32	1.04	0.239	0.254	0.0089	1.18	1.553	5.00	Bridge piers
				0.237	*0.254*	0.0145	1.20	1.579	4.55	
				0.238	*0.248*	0.0079	1.16	1.526	4.00	
090417_64	0.1910	1.32	1.11	0.220	0.233	0.0093	1.10	1.447	5.00	No pier
				0.220	0.232	0.0092	1.10	1.447	4.55	
				0.219	0.232	0.0098	1.14	1.500	4.00	
090417_65	0.1170	0.89	1.14	0.155	*0.213*	*0.0454*	0.96	0.857	5.00	Bridge piers
				0.156	*0.190*	*0.0353*	0.92	0.821	4.55	
				0.154	*0.175*	*0.0243*	0.98	0.875	4.00	
090417_66	0.1145	0.88	1.15	0.150	0.196	0.0348	0.76	0.667	5.00	1/2 bridge pier
				0.155	*0.186*	*0.0306*	0.98	0.860	4.55	
				0.157	*0.189*	*0.0311*	0.94	0.825	4.00	
090417_67	0.1122	1.00	1.28	0.149	0.188	0.0311	0.88	0.880	5.00	No pier
				0.150	*0.187*	*0.0311*	0.92	0.920	4.55	
				0.149	*0.188*	*0.0326*	0.94	0.940	4.00	
090423_803	0.1163	1.00	1.25	0.149	0.188	0.0311	0.88	0.880	5.00	Bridge piers
				0.150	*0.187*	*0.0311*	0.92	0.920	4.55	
				0.149	*0.188*	*0.0326*	0.94	0.940	4.00	
090424_901a	0.1147	0.90	1.16	0.153	0.204	*0.0404*	0.98	0.881	5.00	Bridge piers
				0.155	0.191	0.0357	0.95	0.854	4.55	
				--	--	--	1.03	0.921	4.00	
090427_911a	0.1703	1.20	1.10	0.203	0.222	0.0129	1.07	1.287	5.00	Bridge piers
				0.197	0.223	0.0228	1.05	1.257	4.55	
				--	--	--	1.11	1.329	4.00	
090427_921a	0.1651	1.21	1.13	0.165	0.242	0.0211	1.10	1.333	5.00	No pier
				--	--	--	1.02	1.236	4.55	
				0.203	0.242	0.0211	1.10	1.333	4.00	
090429_931a	0.1989	1.32	1.08	0.228	0.242	0.0090	1.13	1.494	5.00	Bridge piers
				0.226	0.237	0.0080	1.18	1.554	4.00	
090429_938a	0.1989	1.32	1.08	0.223	0.236	0.0100	1.16	1.527	5.00	No pier
				0.223	0.236	0.0100	1.16	1.527	4.00	

Notes: *Italic data*: suspicious data; x: longitudinal distance downstream of the upstream channel end; x = 5 m: downstream of channel constriction; x = 4.55 m: between channel constriction (Fig. C-1); x = 4.0 m: upstream of channel constriction; (--): data not available.

Appendix D - Undular wave theory

D.1 Presentation

The majority of tidal bores have an undular shape where the leading front is followed by a train of well-developed, quasi-periodic undulations (Fig. D-1). The train of quasi-periodic waves is called whelps or 'éteules' and it is observed when the bore Froude number Fr is less than 1.5 to 1.8. For larger Froude numbers, a breaking bore is observed (section 3).

In an undular tidal bore, the first wave crest is followed by a train of well-defined waves whose shape was investigated during the last two centuries (BOUSSINESQ 1877, LEMOINE 1948, BENJAMIN and LIGHTHILL 1954). The experimental measurements showed that the profile of the free-surface undulations followed closely a solution of the linear wave theory as well as a solution of the Boussinesq equation (section 3). The former is based upon a sinusoidal wave shape, while the latter yields a cnoidal function squared. Relevant references on the cnoidal function and wave theory include ABRAMOWITZ and STEGUN (1972), FENTON (1979, 1998), WIEGEL (1960) and MONTES (1998).

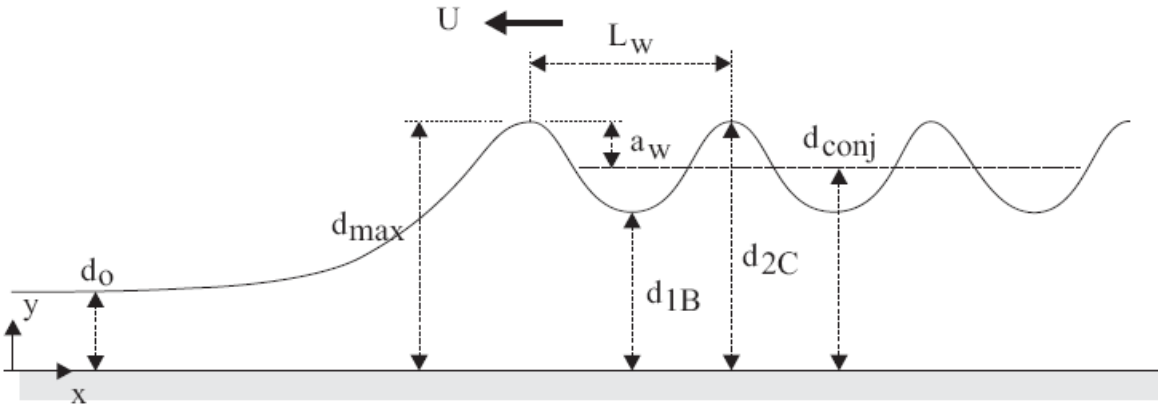

Fig. D-1 - Definition sketch of an undular tidal bore

D.2 Mathematical functions

D.2.1 Linear wave

$$d = d_{conj} + a_w \times \cos\left(2 \times \pi \times \frac{x}{L_w}\right)$$ from first wave crest (x=0)

$$\frac{d - d_{1B}}{d_{max} - d_{1B}} = \frac{1}{2} \times \left(1 + \cos\left(2 \times \pi \times \frac{x}{L_w}\right)\right)$$ between wave crest and trough

D.2.2 Cnoidal wave

$$\frac{d - d_{1B}}{d_{max} - d_{1B}} = cn^2\left(2 \times K \times \frac{x}{L_w}\right)$$ between wave crest and trough (FENTON 1998)

D.2.2.1 Cnoidal function

The cnoidal function is an elliptic integral of the first kind.

$$\mathrm{cn}\ u = \cos\varphi$$

$$u = \int_0^{\varphi} \frac{d\theta}{\sqrt{1 - m \times \sin^2\theta}} \qquad 0 \le m \le 1$$

Particular cases (ABRAMOWITZ and STEGUN 1972)

$$\mathrm{cn}\ u = \cos u + \frac{1}{4} \times m \times (u - \sin u \times \cos u) \times \sin u \qquad m << 1$$

$$\mathrm{cn}\ u = \mathrm{sech}\ u - \frac{1}{4} \times m_1 \times (\sinh u \times \cosh u - u) \times \tanh u \times \mathrm{sech}\ u$$

$$m_1 = 1 - m << 1$$

Case $1/2 \le m \le 1$ (FENTON 1998)

$$K(m) = \frac{2}{(1 + m^{1/4})^2} \times \mathrm{Ln}\left(\frac{2 \times (1 + m^{1/4})}{1 - m^{1/4}}\right) \qquad \text{complete elliptic integral of first kind}$$

$$K'(m) = \frac{2 \times \pi}{(1 + m^{1/4})^2} \qquad \text{complementary elliptic integral of first kind}$$

$$q_1 = \exp\left(-\frac{K}{K'}\right) \qquad \text{complementary nome}$$

$$\mathrm{cn}\ (u \mid m) = \frac{1}{2} \times \left(\frac{m_1}{m \times q_1}\right)^{1/4} \times \frac{1 - 2 \times q_1 \times \cosh(2 \times w)}{\cosh w + {q_1}^2 \times \cosh(3 \times w)} \qquad \text{Jacobian elliptic function}$$

with $m_1 = (1 - m)$ and $w = \pi \times u / (2 \times K')$.

Appendix E - Observations of tidal bore propagation between bridge piers and short channel constrictions

E.1 Pont Aubault, Pontaubault (France)

Fig. E-1 - Propagation of the Sélune River tidal bore beneath the Pont Aubault, Pontaubault (France) on 7 April 2004 at 09:00 - View from the left bank - Shutter speed: 1/800 to 1/1,000 s (Filenames: Selun53.jpg to Selun56.jpg)

Fig. E-2 - Propagation of the Sélune River tidal bore beneath the Pont Aubault, Pontaubault (France) on 2 August 2008 at 20:58 - View from the left bank - From left to right, top to bottom: $t = t_o$, t_o+22 s, t_o+30 s, t_o+39 s, Shutter speed: 1/80 s (Filenames: Selun209.jpg to Selun225.jpg)

Fig. E-3 - Propagation of the Sélune River tidal bore beneath the Pont Aubault, Pontaubault (France) on 3 August 2008 at 09:37 - View from the left bank - From left to right looking upstream, top to bottom: $t = t_o$, t_o+5 s, t_o+29 s, t_o+59 s, Shutter speed: 1/125 to 1/320 s (Filenames: Selun331.jpg to Selun340.jpg)

Fig. E-4 - Propagation of the Sélune River tidal bore beneath the Pont Aubault, Pontaubault (France) on 31 August 2008 at 20:35 - View from the left bank; note the kayaker riding the first wave of the undular tidal bore - From left to right looking upstream, top to bottom: t = t_o, t_o+5 s, t_o+29 s, t_o+59 s, t_o+59 s, t_o+59 s, Shutter speed: 1/50 s (Filenames: Selun539.jpg to Selun558.jpg)

Fig. E-5 - Propagation of the Sélune River tidal bore beneath the Pont Aubault, Pontaubault (France) on 1 September 2008 at 09:04 - View from the left bank; note the kayaker riding the first wave of the undular tidal bore beneath the bridge - From left to right looking upstream, top to bottom: $t = t_o$, t_o+13 s, t_o+35 s, t_o+43 s, Shutter speed: 1/400 to 1/1,400 s (Filenames: Selun663.jpg to Selun667.jpg)

E.2 Stone bridge over a drainage channel off the Sélune River

Fig. E-6 - Propagation of a small undular tidal bore beneath a stone bridge over a drainage channel off the Sélune River (France) on 31 August 2008 at 19:45 - Bore propagation through the partially-opened gate, with some reflection effect ($t=t_o$+9 to 12 s) and continuing past the bridge ($t=t_o$+40 s)- From left to right looking upstream, top to bottom: $t = t_o$, t_o+2 s, t_o+4 s, t_o+9 s, t_o+12 s, t_o+40 s, Shutter speed: 1/50 to 1/80 s (Filenames: Selun443.jpg to Selun448.jpg)

Fig. E-7 - Propagation of a small undular tidal bore beneath a stone bridge over a drainage channel off the Sélune River (France) on 19 September 2008 at 09:20 - Bore propagation through the partially-opened gate, with some reflection effect ($t=t_o+8$ to 11.5 s) - From left to right looking upstream, top to bottom: $t = t_o$, $t_o+1.0$ s, $t_o+8.0$ s, $t_o+82.5$ s, $t_o+10.0$ s, $t_o+11.5$ s, Shutter speed: 1/100 to 1/320 s (Filenames: Selun817.jpg to Selun8247.jpg)

Appendix F - Free-surface measurements of tidal bore propagation through a short channel constriction

F.1 Presentation

The propagation of an undular tidal was tested in a physical model. New experiments were performed in a large tilting flume at the University of Queensland (Table F-1). The channel was 0.5 m wide 12 m long, and its slope was set horizontal for all experiments.

For a series of experiments, two half-channel constrictions (Fig. F-1) were introduced between x = 4.88 m and 4.21 m. Both sides were identical, made of mortar and painted. The convergent and divergent shapes were sloped at 1:1 roughly. For one experiment (Run 090417_66), only one half-channel constriction was installed. Table F-1 summarises the experimental flow conditions and the free-surface measurements are presented in section F.2.

In steady flows, the water depths were measured using rail mounted pointer gauges and acoustic displacement meters. Unsteady water depths were measured with a series of acoustic displacement meters located on the channel centreline.

F1.1 Experimental procedure

The experimental setup was selected to generate an initially steady, subcritical flow for a given initial flow rate Q. The opening of the downstream radial gate (x = 11.9 m) was set to control the initial steady flow depth, and the opening was kept constant during each tidal bore experiment. The tidal bore was generated by the rapid (partial or complete) closure of the downstream tainter gate located at x = 11.15 m. The gate closure time was less than 0.2 s. Some photographs of the bore formation immediately after the tainter gate closure are presented in Appendix A. After the rapid tainter gate closure, the tidal bore propagated upstream and each experiment was stopped when the bore front reached the intake structure to avoid wave reflection interference.

A series of experiments were repeated carefully with and without channel constriction. The discharge and the radial gate opening were kept constant. The free-surface measurements were conducted first with the channel constriction in place. Then, while the flow rate while still running, the channel constriction elements were removed. The steady gradually-varied flow conditions were established for at least 15 minutes, and the free-measurements were repeated without the constriction.

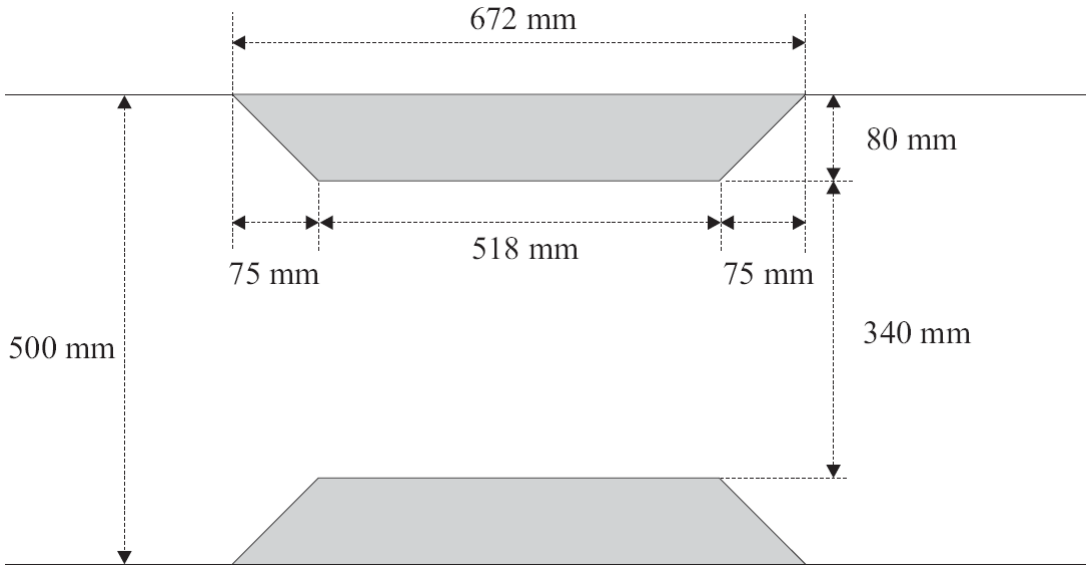

Fig. F-1 - Dimensioned sketch of the channel constriction - View in elevation

Table F-1 - Experiment flow conditions for free-surface measurements of tidal bore propagation through a short channel constriction

Run	Q	d_o	Radial gate open.	U x=5m	Fr x=5m	d_{max}-d_o x=5m	a_w	T	Comment
	m3/s	m	m	m/s		m	m	s	
(1)	(2)	(3)	(4)	(5)	(6)	(7)	(8)	(9)	(10)
090415_61	0.0089	0.0845	0.015	0.847	1.16	0.0253	0.0216	0.84	Channel constriction.
090415_62	0.0089	0.0802	0.015	0.862	1.22	0.0210	0.0168	0.74	No constriction
090417_63	0.0190	0.2120	0.015	1.316	1.04	0.0149	0.0089	1.18	Channel constriction.
090417_64	0.0190	0.1910	0.015	1.316	1.11	0.0121	0.0093	1.10	No constriction
090417_65	0.0193	0.1170	0.03	0.893	1.14	0.0574	0.0454	0.96	Channel constriction.
090417_66	0.0193	0.1145	0.03	0.877	1.15	0.0461	0.0348	0.76	1/2 channel constriction.
090417_67	0.0193	0.1122	0.03	1.000	1.28	0.0397	0.0311	0.88	No constriction
090427_911a	0.0190	0.1703	0.02	1.203	1.10	0.0191	0.0129	1.07	Channel constriction.
090427_921a	0.0190	0.1651	0.02	1.212	1.13	0.0768	0.0211	1.10	No constriction
090429_931a	0.0188	0.1989	0.0165	1.322	1.08	0.0143	0.0090	1.13	Channel constriction.
090429_938a	0.0188	0.1989	0.0165	1.322	1.08	0.0131	0.0100	1.16	No constriction

Notes: a_w: amplitude of the first wave length; d_{max}: maximum flow depth measured at first wave crest; d_o: initial flow depth (at x = 3.6 m); Fr: bore Froude number; Q: initial discharge; T wave period (first wave length); U: bore celerity positive upstream.

F.2 Experimental data

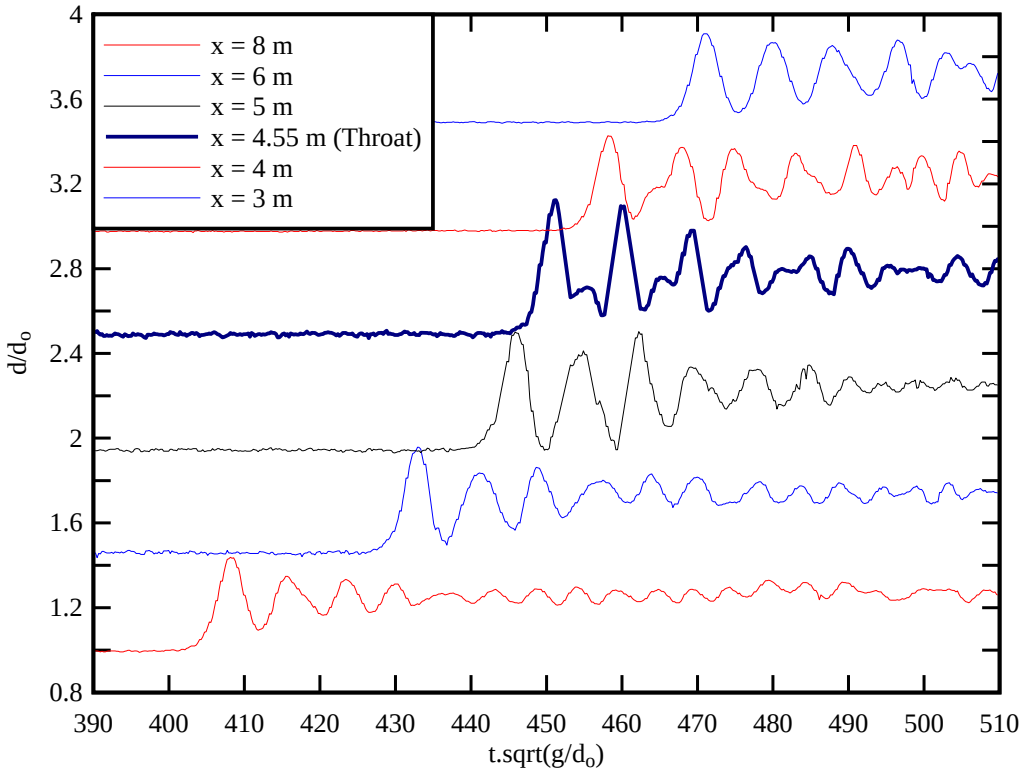

(A) Run 090417_61, Q = 0.0089 m^3/s, d_o = 0.0845 m, Fr = 1.16, U = 0.847 m/s, Channel constriction

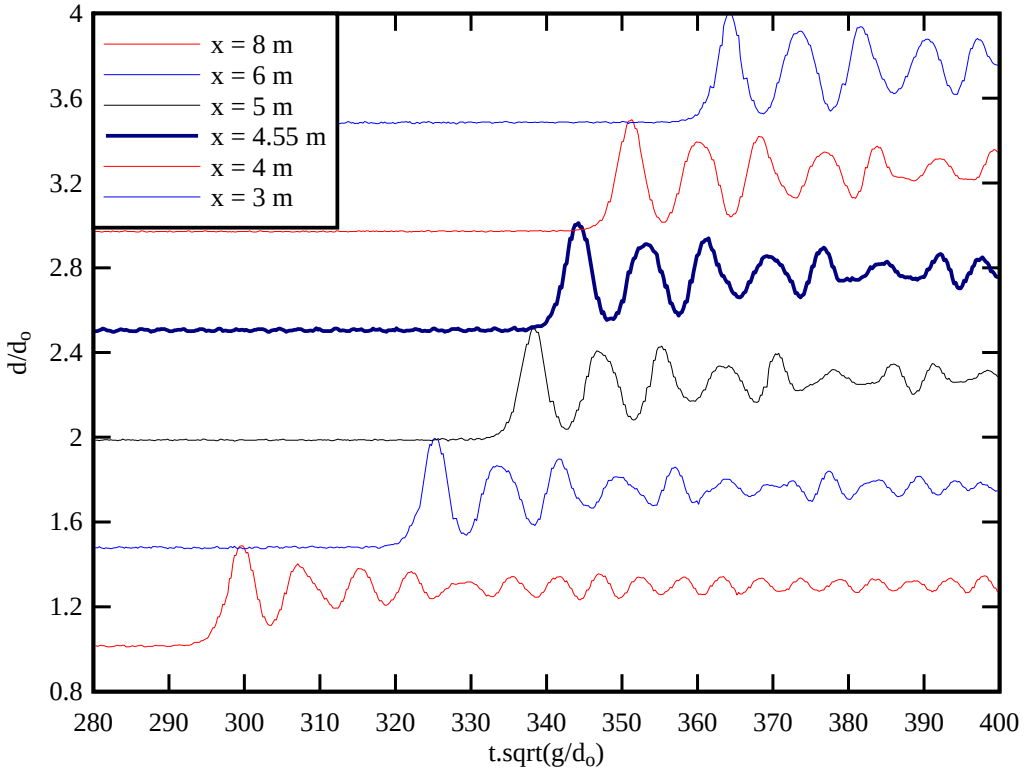

(B) Run 090417_62, Q = 0.0089 m^3/s, d_o = 0.0802 m, Fr = 1.22, U = 0.862 m/s, No channel constriction

Fig. F-1 - Dimensionless time-variations of the flow depth during the propagation of an undular tidal bore with and without bridge pier model: Q = 0.0089 m^3/s, d_o = 0.08 m, Fr = 1.16-1.22, U = 0.8 m/s - Each curve was offset vertically by 0.5

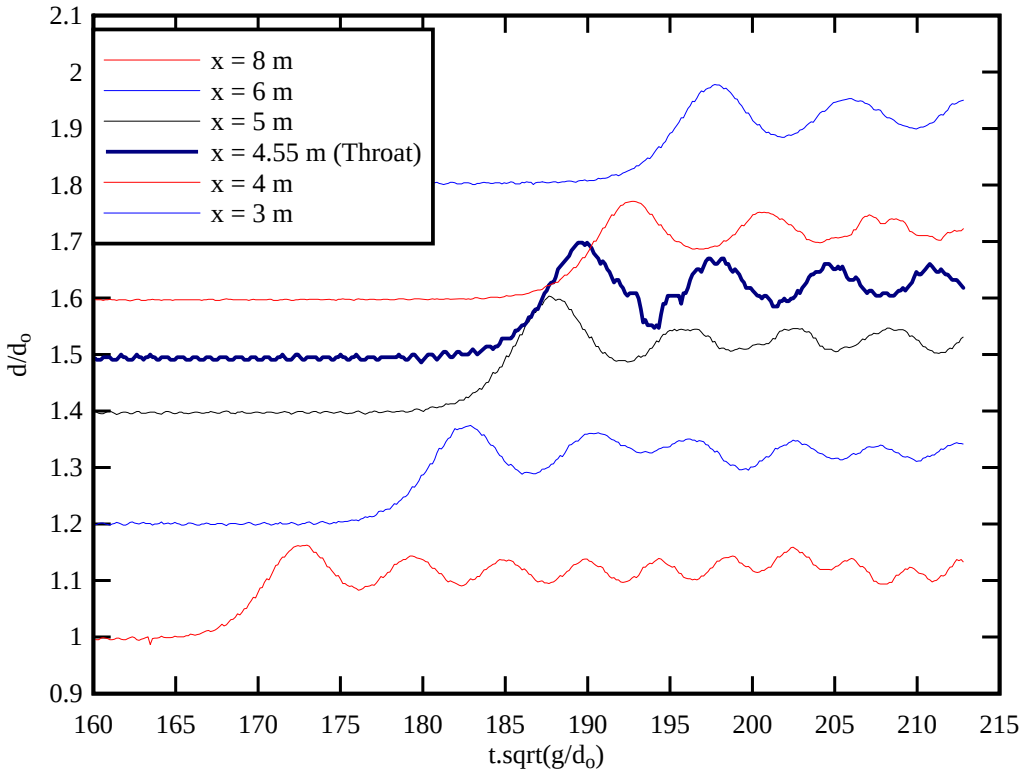

(A) Run 090417_63, Q = 0.0190 m^3/s, d_o = 0.212 m, Fr = 1.04, U = 1.32 m/s, Channel constriction

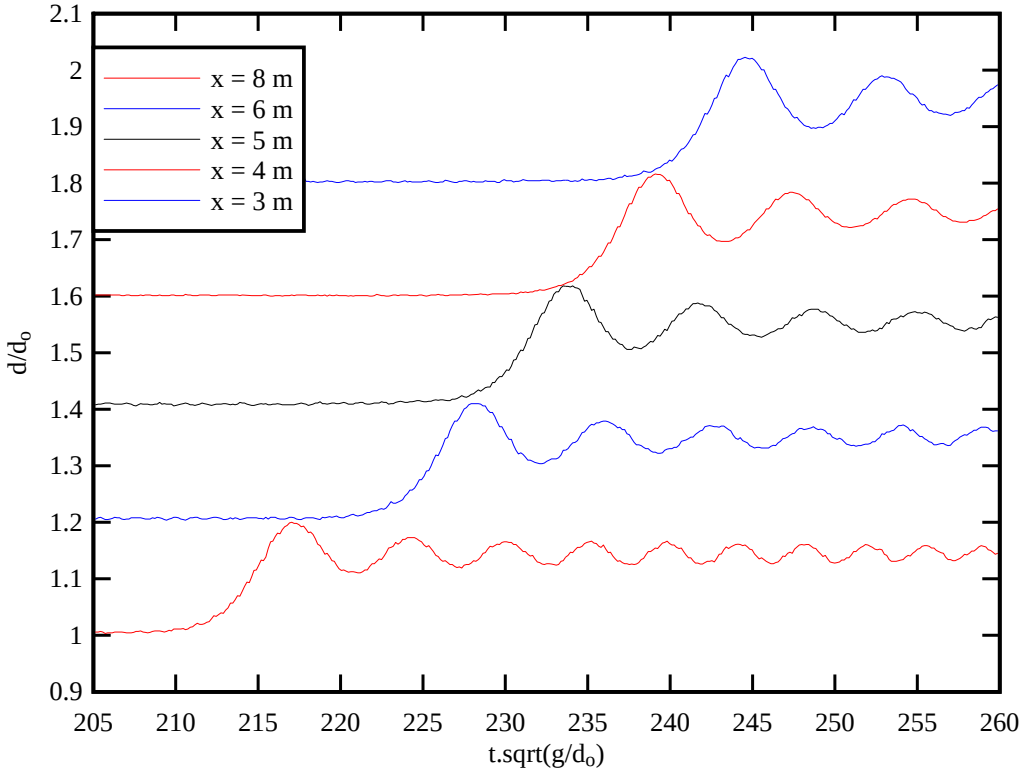

(B) Run 090417_64, Q = 0.0190 m^3/s, d_o = 0.191 m, Fr = 1.11, U = 1.32 m/s, No channel constriction

Fig. F-2 - Dimensionless time-variations of the flow depth during the propagation of an undular tidal bore with and without bridge pier model: Q = 0.0190 m^3/s, d_o = 0.2 m, Fr = 1.04-1.1, U = 1.32 m/s - Each curve was offset vertically by 0.2, but the throat data by 0.1

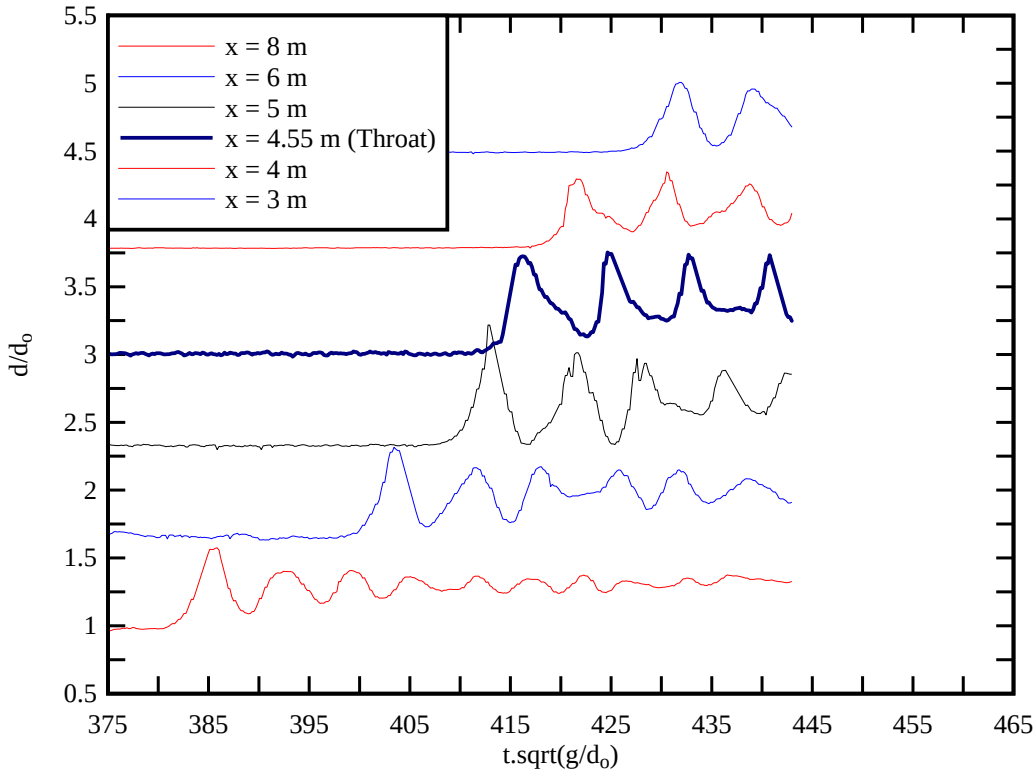

(A) Run 090417_65, Q = 0.0193 m^3/s, d_o = 0.117 m, Fr = 1.14, U = 0.893 m/s, Channel constriction

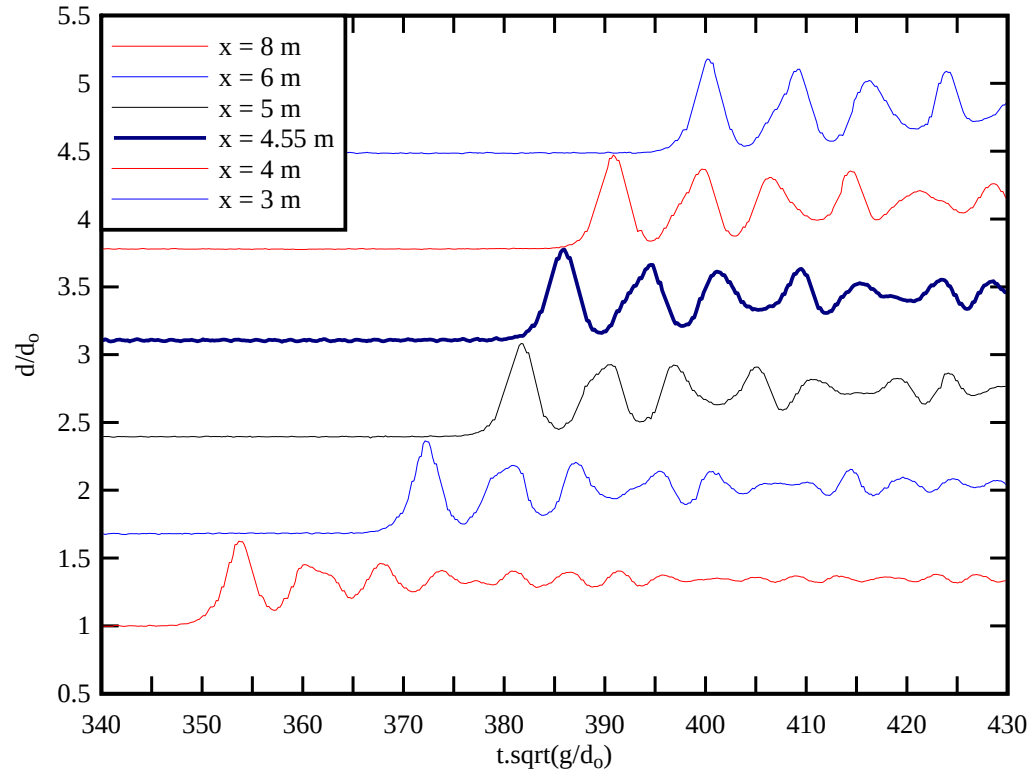

(B) Run 090417_67, Q = 0.0193 m^3/s, d_o = 0.1122 m, Fr = 1.28, U = 1.0 m/s, No channel constriction

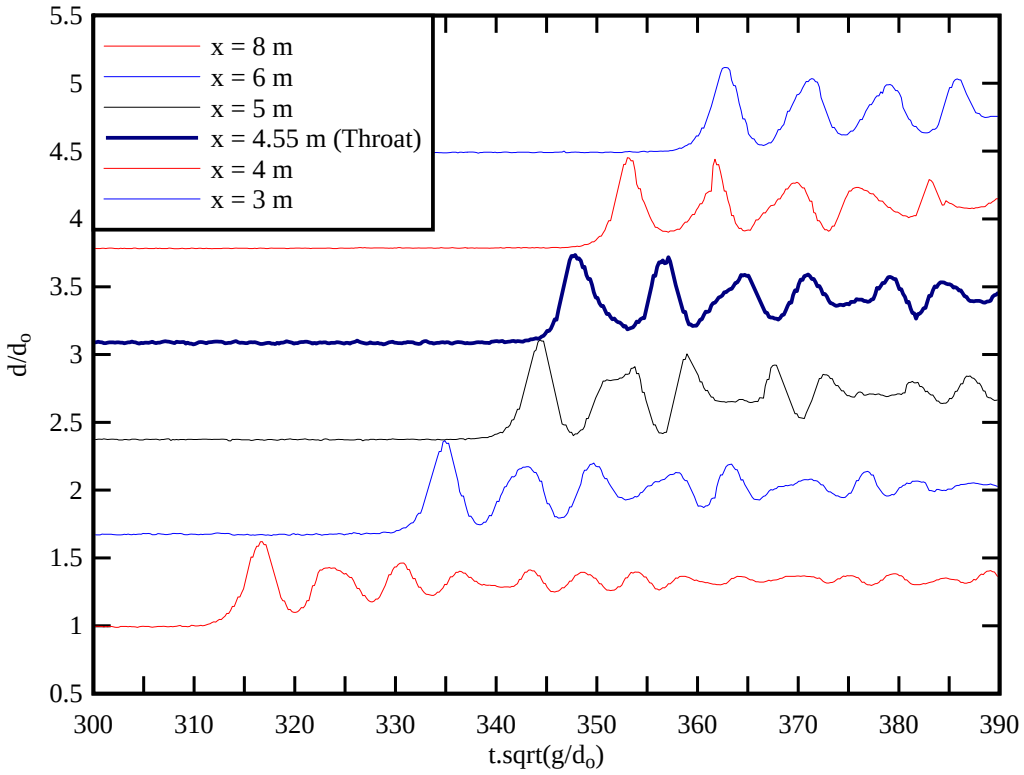

(C) Run 090417_66, Q = 0.0193 m^3/s, d_o = 0.1145 m, Fr = 1.15, U = 0.877 m/s, One half-channel constriction only, Centreline data

Fig. F-3 - Dimensionless time-variations of the flow depth during the propagation of an undular tidal bore with and without bridge pier model: Q = 0.0193 m^3/s, d_o = 0.11 m, Fr = 1.14-1.28, U = 0.9-1.0 m/s - Each curve was offset vertically by 0.7

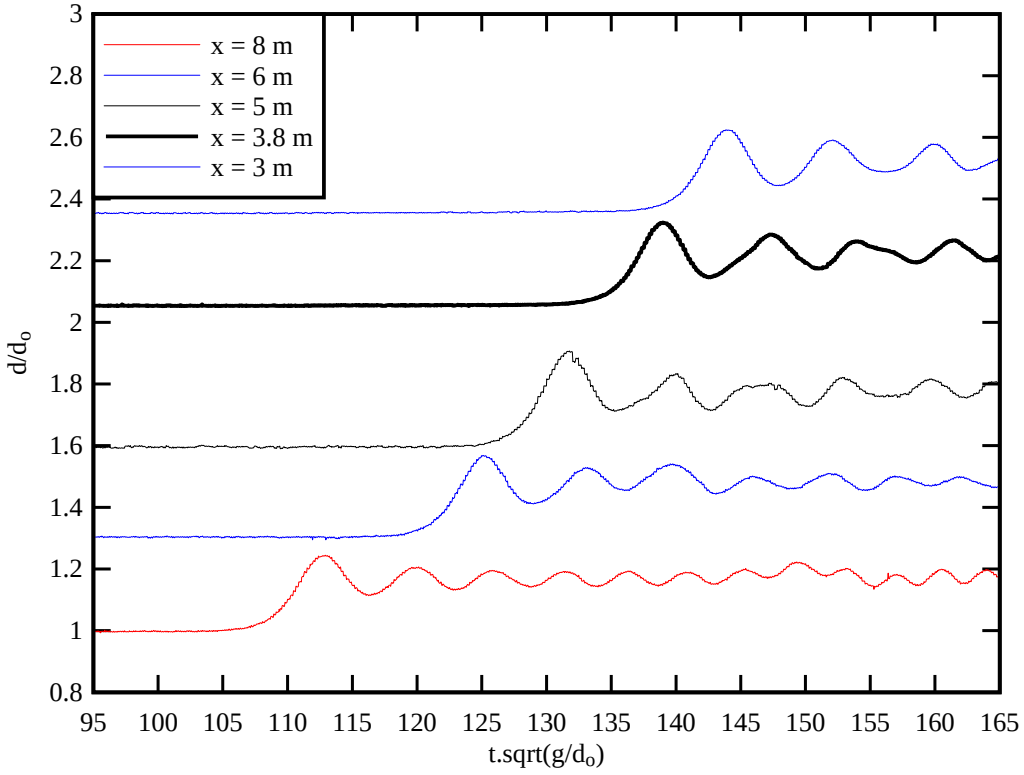

(A) Run 090427_911a, Q = 0.0190 m^3/s, d_o = 0.1703 m, Fr = 1.10, U = 1.203 m/s, Channel constriction

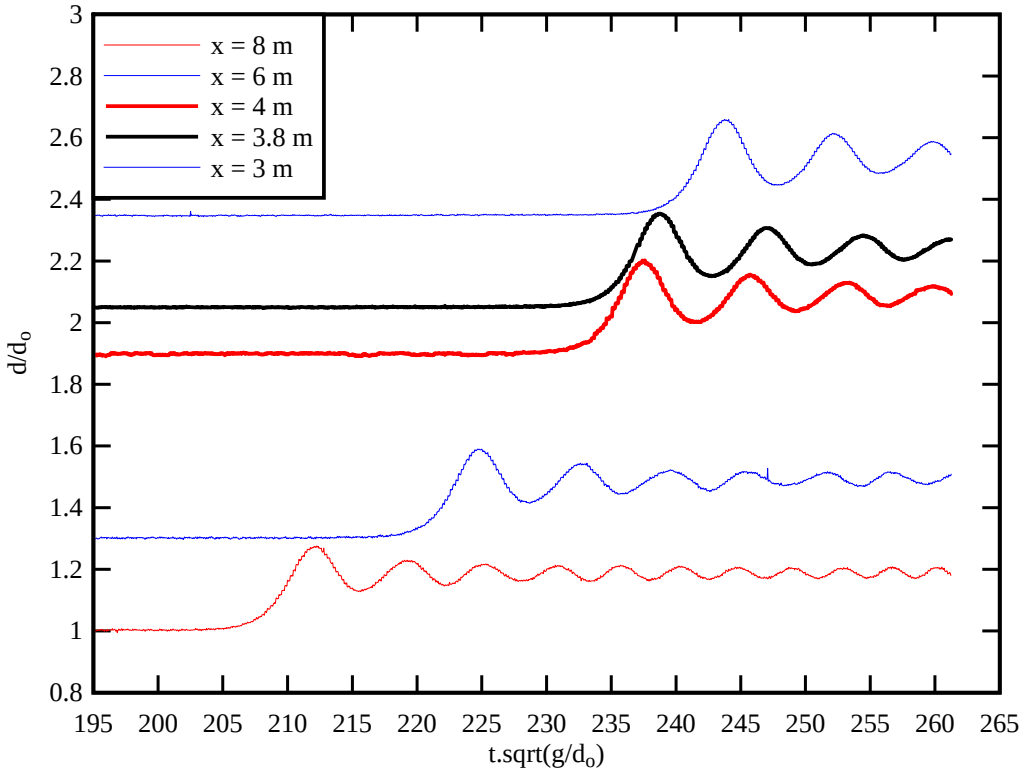

(B) Run 090427_921a, Q = 0.0190 m^3/s, d_o = 0.1651 m, Fr = 1.13, U = 1.212 m/s, No channel constriction

Fig. F-4 - Dimensionless time-variations of the flow depth during the propagation of an undular tidal bore with and without bridge pier model: Q = 0.0190 m^3/s, d_o = 0.17 m, Fr = 1.1, U = 1.2 m/s - Each curve was offset vertically by 0.3, but the x=3.8 m data by 0.15

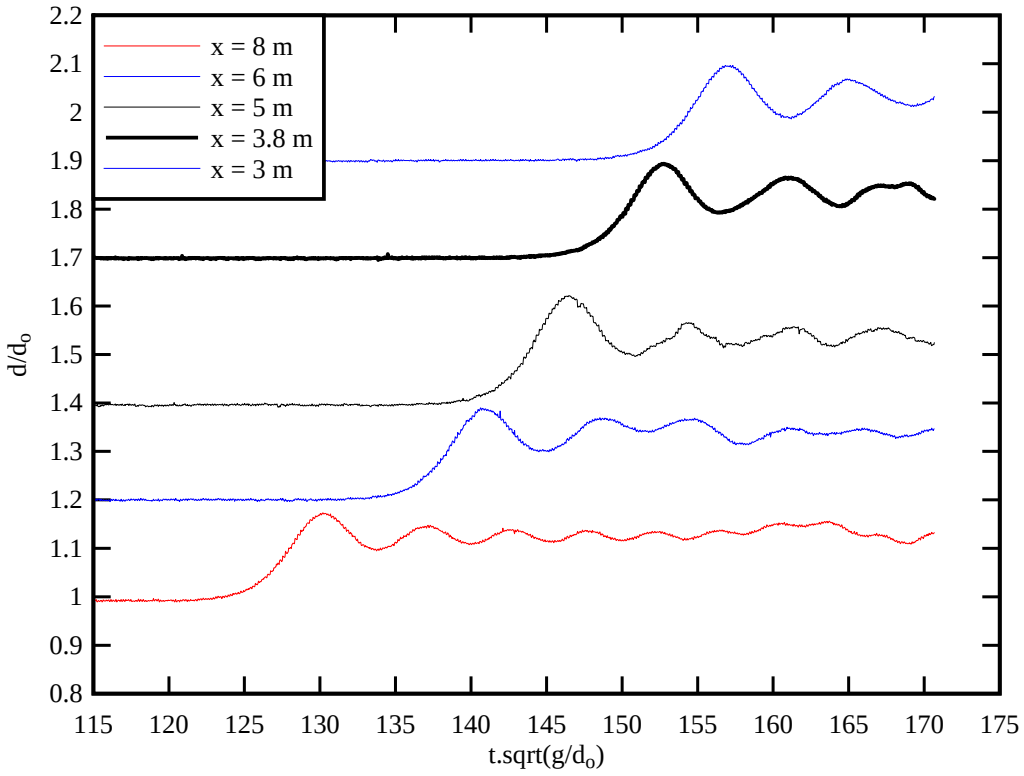

(A) Run 090429_931a, Q = 0.0188 m^3/s, d_o = 0.1989 m, Fr = 1.08, U = 1.32 m/s, Channel constriction

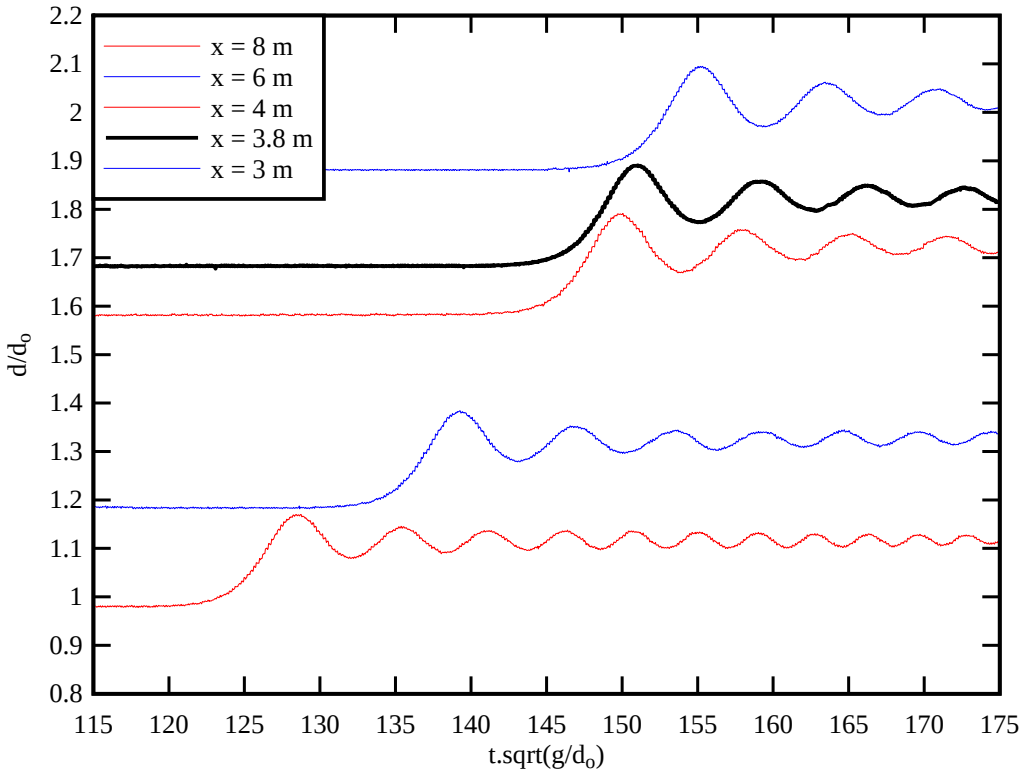

(B) Run 090429_938a, Q = 0.0188 m^3/s, d_o = 0.1989 m, Fr = 1.08, U = 1.32 m/s, No channel constriction

Fig. F-5 - Dimensionless time-variations of the flow depth during the propagation of an undular tidal bore with and without bridge pier model: Q = 0.0188 m^3/s, d_o = 0.199 m, Fr = 1.08-1.1, U = 1.32 m/s - Each curve was offset vertically by 0.2, but the x=3.8 m data by 0.1

References

ABRAMOWITZ, M., and STEGUN, I.E. (1972). "Handbook of Mathematical Functions with Formulas, Graphs and Mathematical Tables." *Dover Publications*, 9th Printing, New York, USA, 1046 pages.

ANDERSEN, V.M. (1978). "Undular Hydraulic Jump." *Jl of Hyd. Div.*, ASCE, Vol. 104, No. HY8, pp. 1185-1188. Discussion : Vol. 105, No. HY9, pp. 1208-1211.

BAKHMETEFF, B.A. (1932). "Hydraulics of Open Channels." *McGraw-Hill*, New York, USA, 1st ed., 329 pages.

BARRÉ de SAINT-VENANT, A.J.C. (1871). "Théorie et Equations Générales du Mouvement Non Permanent des Eaux Courantes." *Comptes Rendus des séances de l'Académie des Sciences*, Paris, France, Séance 17 July 1871, Vol. 73, pp. 147-154 (in French).

BAZIN, H. (1865). "Recherches Expérimentales sur la Propagation des Ondes." ('Experimental Research on Wave Propagation.') *Mémoires présentés par divers savants à l'Académie des Sciences*, Paris, France, Vol. 19, pp. 495-644 (in French).

BENET, F., and CUNGE, J.A. (1971). "Analysis of Experiments on Secondary Undulations caused by Surge Waves in Trapezoidal Channels." *Jl of Hyd. Res.*, IAHR, Vol. 9, No. 1, pp. 11-33.

BENJAMIN, T.B., and LIGHTHILL, M.J. (1954). "On Cnoidal Waves and Bores." *Proc. Royal Soc. of London, Series A, Math. & Phys. Sc.*, Vol. 224, No. 1159, pp. 448-460.

BEN MEFTAH, M., DE SERIO, F., MOSSA, M., and POLLIO, A. (2007). "Analysis of the Velocity Field in a Large Rectangular Channel with Lateral Shockwave." *Env. Fluid Mech.*, Vol. 7, No. 6, pp. 519-536 (DOI: 10.1007/s10652-007-9034-7).

BOUSSINESQ, J.V. (1877). "Essai sur la Théorie des Eaux Courantes." ('Essay on the Theory of Water Flow.') *Mémoires présentés par divers savants à l'Académie des Sciences*, Paris, France, Vol. 23, Série 3, No. 1, supplément 24, pp. 1-680 (in French).

BRADSHAW, P. (1971). "An Introduction to Turbulence and its Measurement." *Pergamon Press*, Oxford, UK, The Commonwealth and International Library of Science and technology Engineering and Liberal Studies, Thermodynamics and Fluid Mechanics Division, 218 pages.

British Standard (1943). "Flow Measurement." *British Standard Code BS 1042:1943*, British Standard Institution, London.

CHANSON, H. (1995). "Flow Characteristics of Undular Hydraulic Jumps. Comparison with Near-Critical Flows." *Report CH45/95*, Dept. of Civil Engineering, University of Queensland, Australia, June, 202 pages (ISBN 0 86776 612 3).

CHANSON, H. (2004). "The Hydraulics of Open Channel Flow: An Introduction." *Butterworth-Heinemann*, 2nd edition, Oxford, UK, 630 pages.

CHANSON, H. (2005). "Physical Modelling of the Flow Field in an Undular Tidal Bore." *Jl of Hyd. Res.*, IAHR, Vol. 43, No. 3, pp. 234-244.

CHANSON, H. (2008a). "Turbulence in Positive Surges and Tidal Bores. Effects of Bed Roughness and Adverse Bed Slopes." *Hydraulic Model Report No. CH68/08*, Div. of Civil Engineering, The University of Queensland, Brisbane, Australia, 121 pages & 5 movie files.

CHANSON, H. (2008b). "Acoustic Doppler Velocimetry (ADV) in the Field and in Laboratory: Practical Experiences." *Proceedings of the International Meeting on Measurements and Hydraulics of Sewers IMMHS'08*, Summer School GEMCEA/LCPC, 19-21 Aug. 2008, Bouguenais, Frédérique LARRARTE and Hubert CHANSON Eds., Hydraulic Model Report No. CH70/08, Div. of Civil Engineering, The University of Queensland, Brisbane, Australia, Dec., pp. 49-66.

CHANSON, H. (2009). "Applied Hydrodynamics: An Introduction to Ideal and Real Fluid Flows." *CRC Press/Balkema*, Taylor & Francis Group, Leiden, The Netherlands, 478 pages.

CHANSON, H., and MONTES, J.S. (1995). "Characteristics of Undular Hydraulic Jumps. Experimental Apparatus and Flow Patterns." *Jl of Hyd. Engrg.*, ASCE, Vol. 121, No. 2, pp. 129-144. Discussion : Vol. 123, No. 2, pp. 161-164.

CHANSON, H., TREVETHAN, M., and AOKI, S. (2008). "Acoustic Doppler Velocimetry (ADV) in Small Estuary : Field Experience and Signal Post-Processing." *Flow Measurement and Instrumentation*, Vol. 19, No. 5, pp. 307-313 (DOI: 10.1016/j.flowmeasinst.2008.03.003).

CHEN, S. (2003). "Tidal Bore in the North Branch of the Changjiang Estuary." *Proc. Intl Conf. on Estuaries & Coasts ICEC-2003*, Hangzhou, China, Nov. 8-11, Intl Research & Training Center on Erosion & Sedimentation Ed., Vol. 1, pp. 233-239.

CHOW, V.T. (1959). "Open Channel Hydraulics." *McGraw-Hill*, New York, USA.

CLANCY, E.P. (1968). "The Tides Pulses of the Earth." *Anchor Books*, New York, USA, 228 pages.

DONNELLY, C., and CHANSON, H. (2005). "Environmental Impact of Undular Tidal Bores in Tropical Rivers." *Environmental Fluid Mechanics*, Vol. 5, No. 5, pp. 481-494 (DOI: 10.1007/s10652-005-0711-0).

DYER, K.R. (1997). "Estuaries. A Physical Introduction." *John Wiley*, New York, USA, 2nd edition, 195 pages.

FAVRE, H. (1935). "Etude Théorique et Expérimentale des Ondes de Translation dans les Canaux Découverts." ('Theoretical and Experimental Study of Travelling Surges in Open Channels.') *Dunod*, Paris, France (in French).

FENTON, J.D. (1979). "A High-Order Cnoidal Wave Theory." *Jl of Fluid Mech.*, Vol. 94, Part I, pp. 129-161.

FENTON, J.D. (1998). "The Cnoidal Theory of Water Waves." in "Developments in Offshore Engineering: Wave Phenomena and Offshore Topics (Handbook of Coastal & Ocean Engineering)", Ed. J.B. HERBICH, *Gulf Professional Publishing*, Houston, USA, pp. 55-101.

FURUYAMA, S., and CHANSON, H. (2008). "A Numerical Study of Open Channel Flow Hydrodynamics and Turbulence of the Tidal Bore and Dam-Break Flows." *Report No. CH66/08*, Div. of Civil Engineering, The University of Queensland, Brisbane, Australia, May, 88 pages.

GORING, D.G., and NIKORA, V.I. (2002). "Despiking Acoustic Doppler Velocimeter Data." *Jl of Hyd. Engrg.*, ASCE, Vol. 128, No. 1, pp. 117-126. Discussion: Vol. 129, No. 6, pp. 484-489.

HINZE, J.O. (1967). "Secondary Currents in Wall Turbulence." *Physics of Fluids*, Suppl. 10, pp. S122-S125.

HINZE, J.O., (1973). "Experimental Investigation of secondary Currents in the Turbulent Flow through a Straight Conduit." *Appl. Science Res.*, Vol. 28, pp. 453-465.

HORNUNG, H.G., WILLERT, C., and TURNER, S. (1995). "The Flow Field Downsteam of a Hydraulic Jump." *Jl of Fluid Mech.*, Vol. 287, pp. 299-316.

JAEGER, C. (1956). "Engineering Fluid Mechanics." *Blackie & Son*, Glasgow, UK, 529 pages.

KJERFVE, B., and FERREIRA, H.O. (1993). "Tidal Bores: First Ever Measurements." *Ciência e Cultura (Jl of the Brazilian Assoc. for the Advancement of Science)*, Vol. 45, No. 2, March/April, pp. 135-138.

KOCH, C., and CHANSON, H. (2005). "An Experimental Study of Tidal Bores and Positive Surges: Hydrodynamics and Turbulence of the Bore Front." *Report No. CH56/05*, Dept. of Civil Engineering, The University of Queensland, Brisbane, Australia, July, 170 pages (ISBN 978-1-86499-824-5).

KOCH, C., and CHANSON, H. (2008). "Turbulent Mixing beneath an Undular Bore Front." *Journal of Coastal Research*, Vol. 24, No. 4, pp. 999-1007 (DOI: 10.2112/06-0688.1).

KOCH, C., and CHANSON, H. (2009). "Turbulence Measurements in Positive Surges and Bores." *Journal of Hydraulic Research*, IAHR, Vol. 47, No. 1, pp. 29-40 (DOI: 10.3826/jhr.2009.2954).

LEMOINE, R. (1948). "Sur les Ondes Positives de Translation dans les Canaux et sur le Ressaut Ondulé de Faible Amplitude." ('On the Positive Surges in Channels and on the Undular Jumps of Low Wave Height.') *Jl La Houille Blanche*, Mar-Apr., pp. 183-185 (in French).

LE MÉHAUTÉ, B., DIVOKY, D., and LIN, A. (1968). "Shallow Water Waves: a Comparison of Theories and Experiments." *Proc. 11th Intl Conf. on Coastal Eng.*, London, UK, ASCE Publ., Vol. I, pp. 86-107.

LEWIS, A.W. (1972). "Field Studies of a Tidal Bore in the River Dee." *M.Sc. thesis*, Marine Science Laboratories, University College of North Wales, Bangor, UK.

LIGGETT, J.A. (1994). "Fluid Mechanics." *McGraw-Hill*, New York, USA.

LUBIN, P., GLOCKNER, S., and CHANSON, H. (2009). "Numerical simulation of a weak breaking tidal bore." *Mechanics Research Communications*, Vol. 36 (DOI: 10.1016/j.mechrescom.2009.09.008).

McLELLAND, S.J., and NICHOLAS, A.P. (2000). "A New Method for Evaluating Errors in High-Frequency ADV Measurements." *Hydrological Processes*, Vol. 14, pp. 351-366.

MADSEN, P.A., SIMONSEN, H.J., and PAN, C.H. (2005). "Numerical Simulation of Tidal Bores and Hydraulic Jumps." Coastal Eng., Vol. 52, pp. 409-433 (DOI: 10.1016/j.coastaleng.2004.12.007).

MONTES, J.S. (1986). "A Study of the Undular Jump Profile." *Proc. 9th Australasian Fluid Mechanics Conference AFMC*, Auckland, New Zealand, pp. 148-151.

MONTES, J.S. (1998). "Hydraulics of Open Channel Flow." *ASCE Press*, New-York, USA, 697 pages.

MONTES, J.S., and CHANSON, H. (1998). "Characteristics of Undular Hydraulic Jumps. Results and Calculations." *Jl of Hyd. Engrg.*, ASCE, Vol. 124, No. 2, pp. 192-205.

NAVARRE, P. (1995). "Aspects Physiques du Caracteres Ondulatoire du Macaret en Dordogne." ('Physical Features of the Undulations of the Dordogne River Tidal Bore.') *D.E.A. thesis*, Univ. of Bordeaux, France, 72 pages (in French).

Open University Course Team (1999). "Waves, Tides and Shallow-Water Processes." *Butterworth-Heinemann*, Oxford, UK, 2nd edition, 227 pages.

PEREGRINE, D.H. (1966). "Calculations of the Development of an Undular Bore." *Jl. Fluid Mech.*, Vol 25, pp.321-330.

ROUSE, H. (1938). "Fluid Mechanics for Hydraulic Engineers." *McGraw-Hill Publ.*, New York, USA (also Dover Publ., New York, USA, 1961, 422 pages)

ROUSE, H. (1959). "Advanced Mechanics of Fluids." *John Wiley*, New York, USA, 444 pages.

SERRE, F. (1953). "Contribution à l'Etude des Ecoulements Permanents et Variables dans les Canaux." ('Contribution to the Study of Permanent and Non-Permanent Flows in Channels.') *Jl La Houille Blanche*, Dec., pp. 830-872 (in French).

THORNE, C.R., and HEY, R.D. (1979). "Direct Measurements of Secondary Currents at a River Inflexion Point." *Nature*, Vol. 280, 19 July, pp. 226-228.

TRESKE, A. (1994). "Undular Bores (Favre-Waves) in Open Channels - Experimental Studies." *Jl of Hyd. Res.*, IAHR, Vol. 32, No. 3, pp. 355-370. Discussion : Vol. 33, No. 3, pp. 274-278.

TREVETHAN, M., CHANSON, H., and BROWN, R. (2008). "Turbulence Characteristics of a Small Subtropical Estuary during and after some Moderate Rainfall." *Estuarine Coastal and Shelf Science*, Vol. 79, No. 4, pp. 661-670 (DOI: 10.1016/j.ecss.2008.06.006).

VOULGARIS, G., and TROWBRIDGE, J.H. (1998). "Evaluation of the Acoustic Doppler Velocimeter (ADV) for Turbulence Measurements." *Jl Atmosph. and Oceanic Tech.*, Vol. 15, pp. 272-289.

WAHL, T.L. (2003). "Despiking Acoustic Doppler Velocimeter Data. Discussion." *Jl of Hyd. Engrg.*, ASCE, Vol. 129, No. 6, pp. 484-487.

WIEGEL, R.L. (1960). "A Presentation of Cnoidal Wave Theory for Practical Application." *Jl of Fluid Mech.*, Vol. 7, No. 2, pp. 273-286.

WOLANSKI, E., WILLIAMS, D., SPAGNOL, S., and CHANSON, H. (2004). "Undular Tidal Bore Dynamics in the Daly Estuary, Northern Australia." *Estuarine, Coastal and Shelf Science*, Vol. 60, No. 4, pp. 629-636 (DOI: 10.1016/j.ecss.2004.03.001).

XIE, Q. (1998). "Turbulent Flows in Non-Uniform Open Channels : Experimental Measurements and Numerical Modelling." *Ph.D. thesis*, Dept. of Civil Eng., University Of Queensland, Australia, 339 pages.

ZHU, A.Z., and CHENG, X. (2008). "Test and Analyses of a New Double-Arch Steel Gate under Cyclic Loading." *Jl Const. Steel Res.*, Vol. 64, pp. 454-464.

Internet references

Tidal bores, Mascaret, Pororoca. Myths, Fables and Reality !!!	{http://www.uq.edu.au/~e2hchans/tid_bore.html}
The tidal bore of the Seine river, France. Le Mascaret de la Seine.	{http://www.uq.edu.au/~e2hchans/mascaret.html}
Free-Surface Undulations in Open Channel Flows: Undular Jumps, Undular Surges, Standing Waves	{http://www.uq.edu.au/~e2hchans/undular.html}
Photographs of tidal bores	{http://www.uq.edu.au/~e2hchans/photo.html#Tidal_bores}
Open access repository UQeSpace	{http://espace.library.uq.edu.au/}
Software 7-zip	{http://www.7-zip.org/}
Software Quicktime	{http://www.apple.com/quicktime/download/}

Bibliographic reference of the Report CH74/09

The Hydraulic Model research report series CH is a refereed publication published by the Division of Civil Engineering at the University of Queensland, Brisbane, Australia.

The bibliographic reference of the present report is :

CHANSON, H. (2009). "An Experimental Study of Tidal Bore Propagation: the Impact of Bridge Piers and Channel Constriction." *Hydraulic Model Report No. CH74/09*, School of Civil Engineering, The University of Queensland, Brisbane, Australia, 110 pages and 5 movies (ISBN 9781864999600).

The Report CH74/09 is available, in the present form, as a PDF file on the Internet at UQeSpace:

http://espace.library.uq.edu.au/

It is listed at:

http://espace.library.uq.edu.au/list/author_id/193/

Hydraulic model research report CH

The Hydraulic Model Report CH series is published by the School of Civil Engineering at the University of Queensland. Orders of any reprint(s) of the Hydraulic Model Reports should be addressed to the School Secretary.

School Secretary, School of Civil Engineering, The University of Queensland
Brisbane 4072, Australia - Tel.: (61 7) 3365 3619 - Fax : (61 7) 3365 4599
Url: http://www.eng.uq.edu.au/civil/ Email: hodciveng@uq.edu.au

Report CH	**Unit price**	Quantity	**Total price**
CHANSON, H. (2009). "An Experimental Study of Tidal Bore Propagation: the Impact of Bridge Piers and Channel Constriction." *Hydraulic Model Report No. CH74/09*, School of Civil Engineering, The University of Queensland, Brisbane, Australia, 110 pages and 5 movies (ISBN 9781864999600).	AUD$60.00		
CHANSON, H. (2008). "Jean-Baptiste Charles Joseph BÉLANGER (1790-1874), the Backwater Equation and the Bélanger Equation." *Hydraulic Model Report No. CH69/08*, Div. of Civil Engineering, The University of Queensland, Brisbane, Australia, 40 pages (ISBN 9781864999211).	AUD$60.00		
GOURLAY, M.R., and HACKER, J. (2008). "Reef-Top Currents in Vicinity of Heron Island Boat Harbour, Great Barrier Reef, Australia: 2. Specific Influences of Tides Meteorological Events and Waves." *Hydraulic Model Report No. CH73/08*, Div. of Civil Engineering, The University of Queensland, Brisbane, Australia, 331 pages (ISBN 9781864999365).	AUD$60.00		
GOURLAY, M.R., and HACKER, J. (2008). "Reef Top Currents in Vicinity of Heron Island Boat Harbour Great Barrier Reef, Australia: 1. Overall influence of Tides, Winds, and Waves." *Hydraulic Model Report CH72/08*, Div. of Civil Engineering, The University of Queensland, Brisbane, Australia, 201 pages (ISBN 9781864999358).	AUD$60.00		
LARRARTE, F., and CHANSON, H. (2008). "Experiences and Challenges in Sewers: Measurements and Hydrodynamics." *Proceedings of the International Meeting on Measurements and Hydraulics of Sewers*, Summer School GEMCEA/LCPC, 19-21 Aug. 2008, Bouguenais, Hydraulic Model Report No. CH70/08, Div. of Civil Engineering, The University of Queensland, Brisbane, Australia (ISBN 9781864999280).	AUD$60.00		
CHANSON, H. (2008). "Photographic Observations of Tidal Bores (Mascarets) in France." *Hydraulic Model Report No. CH71/08*, Div. of Civil Engineering, The University of Queensland, Brisbane, Australia, 104 pages, 1 movie and 2 audio files (ISBN 9781864999303).	AUD$60.00		
CHANSON, H. (2008). "Turbulence in Positive Surges and Tidal Bores. Effects of Bed Roughness and Adverse Bed Slopes." *Hydraulic Model Report No. CH68/08*, Div. of Civil Engineering, The University of Queensland, Brisbane, Australia, 121 pages & 5 movie files (ISBN 9781864999198)	AUD$70.00		
FURUYAMA, S., and CHANSON, H. (2008). "A Numerical Study of Open Channel Flow Hydrodynamics and Turbulence of the Tidal Bore and Dam-Break Flows." *Report No. CH66/08*, Div. of Civil Engineering, The University of Queensland, Brisbane, Australia, May, 88 pages (ISBN 9781864999068).	AUD$60.00		

GUARD, P., MACPHERSON, K., and MOHOUPT, J. (2008). "A Field Investigation into the Groundwater Dynamics of Raine Island." *Report No. CH67/08*, Div. of Civil Engineering, The University of Queensland, Brisbane, Australia, February, 21 pages (ISBN 9781864999075).	AUD$40.00		
FELDER, S., and CHANSON, H. (2008). "Turbulence and Turbulent Length and Time Scales in Skimming Flows on a Stepped Spillway. Dynamic Similarity, Physical Modelling and Scale Effects." *Report No. CH64/07*, Div. of Civil Engineering, The University of Queensland, Brisbane, Australia, March, 217 pages (ISBN 9781864998870).	AUD$60.00		
TREVETHAN, M., CHANSON, H., and BROWN, R.J. (2007). "Turbulence and Turbulent Flux Events in a Small Subtropical Estuary." Report No. CH65/07, Div. of Civil Engineering, The University of Queensland, Brisbane, Australia, November, 67 pages (ISBN 9781864998993)	AUD$60.00		
MURZYN, F., and CHANSON, H. (2007). "Free Surface, Bubbly flow and Turbulence Measurements in Hydraulic Jumps." *Report CH63/07*, Div. of Civil Engineering, The University of Queensland, Brisbane, Australia, August, 116 pages (ISBN 9781864998917).	AUD$60.00		
KUCUKALI, S., and CHANSON, H. (2007). "Turbulence in Hydraulic Jumps: Experimental Measurements." *Report No. CH62/07*, Div. of Civil Engineering, The University of Queensland, Brisbane, Australia, July, 96 pages (ISBN 9781864998825).	AUD$60.00		
CHANSON, H., TAKEUCHI, M, and TREVETHAN, M. (2006). "Using Turbidity and Acoustic Backscatter Intensity as Surrogate Measures of Suspended Sediment Concentration. Application to a Sub-Tropical Estuary (Eprapah Creek)." *Report No. CH60/06*, Div. of Civil Engineering, The University of Queensland, Brisbane, Australia, July, 142 pages (ISBN 1864998628).	AUD$60.00		
CAROSI, G., and CHANSON, H. (2006). "Air-Water Time and Length Scales in Skimming Flows on a Stepped Spillway. Application to the Spray Characterisation." *Report No. CH59/06*, Div. of Civil Engineering, The University of Queensland, Brisbane, Australia, July (ISBN 1864998601).	AUD$60.00		
TREVETHAN, M., CHANSON, H., and BROWN, R. (2006). "Two Series of Detailed Turbulence Measurements in a Small Sub-Tropical Estuarine System." *Report No. CH58/06*, Div. of Civil Engineering, The University of Queensland, Brisbane, Australia, Mar. (ISBN 1864998520).	AUD$60.00		
KOCH, C., and CHANSON, H. (2005). "An Experimental Study of Tidal Bores and Positive Surges: Hydrodynamics and Turbulence of the Bore Front." *Report No. CH56/05*, Dept. of Civil Engineering, The University of Queensland, Brisbane, Australia, July (ISBN 1864998245).	AUD$60.00		
CHANSON, H. (2005). "Applications of the Saint-Venant Equations and Method of Characteristics to the Dam Break Wave Problem." *Report No. CH55/05*, Dept. of Civil Engineering, The University of Queensland, Brisbane, Australia, May (ISBN 1864997966).	AUD$60.00		
CHANSON, H., COUSSOT, P., JARNY, S., and TOQUER, L. (2004). "A Study of Dam Break Wave of Thixotropic Fluid: Bentonite Surges down an Inclined plane." *Report No. CH54/04*, Dept. of Civil Engineering, The University of Queensland, Brisbane, Australia, June, 90 pages (ISBN 1864997710).	AUD$60.00		
CHANSON, H. (2003). "A Hydraulic, Environmental and Ecological Assessment of a Sub-tropical Stream in Eastern Australia: Eprapah Creek, Victoria Point QLD on 4 April 2003." *Report No. CH52/03*, Dept. of Civil Engineering, The University of Queensland, Brisbane, Australia, June, 189 pages (ISBN 1864997044).	AUD$90.00		
CHANSON, H. (2003). "Sudden Flood Release down a Stepped Cascade. Unsteady Air-Water Flow Measurements. Applications to Wave Run-up, Flash Flood and Dam Break Wave." *Report CH51/03*, Dept of Civil Eng., Univ. of Queensland, Brisbane, Australia, 142 pages (ISBN 1864996552).	AUD$60.00		

CHANSON, H,. (2002). "An Experimental Study of Roman Dropshaft Operation : Hydraulics, Two-Phase Flow, Acoustics." *Report CH50/02*, Dept of Civil Eng., Univ. of Queensland, Brisbane, Australia, 99 pages (ISBN 1864996544).	AUD$60.00		
CHANSON, H., and BRATTBERG, T. (1997). "Experimental Investigations of Air Bubble Entrainment in Developing Shear Layers." *Report CH48/97*, Dept. of Civil Engineering, University of Queensland, Australia, Oct., 309 pages (ISBN 0 86776 748 0).	AUD$90.00		
CHANSON, H. (1996). "Some Hydraulic Aspects during Overflow above Inflatable Flexible Membrane Dam." *Report CH47/96*, Dept. of Civil Engineering, University of Queensland, Australia, May, 60 pages (ISBN 0 86776 644 1).	AUD$60.00		
CHANSON, H. (1995). "Flow Characteristics of Undular Hydraulic Jumps. Comparison with Near-Critical Flows." *Report CH45/95*, Dept. of Civil Engineering, University of Queensland, Australia, June, 202 pages (ISBN 0 86776 612 3).	AUD$60.00		
CHANSON, H. (1995). "Air Bubble Entrainment in Free-surface Turbulent Flows. Experimental Investigations." *Report CH46/95*, Dept. of Civil Engineering, University of Queensland, Australia, June, 368 pages (ISBN 0 86776 611 5).	AUD$80.00		
CHANSON, H. (1994). "Hydraulic Design of Stepped Channels and Spillways." *Report CH43/94*, Dept. of Civil Engineering, University of Queensland, Australia, Feb., 169 pages (ISBN 0 86776 560 7).	AUD$60.00		
POSTAGE & HANDLING (per report)	AUD$10.00		
GRAND TOTAL			

Other hydraulic research reports

Reports/Theses	Unit price	Quantity	Total price
TREVETHAN, M. (2008). "A Fundamental Study of Turbulence and Turbulent Mixing in a Small Subtropical Estuary." Ph.D. thesis, Div. of Civil Engineering, The University of Queensland, 342 pages.	AUD$100.00		
GONZALEZ, C.A. (2005). "An Experimental Study of Free-Surface Aeration on Embankment Stepped Chutes." *Ph.D. thesis*, Dept of Civil Engineering, The University of Queensland, Brisbane, Australia, 240 pages.	AUD$80.00		
TOOMBES, L. (2002). "Experimental Study of Air-Water Flow Properties on Low-Gradient Stepped Cascades." *Ph.D. thesis*, Dept of Civil Engineering, The University of Queensland, Brisbane, Australia.	AUD$100.00		
CHANSON, H. (1988). "A Study of Air Entrainment and Aeration Devices on a Spillway Model." *Ph.D. thesis*, University of Canterbury, New Zealand.	AUD$60.00		
POSTAGE & HANDLING (per report)	AUD$10.00		
GRAND TOTAL			

Civil Engineering research report CE

The Civil Engineering Research Report CE series is published by the School of Civil Engineering at the University of Queensland. Orders of any of the Civil Engineering Research Report CE should be addressed to the School Secretary.

School Secretary, School of Civil Engineering, The University of Queensland
Brisbane 4072, Australia
Tel.: (61 7) 3365 3619 Fax : (61 7) 3365 4599
Url: http://www.eng.uq.edu.au/civil/ Email: hodciveng@uq.edu.au

Recent Research Report CE	Unit price	Quantity	Total price
CALLAGHAN, D.P., NIELSEN, P., and CARTWRIGHT, N. (2006). "Data and Analysis Report: Manihiki and Rakahanga, Northern Cook Islands - For February and October/November 2004 Research Trips." *Research Report CE161*, Division of Civil Engineering, The University of Queensland (ISBN No. 1864998318).	AUD$10.00		
GONZALEZ, C.A., TAKAHASHI, M., and CHANSON, H. (2005). "Effects of Step Roughness in Skimming Flows: an Experimental Study." *Research Report No. CE160*, Dept. of Civil Engineering, The University of Queensland, Brisbane, Australia, July (ISBN 1864998105).	AUD$10.00		
CHANSON, H., and TOOMBES, L. (2001). "Experimental Investigations of Air Entrainment in Transition and Skimming Flows down a Stepped Chute. Application to Embankment Overflow Stepped Spillways." *Research Report No. CE158*, Dept. of Civil Engineering, The University of Queensland, Brisbane, Australia, July, 74 pages (ISBN 1 864995297).	AUD$10.00		
HANDLING (per order)	AUD$10.00		
GRAND TOTAL			

Note: Prices include postages and processing.

PAYMENT INFORMATION

1- VISA Card

Name on the card :	
Visa card number :	
Expiry date :	

Amount :	AUD$ .....

2- Cheque/remittance payable to: THE UNIVERSITY OF QUEENSLAND and crossed "Not Negotiable".

N.B. For overseas buyers, cheque payable in Australian Dollars drawn on an office in Australia of a bank operating in Australia, payable to: THE UNIVERSITY OF QUEENSLAND and crossed "Not Negotiable".

Orders of any Research Report should be addressed to the School Secretary.

School Secretary, School of Civil Engineering, The University of Queensland
Brisbane 4072, Australia - Tel.: (61 7) 3365 3619 - Fax : (61 7) 3365 4599
Url: http://www.eng.uq.edu.au/civil/ Email: hodciveng@uq.edu.au